SKB

TECHNICAL REPORT 96-23

Analysis of the Äspö LPT2 pumping test via simulation and inverse modelling with HYDRASTAR

Douglas Walker (ed.)[1], Lars Eriksson[2], Lars Lovius[2]

[1] INTERA KB
[2] Starprog AB

December 1996

SVENSK KÄRNBRÄNSLEHANTERING AB
SWEDISH NUCLEAR FUEL AND WASTE MANAGEMENT CO
P.O.BOX 5864 S-102 40 STOCKHOLM SWEDEN
PHONE +46 8 665 28 00
FAX +46 8 661 57 19

ANALYSIS OF THE ÄSPÖ LPT2 PUMPING TEST VIA SIMULATION AND INVERSE MODELLING WITH HYDRASTAR

Douglas Walker (ed.)[1], *Lars Eriksson*[2], *Lars Lovius*[2]

1 INTERA KB
2 Starprog AB

December 1996

ANALYSIS OF THE ÄSPÖ LPT2 PUMPING TEST VIA SIMULATION AND INVERSE MODELLING WITH HYDRASTAR

Douglas Walker (ed.)[1], Lars Eriksson[2], and Lars Lovius[2]

[1]INTERA KB

[2]Starprog AB

December, 1996

Keywords: stochastic hydrogeology, calibration, conditioning, geostatistics, groundwater modelling, pumping test, fractured rock

ABSTRACT

A stochastic groundwater modelling study is presented for the second Long-term Pumping Test (LPT2) conducted at the Äspö Hard Rock Laboratory (HRL). It is a test case for HYDRASTAR, a stochastic continuum groundwater flow and transport model developed by Starprog AB for Swedish Nuclear Fuel and Waste Management Company (SKB). Unlike previous modelling studies of the LPT2, this study uses the inverse modelling capabilities of HYDRASTAR to condition the model results to the observed hydraulic heads. The purpose of this conditioning via inverse modelling is to improve the reliability of input hydraulic conductivity fields and thus minimise the uncertainty of the model predictions. Preliminary simulations evaluated the boundary conditions, grid extent and grid density, all of which were restricted by the computational demands of a larger domain and by code limitations. The preliminary simulations also indicated that the model is quite sensitive to changes in specific storativity and kriging parameters. The final calibrated model simulations were successful in representing the response of the rock mass to the LPT2. Specifically, the mean of the Monte Carlo realisations of simulated drawdowns generally reproduced the magnitude, timing, and shape of the observed drawdowns. The observed drawdowns generally were bracketed by an interval of plus or minus one standard deviation from the mean of the realisations. Some discrepancies in the magnitude and timing of the observed versus the simulated drawdowns were revealed at several locations, such as the upper sections of borehole KAS07. However, the ensemble of model realisations were centred on the observed drawdowns and bracketed the observed responses. This indicates that the ensemble of realisations has bracketed the true characteristics of the HRL, supporting both the conceptual model and its representation by HYDRASTAR.

SAMMANFATTNING

En stokastisk grundvattenmodellering av det s.k. "Longterm Pumping Test" (LPT2) har utförts. Pumptestet utfördes vid Äspölaboratoriet (HRL). Vid studien användes HYDRASTAR, ett program för stokastisk kontinuum simulering av grundvattenströmning och transport, som ursprungligen är utvecklat av Starprog AB för Svensk Kärnbränslehantering AB:s (SKB) räkning. Till skillnad från tidigare utförda modelleringar av LPT2 används i denna studie den inversa modelleringstekniken som finns i HYDRASTAR för att betinga modelleringsresultaten på de observerade grundvatten-potentialerna. Syftet med betingning via inversmodellering är att förbättra tillförlitligheten hos de hydrauliska konduktivitetsfälten och på så sätt minimera osäkerheterna i modellprediktionerna. Studien är också ämnad som ytterligare en tillämpning med HYDRASTAR på verkliga data. Preliminära simuleringar användes för att utvärdera randvillkoren, elementnätets utbredning och täthet. Flera begränsningar i den aktuella versionen av HYDRASTAR och beräkningstekniska krav inskränkte typen av randvillkor och storleken av beräkningsmodellens nät. De preliminära simuleringarna tyder även på att modellen är tämligen känslig för förändringar i den specifika magasinskoefficienten. De slutgiltiga kalibrerade simuleringarna av modellen återgav väl bergmassans hydrauliska respons i förhållande till LPT2 testet. Framför allt återgav Monte Carlo simuleringarnas medelvärde väl de observerade avsänkningarnas storlek och tidsförlopp. De observerade avsänkningarna beskrivs generellt av ± en standardavvikelse från det simulerade medelvärdet. Dock uppstod viss avvikelse i omfattning och tidpunkt mellan den observerade och den simulerade avsänkningen på flera platser, som t.ex. i den övre delen av borrhålet KAS07. Merparten av simuleringarna beskrev väl de observerade avsänkningarna och återspeglade de observerade responserna. Detta tyder på att simuleringarna väl beskriver de verkliga förhållandena i HRL, vilket stöder både den konceptuella modellen och dess beskrivning med HYDRASTAR.

TABLE OF CONTENTS

LIST OF FIGURES

LIST OF TABLES

1. INTRODUCTION

This report presents a stochastic groundwater modelling study of the second Long-term Pumping Test (LPT2) conducted at the Äspö Hard Rock Laboratory (HRL). It makes use of HYDRASTAR, a stochastic continuum groundwater flow and transport model developed by Starprog AB for Swedish Nuclear Fuel and Waste Management Company (SKB). The LPT2, this study and several related studies were conducted under the supervision of SKB as part of performance assessment studies for the Swedish nuclear waste disposal program.

The main objective of this study is to provide an additional real-world test case for HYDRASTAR. This study also evaluates the Äspö HRL hydrogeologic conceptual model via inverse modelling of the LPT2. The success of this study is to be judged by the degree of accuracy with which HYDRASTAR is able to reproduce the transient borehole responses observed during the LPT2. The study differs from previous LPT2 modelling studies because it uses the inverse modelling capabilities of HYDRASTAR to condition the model results to the observed hydraulic heads. The purpose of this conditioning via inverse modelling is to improve the reliability of input hydraulic conductivity fields and thus minimise the uncertainty of the model predictions.

This report describes HYDRASTAR and summarises its testing and previous applications to other sites. It then briefly describes the current conceptual model of the Äspö HRL and the LPT2 experiments. This is followed by a description of the application of HYDRASTAR to the LPT2 and the results of two stochastic transient simulations. The first simulation conditions the model results only to the measured hydraulic conductivities (uncalibrated), while the second conditions the results to both the measured hydraulic conductivities and to the observed hydraulic heads (calibrated). The report ends with a discussion of the model results and the conclusions of this study. Although HYDRASTAR has the ability to model advective transport of such tracers, this study does not examine the LPT2 tracer tests.

1.1. APPROACH

Hydrogeologists frequently use groundwater flow and transport models to assess the possible outcomes of waste management decisions. Ideally, input parameters for these models would be perfectly known, so that the model results would be deterministic. However, input parameters for groundwater models are usually highly uncertain, requiring that the model be calibrated by adjusting input parameters until the model results match observed conditions. This calibration is also known as inverse modelling, and typically involves modifying the input hydraulic conductivity field until the model simulations match hydraulic head observations. Unfortunately, the inverse problem in hydrogeology is nonunique, that is, many hydraulic conductivity fields will satisfy a given set of head observations with equal probability. This will be true even though subsequent transport model

simulations may be quite different for each hydraulic conductivity field. One solution is to acknowledge that inverse solutions are nonunique, and present the model results as stochastic rather than deterministic. For example, the mean and variance of many nonunique solutions is presented for the hydraulic conductivity fields, contaminant arrival times, etc.

Several algorithms exist to solve the inverse problem (Carrera and Neuman, 1986; Yeh, 1986; RamRao et al., 1995). In general, they rely on kriging and geostatistical simulation to interpolate between known hydraulic conductivities, then calibrate the hydraulic conductivities by comparing the model-simulated responses to observed responses. Whatever approach is used, the method should incorporate all the available data and features of the site conceptual models to ensure that the model results have the minimum level of uncertainty. The model simulations, therefore, should honour (be conditioned on) the measured hydraulic conductivities and other hydrogeologic information as well as the observed hydraulic heads.

1.2. HYDRASTAR

HYDRASTAR is a stochastic groundwater flow and transport model developed as a quantitative tool for support of the SKB 91 safety analysis project (SKB, 1992). HYDRASTAR uses conditional geostatistical simulation to create fields which honour the measured hydraulic conductivities, then calibrates the resulting fields to the observed heads via inverse modelling. HYDRASTAR treats the rock mass of interest as a porous media continuum where flow is governed by Darcy's Law.

Figure 1-1 presents a flow-chart summarising the HYDRASTAR algorithm. The current version, 1.5, uses the Turning Bands algorithm (Journel and Huijbregts, 1978) to generate realisations of the hydraulic conductivity field conditioned on the observed hydraulic conductivities. Trends in the data may be included implicitly through the use of ordinary kriging neighbourhoods or prescribed explicitly for specific regions. Hydraulic conductivity measurements at the borehole scale are upscaled to the model calculation scale using an averaging scheme based on Moye's formula (a corrected arithmetic mean of the packer test hydraulic conductivities within a block; see Norman, 1992b, for details). HYDRASTAR uses the governing equation for either time-dependent or steady state groundwater flow in three dimensions, assuming constant density. The solution to this governing equation is approximated by a node centred finite-difference method to create a linear system equations. A pre-conditioned conjugate-gradient algorithm solves the system of equations to arrive at a solution for the hydraulic head at each node. The pilot point inverse method (de Marsily et al., 1984) then calibrates the input hydraulic conductivity field to minimise the error between the simulated and observed hydraulic heads. Transport in the resulting velocity field is modelled as pure advection using a particle tracking scheme. The process of conditional geostatistical simulation of hydraulic conductivity, calibration of the field via inverse modelling, and particle tracking can be repeated in Monte Carlo fashion to develop empirical probability distributions for the hydraulic conductivity field, contaminant travel paths, and contaminant arrival times.

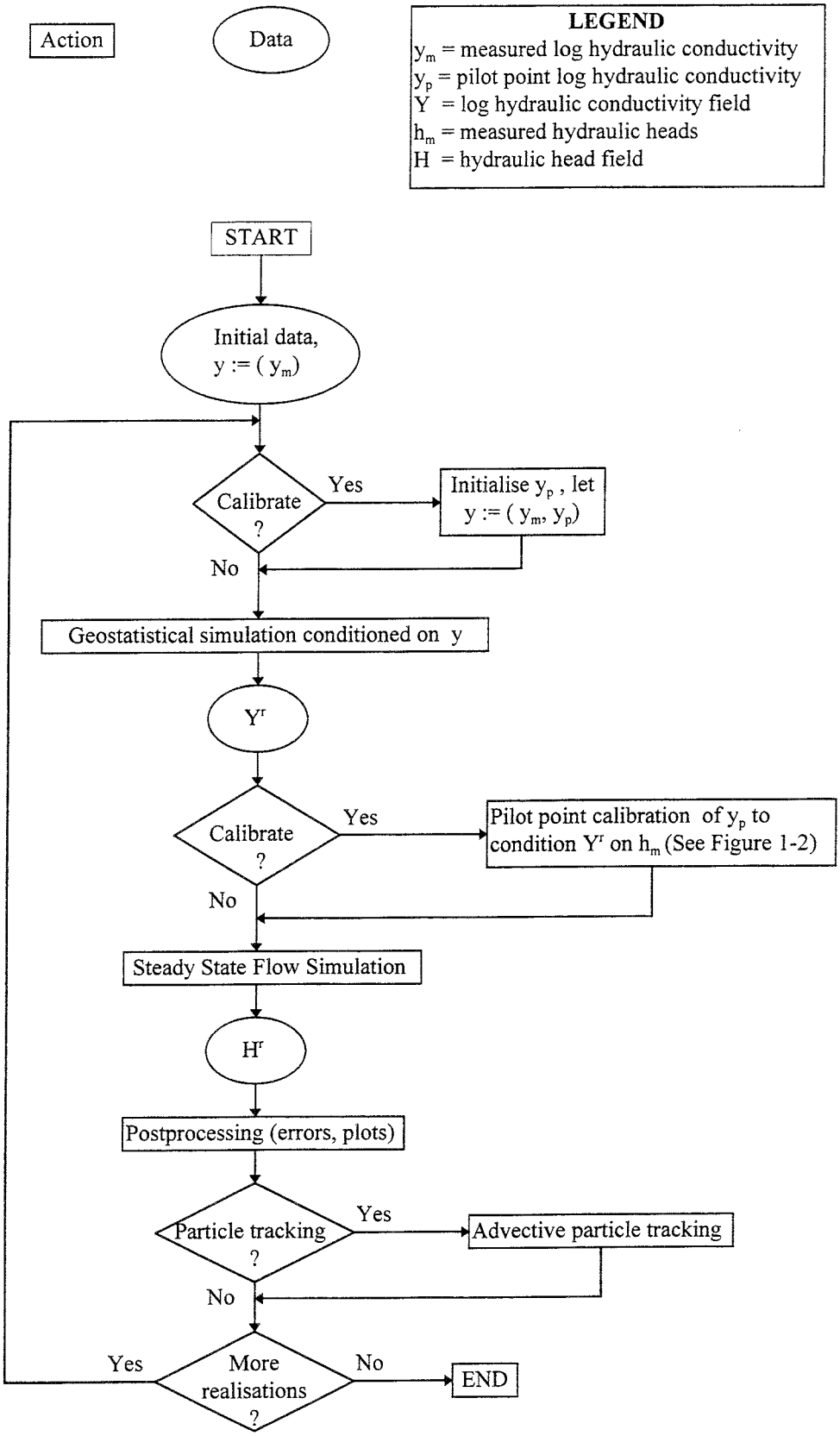

Figure 1-1. *HYDRASTAR flow chart*

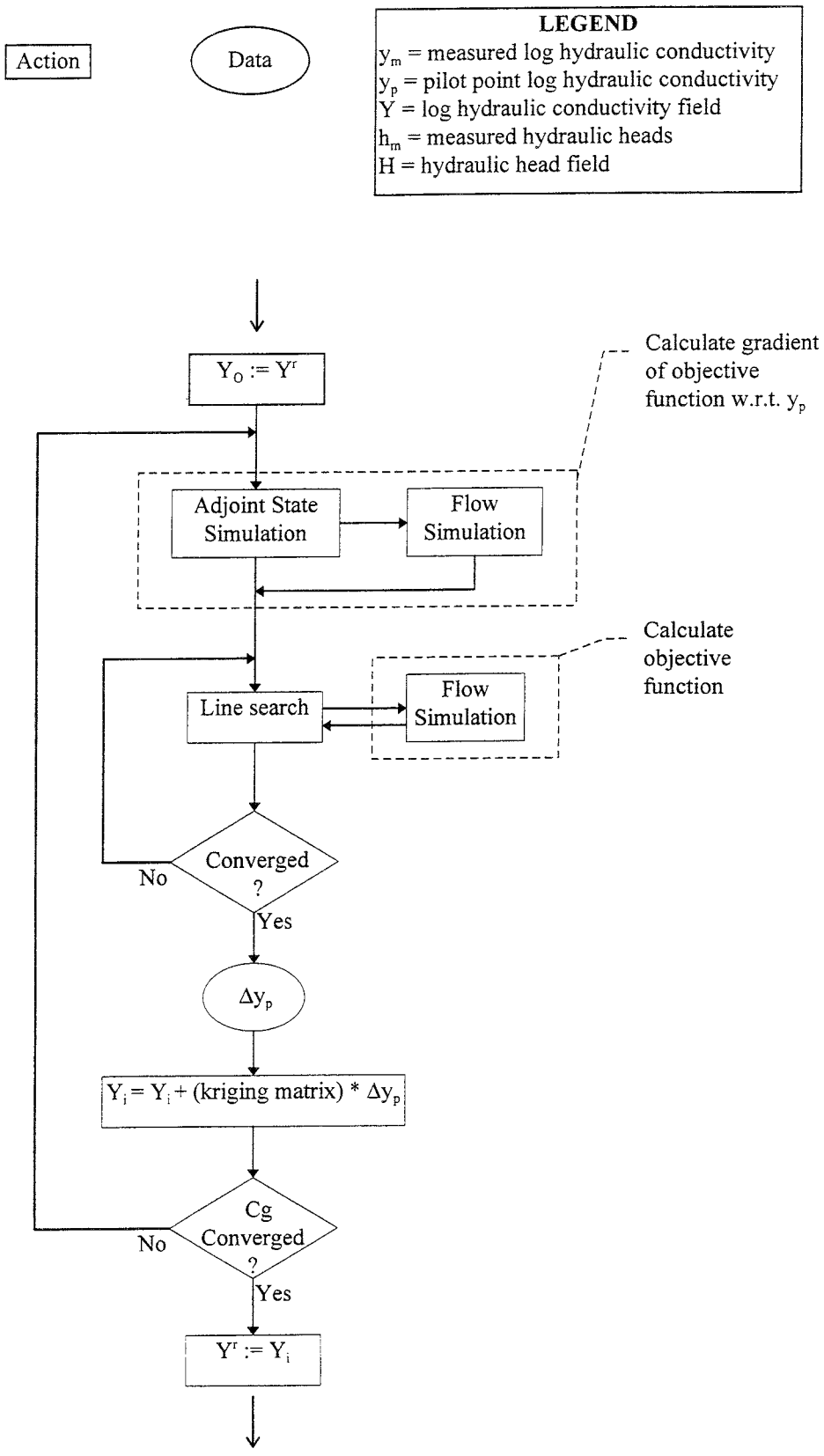

Figure 1-2. *Pilot Point method flow chart*

This is the first HYDRASTAR application to use a newly-implemented pilot point method of calibration (Eriksson and Oppelstrup, 1994). This method adjusts the input hydraulic conductivity field at key locations (pilot points) to minimise the error between the simulated and observed hydraulic heads. These pilot points are included as conditioning data in the geostatistical simulation so that the influence of the pilot point is determined by the range of spatial correlation and the choice of kriging neighbourhood. That is, the influence of the adjustments is governed by the range of the input variogram model, decreasing with distance from the pilot point. An additional larger-scale effect arises from the influence of the pilot points on in the mean of the ordinary kriging neighbourhood. Both of these effects condition the input hydraulic conductivity fields on both the observed hydraulic conductivities and the measured heads. This consequently increases the reliability of the hydraulic conductivity field, and reduces the uncertainty of subsequent simulations. Figure 1-2 presents a flowchart which summarises the pilot point method of calibration.

Starprog AB developed and tested the code under contract to SKB, beginning in 1991 (Norman 1991 and 1992b). Various authors have contributed to the development and testing of the code, most notably Norman (1991 and 1992b), Morris and Cliffe (1994), Lovius and Eriksson (1993, 1994), and Walker (1997). The test problems include comparisons to well-known analytical and numerical solutions, or are taken from the HYDROCOIN series of test problems (OECD, 1983; Hodgkinson and Barker, 1985). The code also has been applied successfully to the Finnsjön site, as part of the SKB-91 Project (Norman, 1992a and SKB 1992).

2. ÄSPÖ HARD ROCK LABORATORY AND THE LPT2 TESTS

2.1. SITE DESCRIPTION

The Äspö Hard Rock Laboratory (HRL) is an underground research facility located near the Oskarshamn nuclear power plant on the east coast of Sweden, approximately 300km south of Stockholm (Figure 2-1).

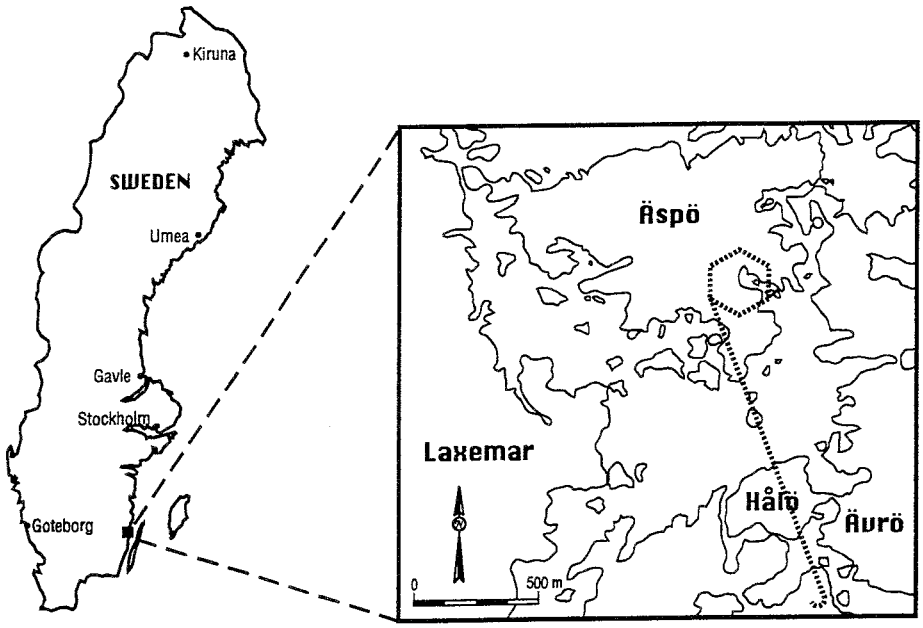

Figure 2-1. Location of the Äspö Hard Rock Laboratory

The HRL lies beneath Äspö island and consists of a vertical shaft and horizontal access tunnels connected to a descending spiral of tunnels which extend to a depth of over 450m below ground surface (Figure 2-2).

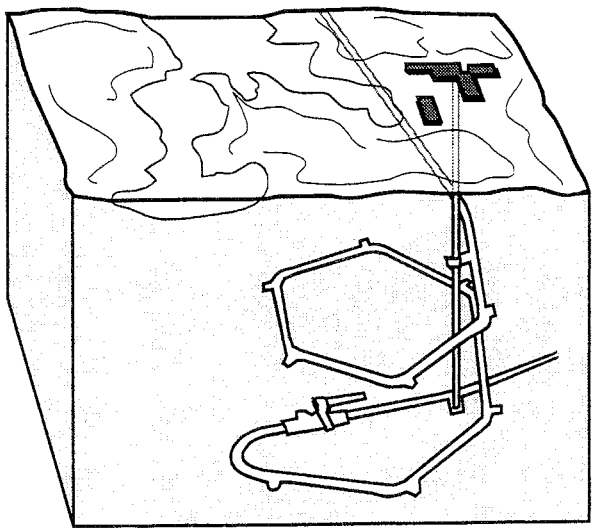

Figure 2-2 Overview of the Äspö Hard Rock Laboratory

Pre-investigations at Äspö started in 1986, and the facility was completed in 1995. It is operated by SKB for the purpose of investigating geological, geochemical, and hydrogeological phenomena associated with the underground disposal of nuclear waste. Nuclear waste management organisations and investigators from several countries participate in research conducted at this facility.

Various investigations have taken place at Äspö before, during and after construction of the laboratory. This included a tracer test and a number of interference pumping tests that were later analysed as training and calibration exercises for the numerical models of the site. A major test of this kind was the second Long-term Pumping Test (LPT2) conducted in the autumn of 1990.

2.2. SITE GEOLOGY AND HYDROGEOLOGY

Pre-investigations of the Äspö area involved a wide variety of remote sensing, surface geophysics, outcrop mapping and drilling programs (Wikberg et al. 1991). The bedrock in the Äspö area is dominated by the 1700-1800Ma old Småland granite suite. The rocks are rather heterogeneous with some older xenoliths, mainly metavulcanites, and younger intrusions of a brittle, light, fine-grained granite. Various seismic, outcrop and borehole studies have revealed a number of steeply dipping fracture zones ranging in width from 10 to 100m, which are conductive in comparison to the surrounding rock mass. This is modelled in a continuum model as an effective porous medium with a rock mass domain and a fracture zone domain. The extensive pre-investigations were aimed at identifying the positions and properties of the fracture zones physically and statistically. Figure 2-3 shows a schematic representation of the conductive fracture zones identified during the pre-investigations and the construction phase (after Rhén, 1995). Note that, although this study incorporates data obtained during the construction phase, the simulations are of events which occurred prior to the construction of the HRL. The tunnels and shafts are shown only for reference, and were not present at the time of the LPT2.

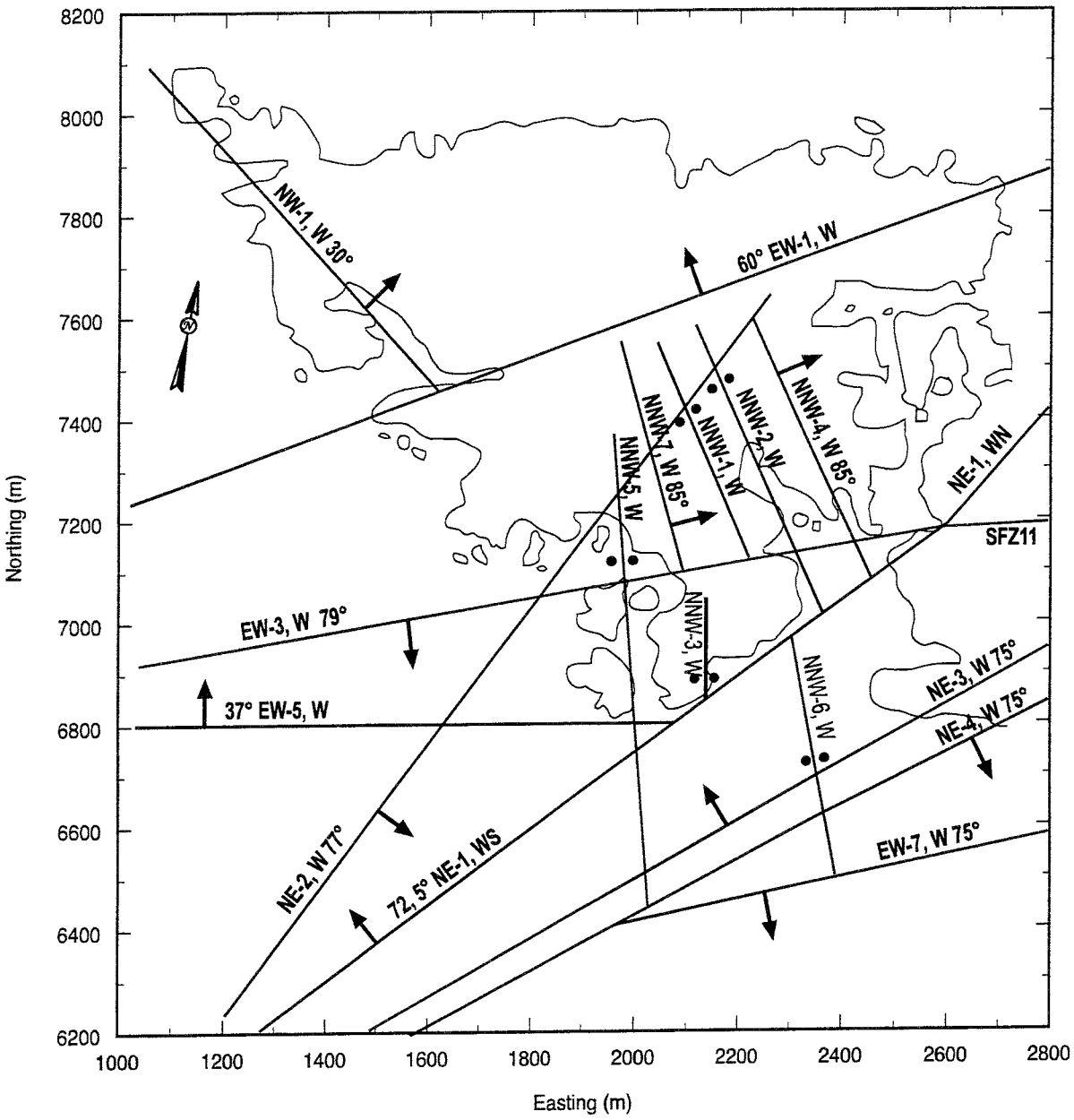

Figure 2-3. Construction phase fracture zones (after Rhén, 1995)

Äspö is an island, and so the level of the brackish Baltic sea is the dominant influence on the groundwater potentiometric level. Because precipitation generally exceeds evapotranspiration, natural recharge on the land surface also influences the preconstruction groundwater flow system. Fresh groundwater near the surface rests on stagnant saline water at depth.

As part of the pre-investigation drilling programme, many tests were conducted in the boreholes in an effort to assess hydraulic conductivities, storage properties, porosities and flow rates. The overall hydraulic conductivity of the rock mass is thought to be in the range of 10^{-6} to 10^{-9} m/sec, decreasing with depth. Specific storativity is thought to be in the range of 10^{-6} to 10^{-8} 1/m (Wikberg et al. 1991). The preliminary analysis of LPT2 reported in Rhén et al. (1992) indicated hydraulic conductivities and

storativities similar to those of Wikberg et al. (1991). The LPT2 tests are discussed in more detail in the following section.

2.3. THE LPT2 EXPERIMENTS

During the extensive pre-investigations for the Äspö HRL, field experiments were carried out to characterise the site geologically, hydrogeologically and hydrochemically. In the autumn of 1990, a combined long term pumping, dilution, and tracer test was conducted in borehole KAS06, referred to as LPT2. The goals of LPT2 included the preliminary identification of major conductive features and the characterisation of the flow and transport within the rock mass at the Äspö HRL (Gustafson and Ström, 1995). Rhén et al. (1992) describes the LPT2 experiments and provides a preliminary analysis of LPT2.

Figure 2-4 shows the wells utilised in LPT2. The pumping phase lasted for three months and was combined with a large scale converging tracer test. Pumping in KAS06 began on September 17, 1990, and continued until December 18, 1990. The initial pumping rate was approximately 2.0 litres/sec which was maintained until steady drawdown was achieved. The rate was then increased to 2.5 litres/sec, then reduced to 2.25 litres/sec. Significant amounts of precipitation were recorded during this time. Recovery of the hydraulic heads within the rock mass continued until January 18, 1991. During pumping and recovery, drawdowns and recoveries were monitored in about 100 packed-off borehole sections, with multiple sections in some boreholes. Groundwater flows through 10 borehole sections were determined by dilution tests before and during LPT2 to help identify important conductive zones. Tracers were injected in 6 borehole sections which penetrate highly conductive fracture zones, and the tracer arrivals in the pumped borehole were recorded.

Rhén et al. (1992) presents a preliminary analysis of the LPT2 data to determine the hydraulic parameters. They reported hydraulic conductivities and storativities as similar to those of the single borehole tests discussed in Wikberg et al. (1991). However, this preliminary analysis in Rhén et al. (1992) has been criticised because the analysis method assumed infinite-acting 2-d radial flow models which are not thought to be applicable to this site (Uchida et al., 1994).

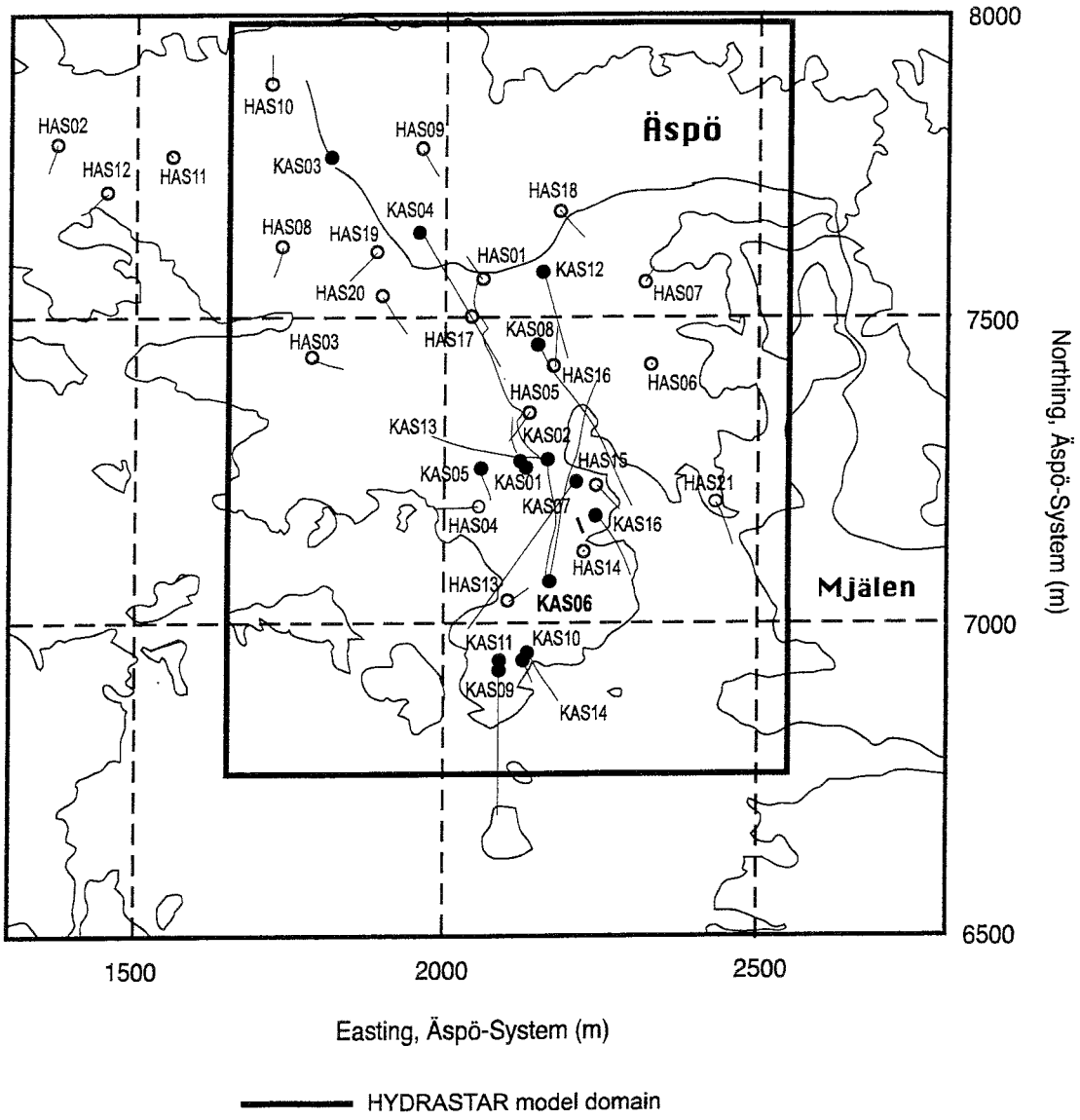

Figure 2-4. *Location of the boreholes and the Hard Rock Laboratory. Borehole KAS06 was pumped during LPT2.*

One use of the LPT2 data has been to provide data for the development and testing of models by the international Äspö Task Force on Modelling of Groundwater Flow and Transport of Solutes (ATFM). Gustafson and Ström (1995) provides an overview of the LPT2 experiments and the modelling studies by members of the Task Force. Eleven (11) of the Task Force members have applied groundwater flow and transport models to the site, with varying degrees of success. To date, no team is known to have applied a stochastic groundwater model which automatically conditions its results on both the observed hydraulic conductivities and the observed head data.

3. HYDRASTAR APPLICATION

3.1. APPROACH

A HYDRASTAR model was constructed to correspond to the Äspö conceptual model of Wikberg et al. (1991), updated with information obtained during construction of the HRL (Rhén, 1995). This updated model includes conductive features not used by members of the Äspö Task Force on Modelling and Groundwater Flow and Transport of Solutes (ATFM) (Gustafson and Ström, 1995). Specifically, an additional fracture zone (NNW-7) was discovered during construction and is included in this model of the HRL. This fracture zone intersects the HRL elevator shaft and may have a significant influence on the drawdowns in that area. Subsequent sections of this report discuss the results of this and the ATFM modelling studies, including the consequences of this additional structure.

Each simulation consists of a Monte Carlo set of realisations, i.e. a single set of boundary conditions and model inputs run repeatedly with different realisations of the conditionally-simulated hydraulic conductivity field. The results of each simulation are presented as of plots of drawdown versus time in sections of the observation boreholes. The multiple realisations are summarised by the mean and standard deviation of the drawdowns at each time step. Note that the drawdowns are not normally-distributed (Gaussian) random variables. As such, the region bounded by the standard deviation should not be interpreted as a confidence interval for the mean simulated drawdown. The standard deviations are presented only as a relative measure of uncertainty, and nothing more. The observed drawdowns are included on each plot for comparison.

Note that the packed-off sections of the boreholes are numbered from the bottom of the hole to the top (i.e., KAS05-5 is the uppermost section in KAS05, and KAS05-1 is the lowest section). In addition, wells designated HAS are shallow percussion-drilled boreholes with only one observation section.

The computer used in these experiments was SKB's Convex C 220. With the typical system demand during the period of this study, each transient uncalibrated realisation required approximately one hour of clock time. Each transient calibrated realisation required approximately 12 to 24 hours of clock time. This greatly restricted the number of realisations which could be computed for any one simulation. An examination of the ensemble statistics revealed that approximately 20 realisations were adequate for stable estimates of the standard deviation of each simulation. A more comprehensive study of the number of realisations would be warranted for use of this method in Performance Assessment modelling.

Several preliminary simulations were run to assess the appropriateness of the boundary conditions and to evaluate the sensitivity of model results to

specific storativity. These preliminary simulations were followed by two final simulations representing the SR-95 model of the HRL. The first simulation was conditioned only on the observed hydraulic conductivities (i.e., not calibrated to observed drawdowns). The second simulation included conditioning on the observed drawdowns via the recently implemented pilot point calibration algorithm.

3.2. FINITE DIFFERENCE REPRESENTATION

The overall modelling approach was to create a smaller-scale submodel based on the regional steady-state NAMMU model of Birgersson et al. (1995). Figure 3-1 shows the relationship between the areas covered by the two models.

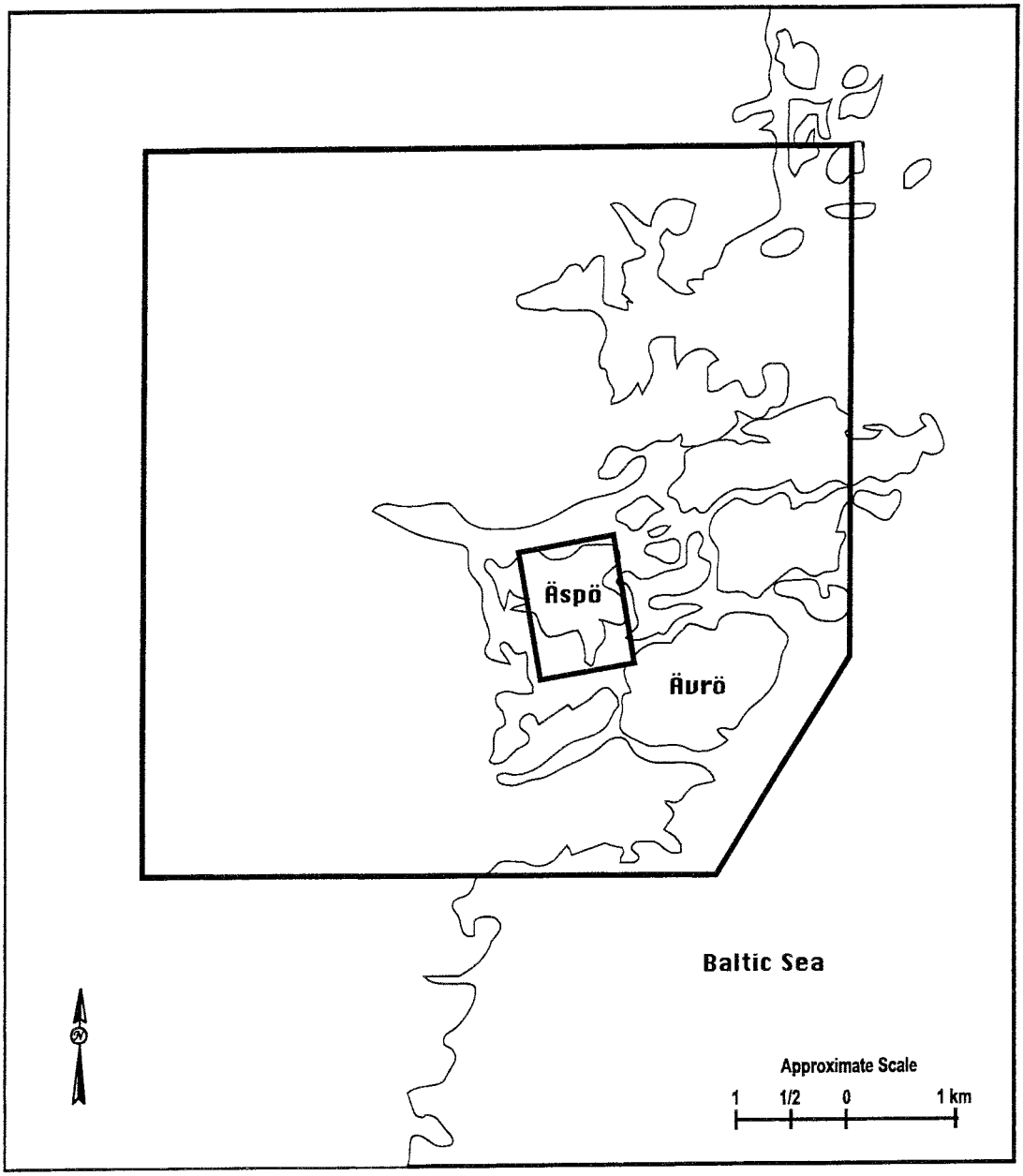

Figure 3-1. Relationship between the Regional NAMMU and Local HYDRASTAR model grids.

The node-centred finite difference grid for this HYDRASTAR model consisted of a 30m regularly spaced grid of 31 x 41 x 31 nodes. The grid covered a width of 900m (east-west), length 1200m (north-south) to a depth of 900m below ground surface (Figure 3-2). This domain was considered to be small relative to the expected radius of influence of the LPT2, but represents a compromise between the need for detail and the computational demands of a larger grid. Grid boundaries were chosen with respect to the regional flow field simulations of Birgersson, et al. (1995). Consequences of this choice are discussed in Section 3.5.3.

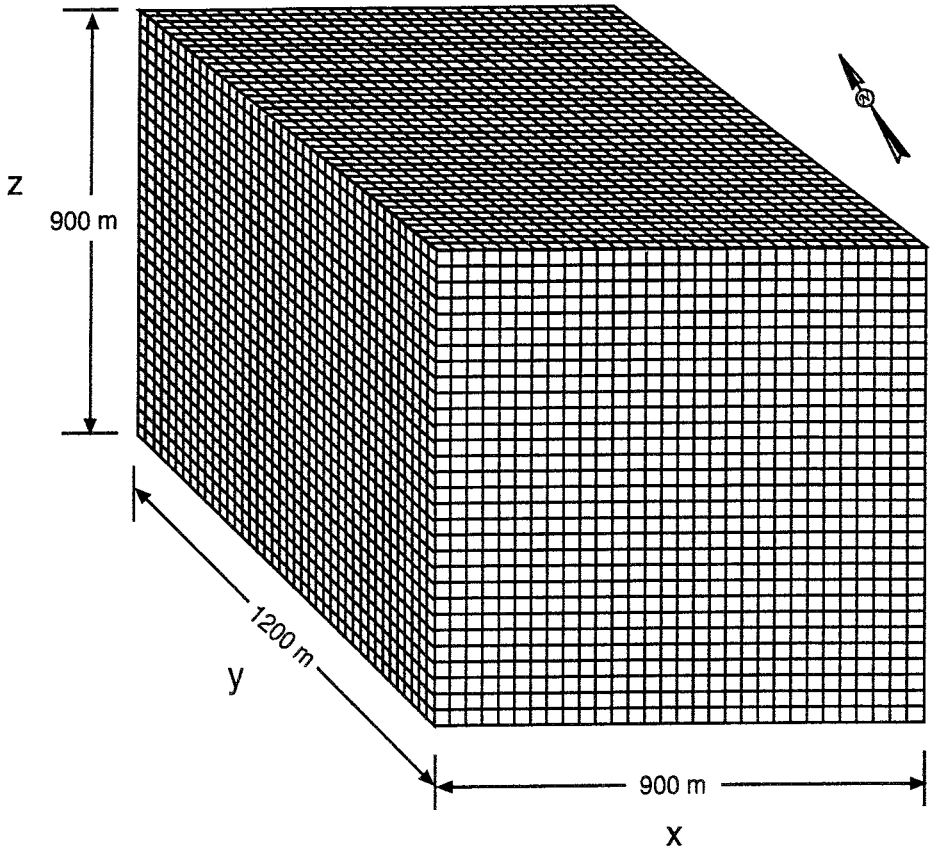

Figure 3-2. *HYDRASTAR finite difference grid for the Äspö LPT2 model.*

Figure 3-3 shows the fracture zones which have been mapped at the HRL based on the available pre-investigation and construction phase data. These fractures were incorporated into the HYDRASTAR model as regions bounded by parallel planes with a trend function of mean $\log_{10}$ hydraulic conductivity, constant with depth. The location, trend function and mean $\log_{10}$ hydraulic conductivity values were interpreted from the structural model of Rhén (1995). The fracture zones are identical to those used in the intermediate-scale HYDRASTAR model of Birgersson et al. (1995). Again, note that this set of fracture zones is different than that used in the ATFM modelling studies (Gustafson and Ström, 1995).

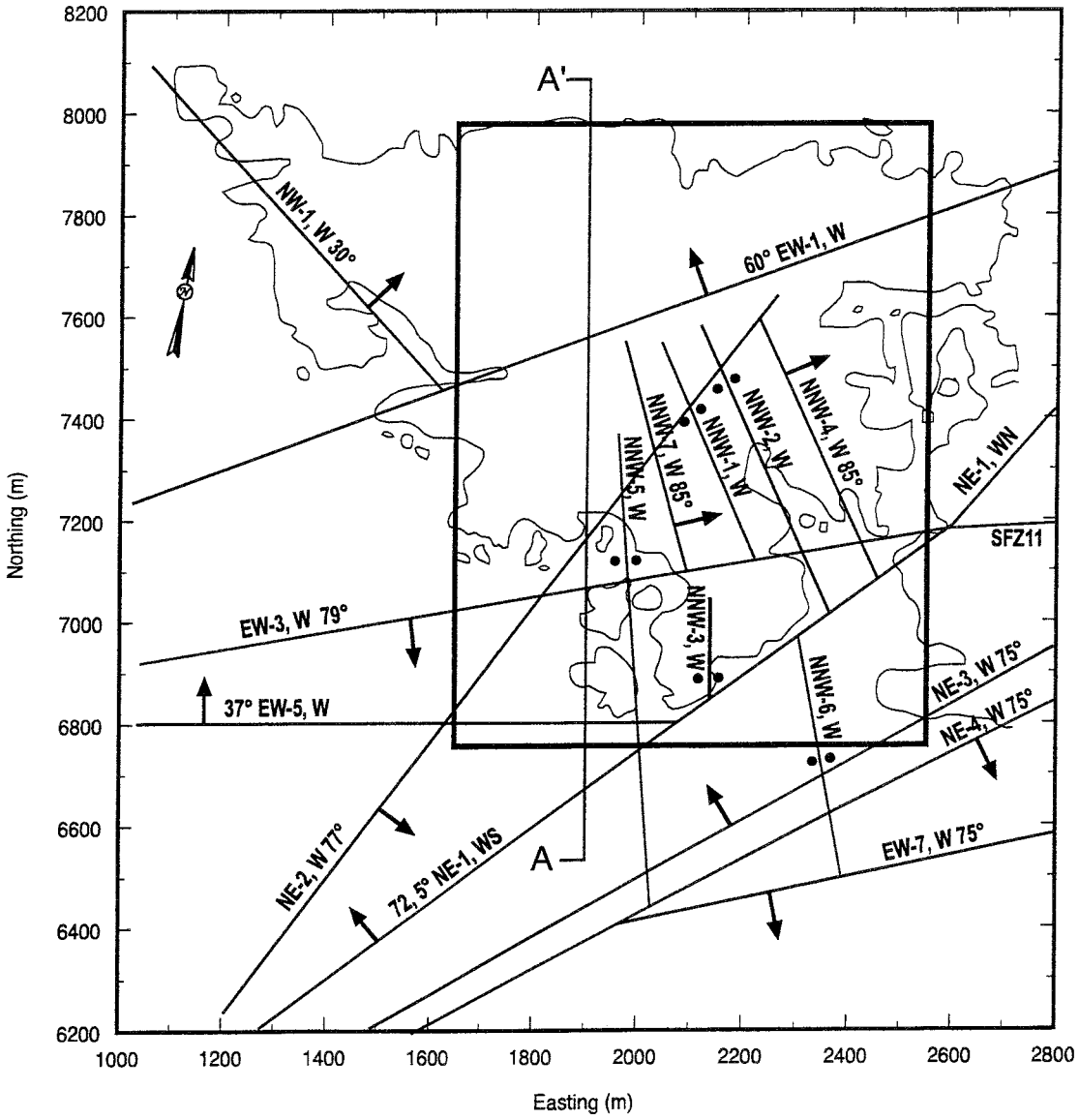

Figure 3-3. *Construction phase fracture zones and HYDRASTAR model location. Cross section A-A' is shown in Figures 3-6, 3-16, 3-17 and 5-8*

A recently implemented feature of HYDRASTAR allows the inclusion of a high conductance term to represent an open borehole (SKB, 1996). This allows an open borehole which spans more than one finite difference block to have approximately the same simulated heads for its entire length. The overall effect is to average the heads along the borehole, just as the real system does. This feature was used to simulate the 602m-length pumped interval of KAS06 and similar open sections of the observation boreholes.

3.3. GEOSTATISTICAL MODELLING OF HYDRAULIC CONDUCTIVITY

The finite difference approximation represents the true hydraulic properties of the rock mass with effective finite difference block properties that honour the physics of flow and the statistical characteristics of the rock mass. These

block-scale effective properties must also rationalise the measurement scale (e.g. packer interval for borehole tests of hydraulic conductivity) and the spatial correlation scale of the properties (e.g. the range of the variogram, the scale of the support, etc.). These problems are referred to as upscaling (Rubin and Gómez-Hernández, 1990; Indelman and Dagan, 1993) or regularisation (Norman, 1992b).

For the governing equation for flow, the hydraulic property of interest is hydraulic conductivity. The HYDRASTAR approach to regularisation uses an extension of Moye's formula (Norman, 1992b) to upscale the small-scale packer tests for hydraulic conductivity to the finite difference block scale. The geostatistical algorithm in HYDRASTAR conditionally simulates the hydraulic conductivity for each face of the finite difference blocks using the regularised measurements, the trend functions, and the model variogram (Norman, 1992a and 1992b). The simulated variability of the conditionally-simulated fields (i.e., the noise level) assumes that the logarithms of the residuals are a multivariate, normally-distributed (Gaussian) random process.

The model variogram for this regularisation scale and set of trends was determined by the application of the geostatistical analysis code INFERENS (Geier, 1993a and 1993b). INFERENS is a complementary code to HYDRASTAR which assists in the inference of geostatistical models for hydraulic conductivities measured at the packer scale. INFERENS upscales the packer-scale measurements of hydraulic conductivity up to the finite difference block scale. It subtracts the estimated trends from the block-scale measurements to get the residual spatially correlated random process. INFERENS uses iterative, generalised least-squares estimation (IGLSE) to fit a model variogram to the experimental variogram of the residuals. The fitted candidate model variograms and trend functions are evaluated via cross-validation, where each measured hydraulic conductivity is estimated using the candidate variogram model, the trend functions, and the remaining measurements. The cross-validation error of measured versus estimated hydraulic conductivity is computed for all the measurements and is used to compare alternative models for the observed data (Geier, 1993b).

Hydraulic conductivity data for the fracture zones and the overall rock mass were taken from the extensive Äspö data base, accessed through the SICADA database management system. The data included 457 single-hole packer tests, analysed by the Jacob method on the 3m scale from 7 boreholes (KAS02, KAS03, KAS04 KAS05, KAS06, KAS07, and KAS08) Figure 3-4 presents a histogram of these $\log_{10}$ transformed measurements. The HYDRASTAR regularization algorithm (a corrected arithmetic mean of the hydraulic conductivity) replaces the 3m measurements with an upscaled set of approximately 110 measurements on the 24m scale.

Although various authors have debated the validity of a decreasing trend with depth for hydraulic conductivities, LaPointe (1994) found that such trends were nonsignificant. Trend functions were prescribed to represent the pre-investigation and construction phase fracture zones corresponding to the zones presented in Birgersson et al. (1995). These fracture zone trends were

simple step increases relative to the rock mass hydraulic conductivities, and were constant with depth. Section 3.5.5 examines the use of ordinary kriging neighbourhoods to imply trends with depth.

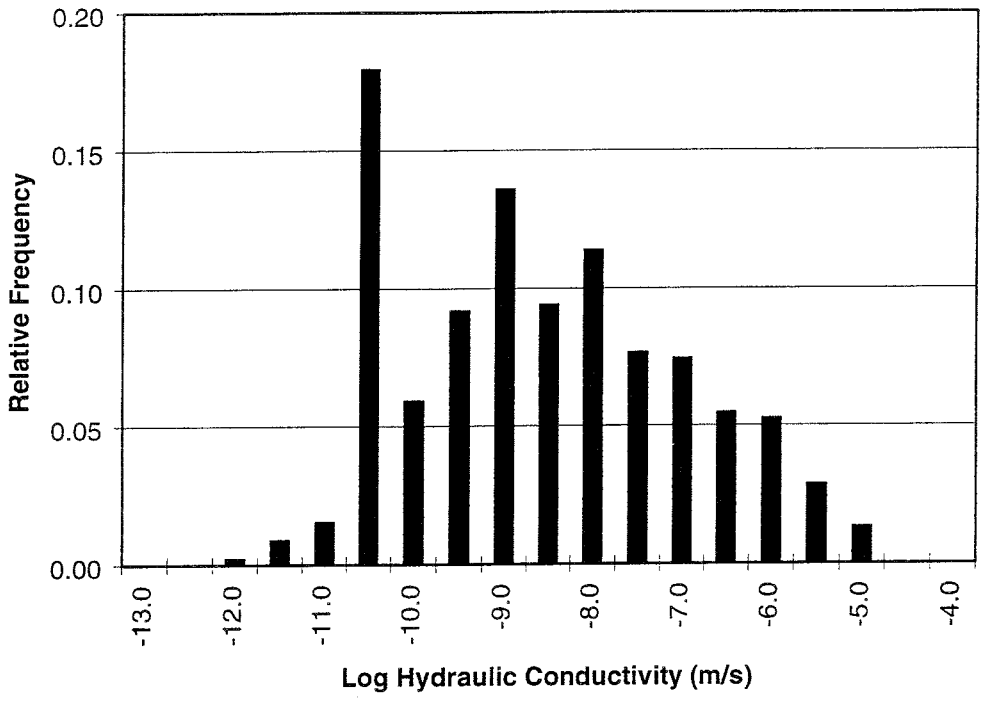

Figure 3-4. *Histogram of 3m scale packer-test measurements of hydraulic conductivity.*

INFERENS incorporated the trend functions with the upscaled hydraulic conductivity measurements to infer a geostatistical model of the HRL. The IGLSE-fitted variogram model for the residuals of this data had a nested structure with a large nugget variance. Unfortunately, HYDRASTAR 1.5 can not use nested variogram models, forcing a compromise specification of a spherical model with a range of 80m, zero nugget, and a sill (variance) of 2.3. Although this variogram model is not ideal for this data set, it is thought to be adequate for testing the inverse modelling capabilities of HYDRASTAR. Figure 3-5 shows the model variogram for the regularised residuals and Figure 3-6 presents a vertical cross-section running north-south through the model domain for one realisation of the simulated $\log_{10}$ hydraulic conductivities.

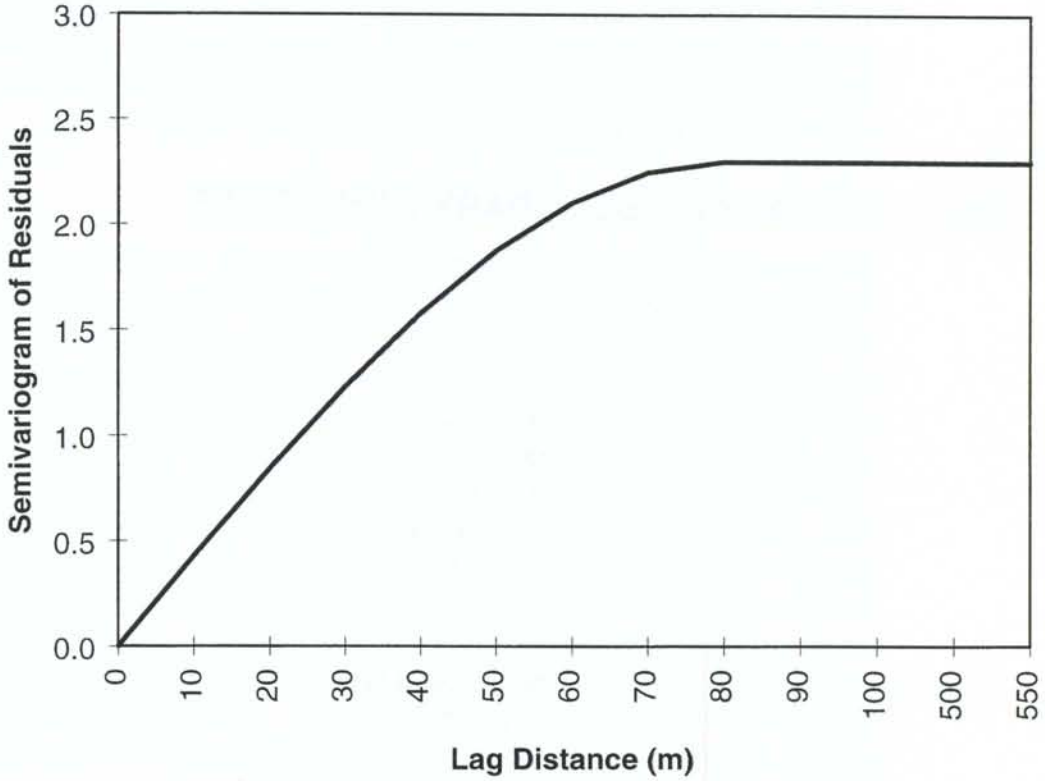

Figure 3-5. *Model variogram for upscaled residual hydraulic conductivity*

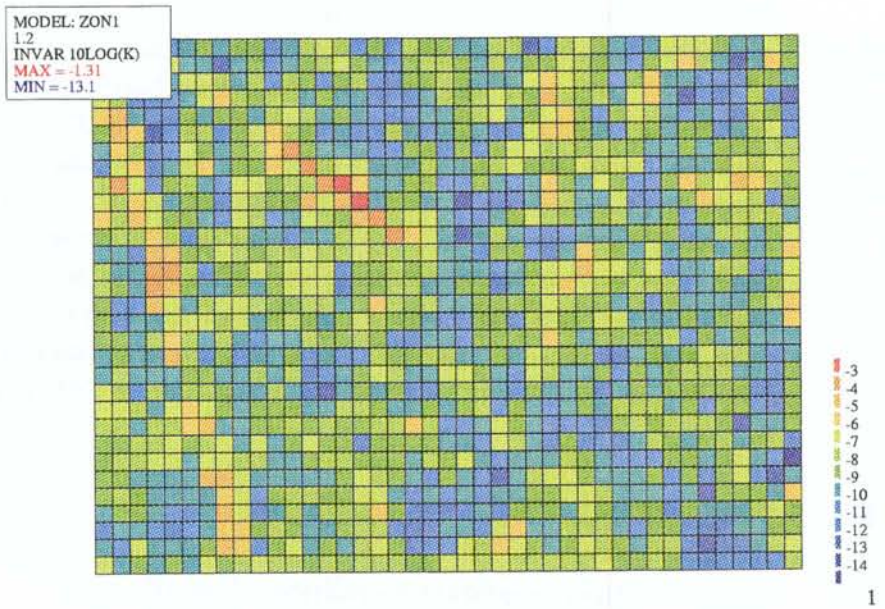

Figure 3-6. *Vertical cross section A-A' through one realisation of conditionally-simulated log hydraulic conductivities (m/s).*

Note that this study assumes that this statistical model of the hydraulic conductivities (i.e., the trends, error distribution, and variogram) is the true model without uncertainty. In reality, the model is inferred from the data and the geological models of the site, and may have great uncertainty. The effects of this uncertainty are not evaluated in this study.

3.4. INITIAL AND BOUNDARY CONDITIONS

These simulations assume steady-state initial conditions and time-independent boundary conditions. This allows the model to take advantage of the principle of superposition for linear, homogeneous differential equations (Freeze and Cherry, 1979). This approach makes knowing the exact boundary values (heads, recharge rates) unnecessary, and the model may calculate only the transient effects of pumping. It is convenient to set an initial head of zero, set zero head for all Dirichlet boundaries, and zero flow (Noflow) for all Neumann boundaries. Under these conditions, the model will calculate the transient effects as the drawdown or change from initial conditions. Similarly, the calibration can be performed in comparison to the observed drawdowns. If it is of interest, the calculated drawdowns can then be added to (superimposed on) the initial heads to view the final results in terms of observed hydraulic head. This superposition approach allows the model to avoid unnecessary computation of the initial head distribution for each transient simulation.

The boundary conditions for the model were assumed to be Dirichlet (constant head) on the sides and bottom. The upper boundary is more problematic, and has been the source of considerable debate amongst modelling groups. Several studies revealed that although a significant amount of precipitation falls on the island surface, a precipitation recharge of only 3 to 5.5mm per year on the upper boundary could be used to successfully model the site (Gustafson and Ström, 1995). Some groups used Dirichlet boundaries to represent the Baltic Sea and coastal marshlands, but found that the recharge from such boundaries was excessive (Barthélémy et al., 1994; Birgersson et al., 1995). These groups chose to limit the inflow from these boundaries by reducing the permeability at the upper boundary, reasoning that fine sediments on the bed of the Baltic Sea were inhibiting infiltration in the real system. The upper boundary condition is evaluated with several preliminary simulations which are described in the following section.

3.5. PRELIMINARY SIMULATIONS

3.5.1. Dirichlet Upper Boundary Condition - Uncalibrated

The regional NAMMU model of Birgersson et al. (1995) was a steady-state model and therefore was able to use Dirichlet (prescribed head) boundary conditions on the upper surface of the model to represent recharge from precipitation and from the Baltic Sea. This study simulates the transient response of the rock mass to pumping, which might be poorly represented by such a boundary condition. This study evaluated the upper boundary

specification using a preliminary model with Dirichlet boundaries on all six sides.

Appendix A presents 30 uncalibrated realisations of the HYDRASTAR model using a Dirichlet upper boundary. This simulation generally underpredicts the observed drawdowns in borehole sections near the upper boundary. For example, drawdowns in KAS08-4 are underpredicted, as are most of the shallow percussion boreholes such as HAS05 (Figures 3-7 and 3-8). This demonstrates that when the influence of the pumping reaches the upper surface of the model, the Dirichlet boundary forces the model to maintain the heads on the upper surface by increasing the flux of water entering this boundary during pumping. As a result, the model computes very little drawdown near the upper surface. The excessive recharge calculated for the model's upper boundary also affects the interior of the model, resulting in underestimated drawdowns in many observation sections (e.g. KAS08-2, Figure 3-9). Notable exceptions are the responses of near-surface sections KAS04-6 and HAS13-1, which are well-modelled by a Dirichlet boundary (Figures 3-10 and 3-11).

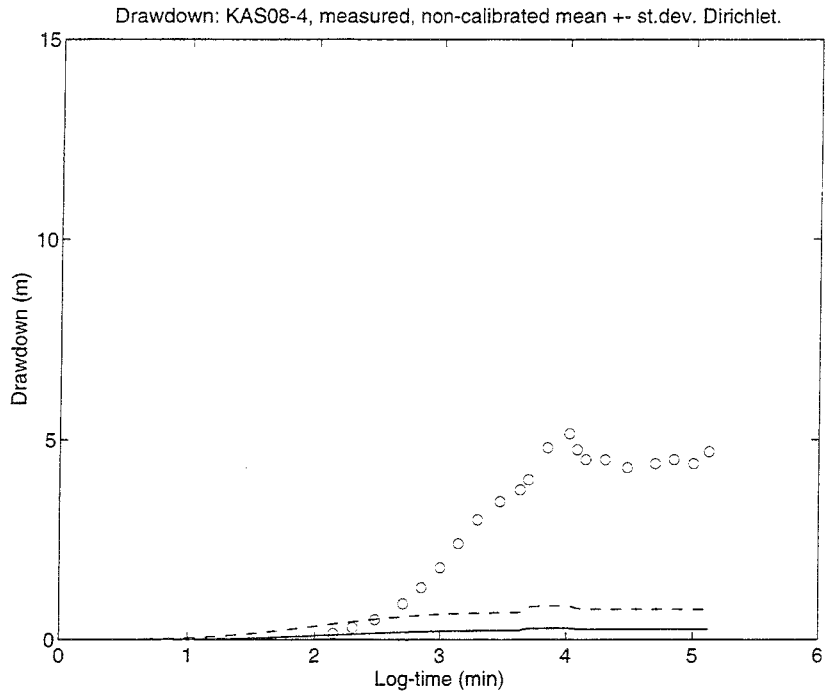

Figure 3-7. *Preliminary simulation of drawdowns versus time for KAS08-4: Uncalibrated, Dirichlet upper boundary.*

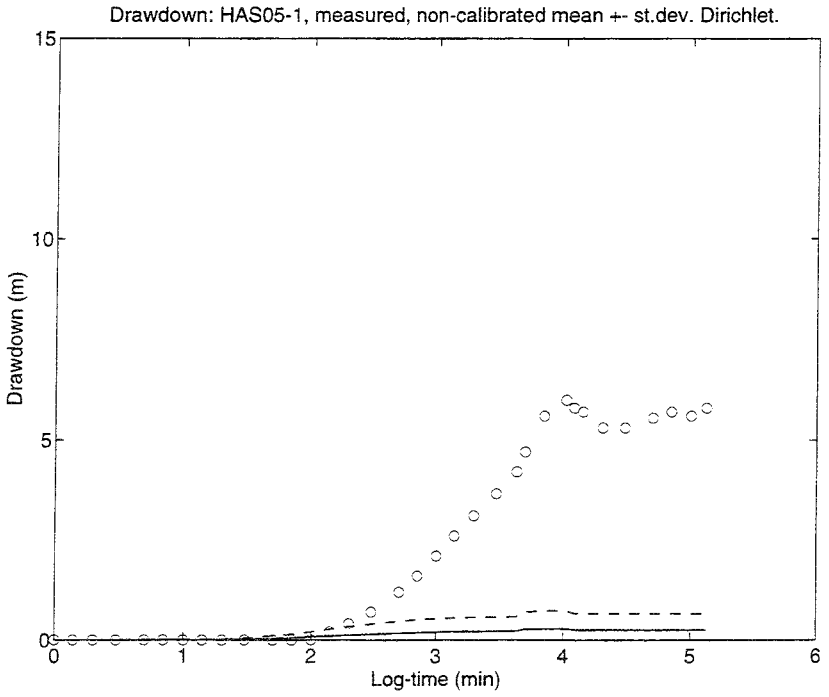

Figure 3-8. *Preliminary simulation of drawdowns versus time for HAS05-1: Uncalibrated, Dirichlet upper boundary.*

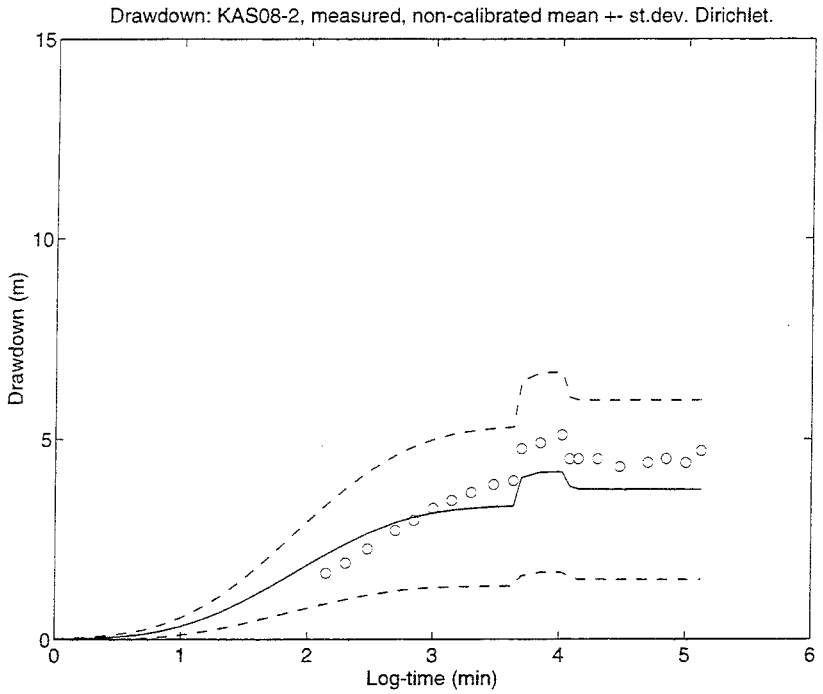

Figure 3-9. *Preliminary simulation of drawdowns versus time for KAS08-2: Uncalibrated, Dirichlet upper boundary.*

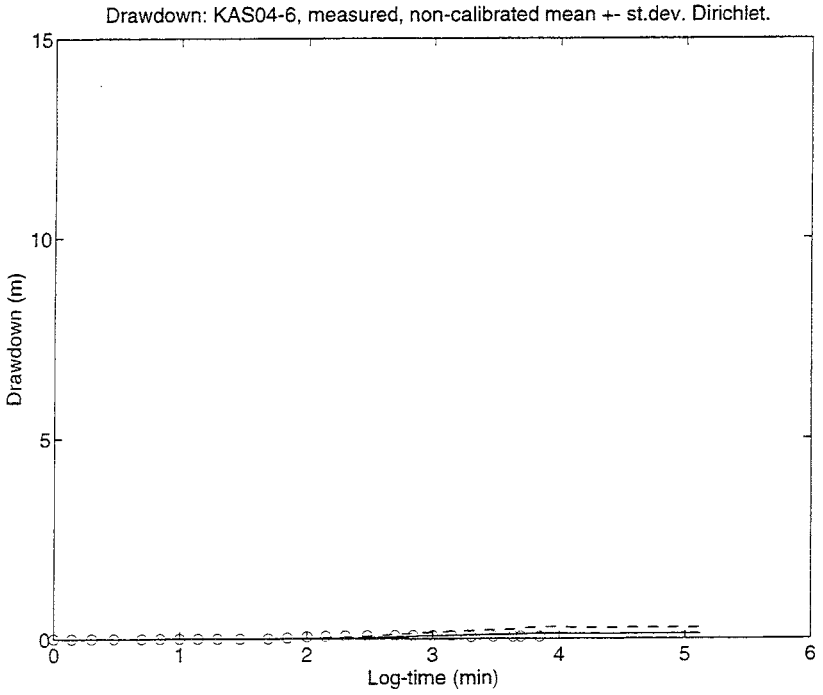

Figure 3-10. *Preliminary simulation of drawdowns versus time for KAS04-6: Uncalibrated, Dirichlet upper boundary.*

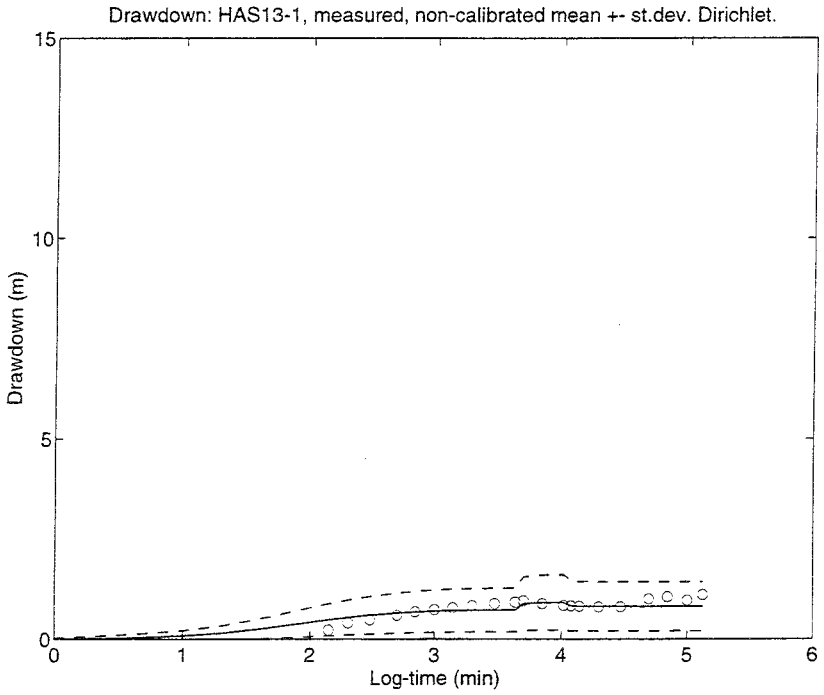

Figure 3-11. *Preliminary simulation of drawdowns versus time for HAS13-1: Uncalibrated, Dirichlet upper boundary.*

3.5.2. Dirichlet Upper Boundary Condition - Calibrated

A second set of realisations was run to examine the effect of calibrating the model with the Dirichlet boundary condition on the upper surface. The pilot point method of calibration was used as described in Sections 1.2 and 5.0, with 32 pilot points (Figure 5-1). The results of 11 realisations for this simulation are also presented in Appendix A. Although only 11 realisations were run, some qualitative conclusions can be drawn. Calibration only slightly improved the fit between the simulated and the observed drawdowns near the boundaries (i.e., KAS08-4, shown in Figure 3-12), while sections in the model's interior do show considerable improvement (i.e., KAS08-2, shown in Figure 3-13). This can partly be attributed to the position of the pilot points; the pilot points are positioned in the model's interior and have little influence beyond the range of the variogram (80m, in this model). If the calibration had been carried out with pilot points near the boundaries, the hydraulic conductivities should have been decreased in order to reduce the boundary fluxes. That is, the effect of calibration would result in Dirichlet boundaries overlying low permeability zones, similar to those used by Barthélémy et al. (1994) and Birgersson et al. (1995). The pilot points also have an additional larger-scale effect of changing the mean of the hydraulic conductivities within a kriging neighbourhood. Consequences of this larger-scale effect are discussed in Section 3.5.5

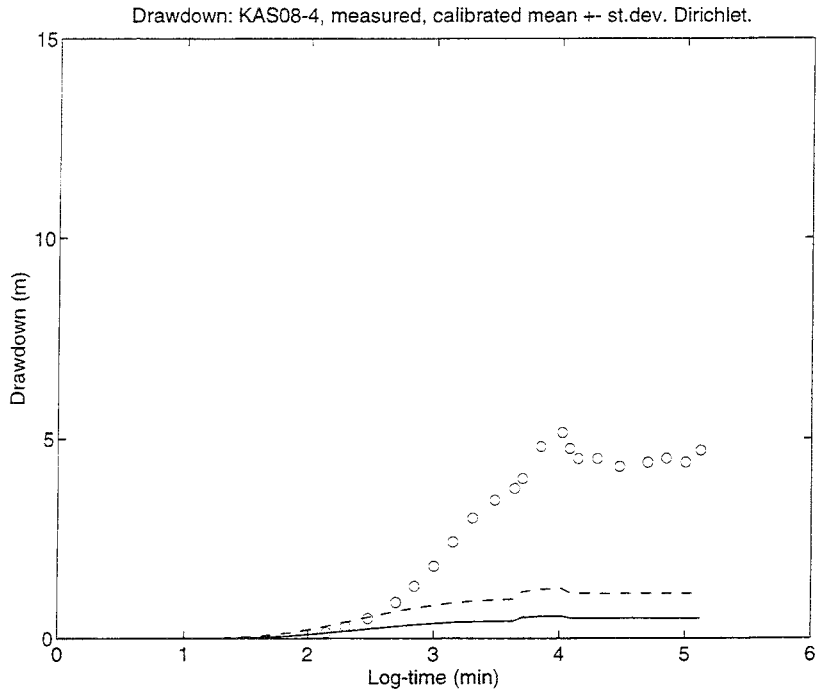

Figure 3-12. *Preliminary simulation of drawdowns versus time for KAS08-4: Calibrated, Dirichlet upper boundary.*

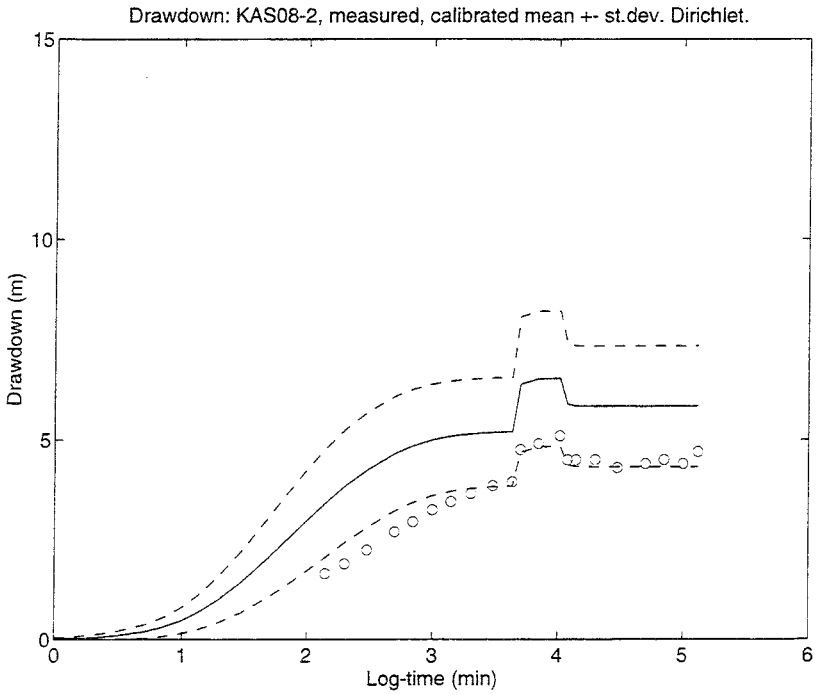

Figure 3-13. *Preliminary simulation of drawdowns versus time for KAS08-2: Calibrated, Dirichlet upper boundary.*

This preliminary analysis suggests that a combination of boundary conditions should be used for the upper model boundary. For example, a seasonally-varying 3-5mm/year recharge rate could be used for the region representing Äspö island, constant head boundaries with low hydraulic conductivity to represent the Baltic sea, etc. This would be best represented as a combination of time-dependent, spatially-varying Neumann, Dirichlet and Mixed-type boundaries for the upper model surface. Unfortunately, the current version of HYDRASTAR (version 1.5) does not support such a complex boundary specification. A compromise is a time independent Neumann boundary for the upper model surface. Using the superposition approach, this would be a Noflow boundary condition for the model's upper surface. Subsequent model simulations used this Noflow boundary condition, noting that seasonal variations in recharge and the effects of the Baltic Sea will not be well-represented.

3.5.3. Adequacy of the Model Grid

For similar reasons, the model underpredicts drawdowns in borehole sections near the bottom (KAS02-2) and side Dirichlet boundaries (all sections of KAS03). Most of the sections in the inner part of the model show reasonable agreement between simulation and measurements. This suggests that either the boundaries might be too close to the area of interest or that an alternative boundary condition should be considered on the sides and bottom. One such alternative boundary condition would be a Carter-Tracy boundary (a so-called Mixed-type boundary condition), which allows both the hydraulic head and flux to be calculated along the model boundary (Kipp, 1986). Computational demands prohibit the use of a larger grid, and the current version of HYDRASTAR (1.5) allows only Dirichlet and Neumann boundary conditions to be specified.

It was anticipated that the model would not reproduce the conditions near the pumping borehole because of the coarseness of the finite difference grid. For example, simulated drawdowns in the pumping borehole, KAS06, are on the order of 6 to 12m, much less than the observed values of approximately 50m at end of pumping. Also it should be noted that the response in KAS06 is not included in the calibration (i.e., the errors of simulated versus observed drawdowns are not included in the objective function). Consequently, the model underestimates both the drawdowns in KAS06 and the drawdowns in nearby observation borehole sections. While this can be addressed with a denser finite difference grid in the region of the pumping well, a dense grid is computationally prohibitive at the present time. Other algorithmic solutions such as telescopic mesh refinement (Ward et al., 1987), or well indexing (Peaceman, 1978) have not been implemented in HYDRASTAR version 1.5.

3.5.4. Specific Storativity

Several previous modelling studies of LPT2 used a wide range of storage parameters, including both single and dual porosity assumptions. Some studies also used unconfined storage parameters for the uppermost level of

their models. The studies were inconclusive as to which model of storage was superior (Gustafson and Ström, 1995). As part of the preliminary analysis of the LPT2 test, Anderson (as summarised in Rhén et al., 1992) analysed the data to estimate the specific storativity. This analysis has since been criticised by Uchida, et al. (1994) as being inadequate, perhaps resulting in inaccurate estimates of specific storativity. Although this suggests that a reanalysis and/or additional hydraulic testing is in order, only a limited sensitivity analysis is performed in this study.

Sensitivity to changes in specific storativity was evaluated with an uncalibrated simulation of 30 realisations with a Noflow upper boundary condition and an increased fracture zone specific storativity of 10^{-6} 1/m (from 10^{-7} 1/m). Figure 3-14 shows the effects of this change on the near-surface section KAS05-5. Note that for this location, the early data is well-modelled by a fracture zone specific storativity of 10^{-6} 1/m. In contrast, the drawdowns in the model's interior are badly predicted with an increased fracture zone storativity (e.g., KAS02-3 as shown in Figure 3-15). This indicates that the model results are sensitive to this parameter, and implies that reanalysis of the existing test data and further transient testing at the HRL may be warranted. The moderate value of 10^{-7} 1/m was used for subsequent modelling since it appears to be most representative of the HRL as a whole. This value also lies in the middle of the range reported by Wikberg et al. (1991).

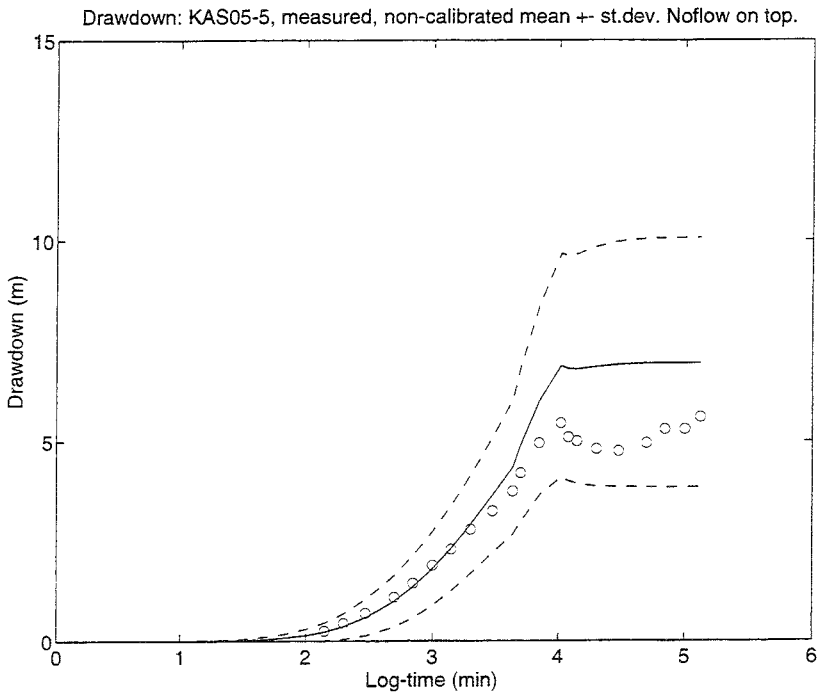

Figure 3-14. *Preliminary simulation of drawdowns versus time for KAS05-5: Uncalibrated, Noflow upper boundary with a fracture zone specific storativity of 10^{-6} 1/m.*

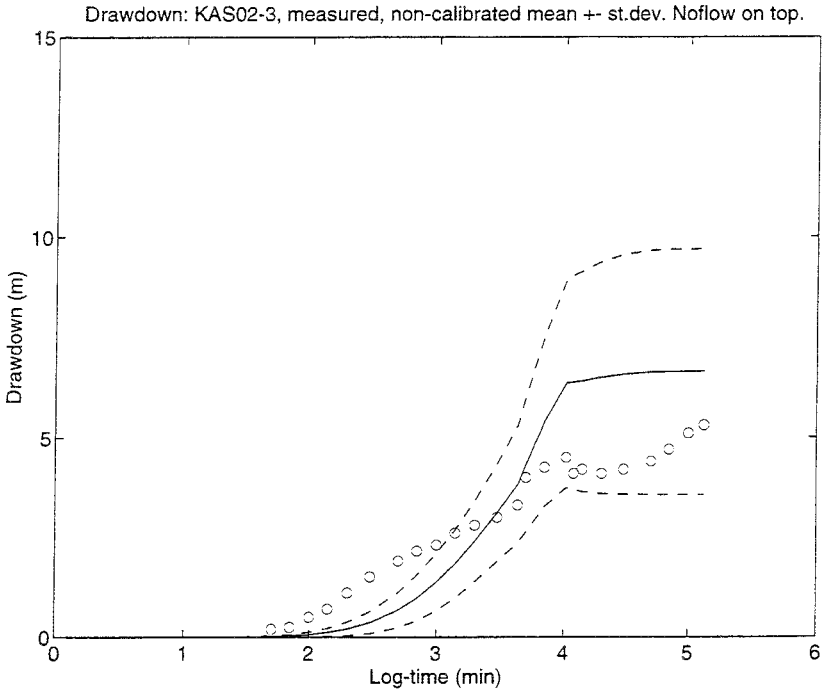

Figure 3-15. *Preliminary simulation of drawdowns versus time for KAS02-3: Uncalibrated, Noflow upper boundary with a fracture zone specific storativity of 10^{-6} 1/m.*

The preliminary simulations also indicate that calibration of hydraulic conductivity has little effect on the simulated responses during the early phase of the pumping. That is, the early system response is insensitive to changes in the conductivity field. Conversely, changing the specific storativity has little impact on the latter part of the simulation when near-steady-state conditions are reached. Thus, calibration of hydraulic conductivity for a transient problem is dominated by the late-time response of the system.

3.5.5. Hydraulic Conductivity, Kriging Neighbourhoods and Trends

As discussed in sections 1.2 and 3.3, HYDRASTAR can include hydraulic conductivity trends implicitly within the model through ordinary kriging. This is possible because each kriging neighbourhood gets a mean based on the measurements falling in that neighbourhood. If there is a trend in the observed data, it is therefore included in the kriged hydraulic conductivity field (and consequently into the conditional simulations and calibration). For example, a decreasing trend with depth can be included implicitly in the model using horizontal kriging neighbourhoods which would reflect the decreasing trend in the data with depth. One consequence of kriging neighbourhoods is that extreme values can have great influence on the conditionally simulated mean for a neighbourhood. Likewise, a single pilot point can also exploit the kriging neighbourhoods to change large areas of the model domain. This may or may not be a desirable effect.

A preliminary specification of kriging neighbourhoods was arbitrarily taken as 200m thick zones with an overlap of 85m, dipping to the SW. The complete set of realizations for both calibrated and uncalibrated cases with Dirichlet and Neumann upper boundary conditions are presented in Appendices A and B. However, after completing these runs it was noticed that the observed data at the bottom of the domain is relatively low (e.g. in KAS02). Consequently the bottom kriging neighbourhood containing this data has a relatively low mean, which appears as a region of low values at the bottom of the uncalibrated hydraulic conductivity field (Figure 3-16a; see also Figure 3-3 for the cross section location). Calibration with this specification of neighbourhood removes this region of low values (Figure 3-16b). This is illustrated more clearly by the plot of the difference of the calibrated minus uncalibrated fields (Figure 3-16c). The relatively large change in $\log_{10}$ hydraulic conductivity of 1.36 arises because there is little observed data in the lowest kriging neighbourhood, allowing the pilot points to control the neighbourhood mean. In order to match the observed heads, the calibration algorithm increases the pilot point conductivity and consequently the conductivity of the entire kriging neighbourhood.

This side left intentionally blank

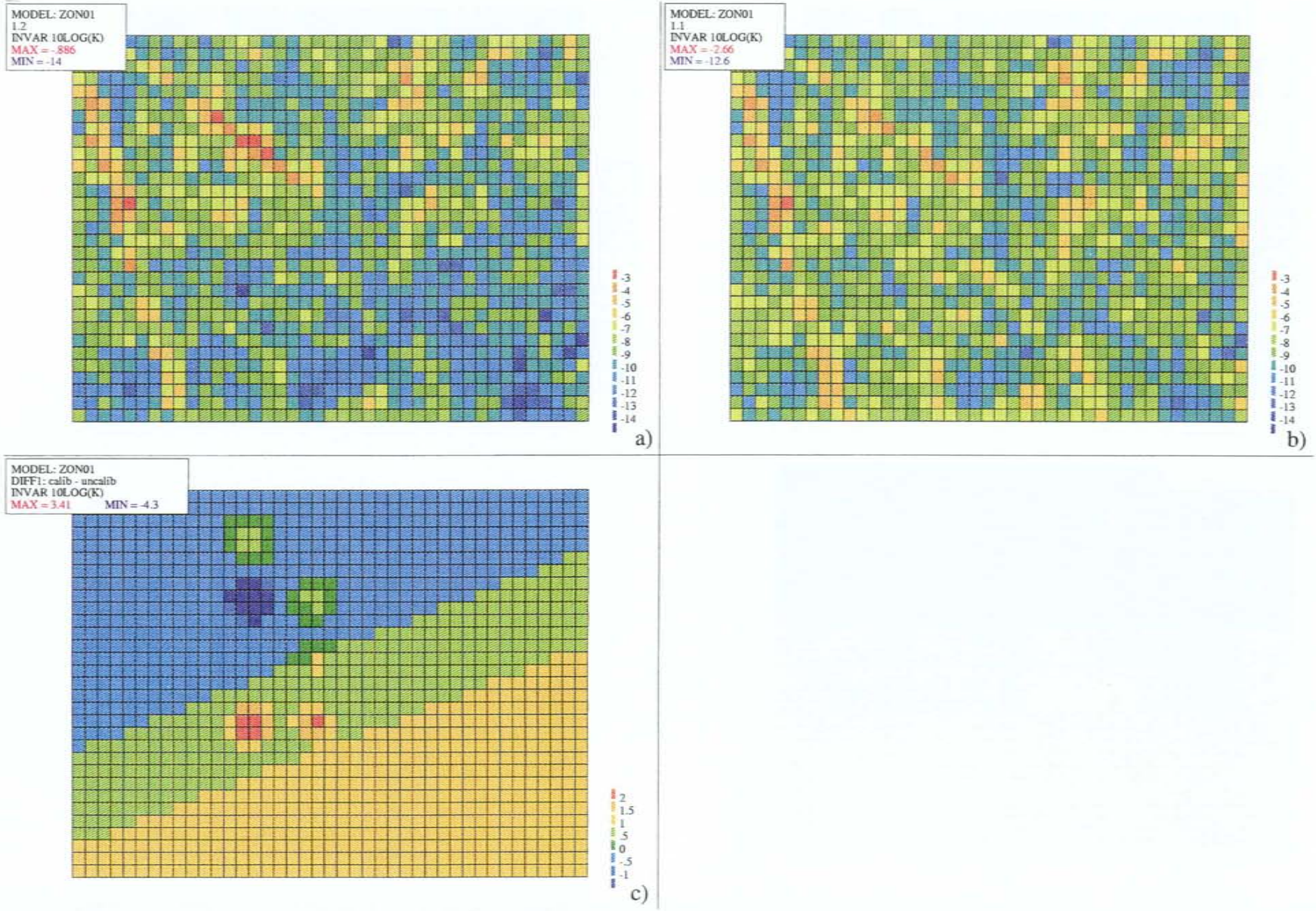

Figure 3-16. *Vertical cross section A-A' through one realisation of a log hydraulic conductivity field (m7s) with three dipping kriging neighbourhoods a) uncalibrated b) calibrated, and c) difference of b minus a.*

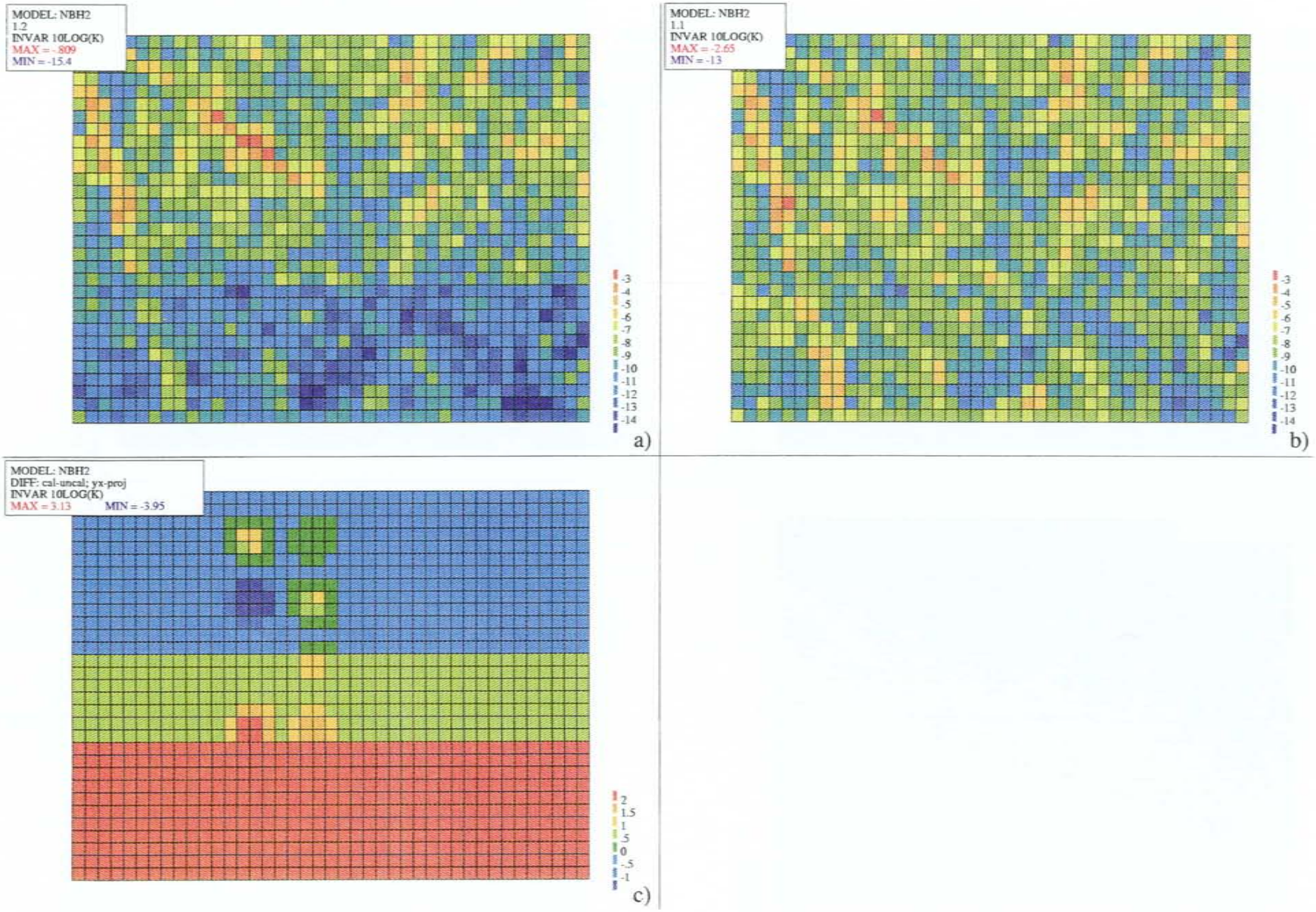

Figure 3-17. *Vertical cross section A-A' through one realisation of a log hydraulic conductivity field (m/s) with three horizontal kriging neighbourhoods, a) uncalibrated b) calibrated, and c) difference of b minus a.*

An alternative specification of kriging neighbourhoods would be horizontal neighbourhoods to reflect the decreasing trend in observations with depth. The rate of decrease is therefore modelled implicitly as the mean of the data within each kriging neighbourhood. This revised specification was used for several simulations to evaluate its consequences for simulation and calibration. Figure 3-17a shows a cross section through an uncalibrated realization of hydraulic conductivity, clearly showing a layer of low values corresponding to the bottom kriging neighbourhood. This again reflects the data observed at the bottom of the modelled domain, whose mean is lower than the remaining data. Subsequent calibration of this field removes this band, as shown in Figure 3-17b. The change in the lowest kriging neighbourhood is more clearly shown in Figure 3-17c, which shows the difference of the calibrated minus uncalibrated fields a change in $\log_{10}$ hydraulic conductivity of 2.37. This indicates that calibration has removed the implied decreasing trend in hydraulic conductivity with depth. This suggests that such a trend is not compatible with the chosen boundary conditions and the observed drawdowns.

A third possible specification of kriging neighbourhoods is to use a single kriging neighbourhood for the entire domain, implying no trend in hydraulic conductivity with depth. This is consistent with the above finding that a decreasing trend is incompatible with the observed drawdowns. A trend-free model is also consistent with LaPointe (1994). This specification of a single kriging neighbourhood and thus no trend was used for all subsequent simulations. The consequences of this specification are discussed in section 5.7 of this report.

4. UNCALIBRATED SIMULATION

This HYDRASTAR simulation models the LPT2 pumping test in Monte Carlo fashion for 30 uncalibrated realisations of the hydraulic conductivity field using the previously described model (i.e., finite difference grid, boundary conditions, and geostatistical model) of the HRL. The pilot point inverse method of calibrating the hydraulic conductivity fields is not used in these runs. The model results are therefore conditioned on the measured hydraulic conductivities but not conditioned on the drawdowns observed during LPT2. These uncalibrated runs serve as a base case for comparison against the calibrated runs discussed in the following section.

As previously discussed, one purpose of this modelling study is to evaluate the current conceptual model of the Äspö HRL via an application of HYDRASTAR to LPT2. The validity of the conceptual model is to be judged by the degree of accuracy with which HYDRASTAR is able to simulate the transient and steady-state borehole responses observed during LPT2. Gustafson and Ström (1995) present several performance criteria used by the international Äspö Task Force on Modelling of Groundwater Flow and Transport of Solutes (ATFM). These include, but are not limited to, comparisons of the simulated versus observed transient and steady-state drawdowns.

4.1. TRANSIENT RESPONSE AT SELECTED WELLS

There are three aspects of the transient response curves which should be evaluated when comparing the observed response versus the simulated responses (Uchida et al., 1994):

- The magnitude of the response at each point in time;
- The timing of the response; and
- The general shape (slope) of the response curve.

Additionally, the ensemble of simulated responses should bracket the observed response. That is, the mean of the realisations should reproduce the magnitude, timing, and shape of the observed response. The set of realisations also should bracket the observed response, for example as indicated by a plus-minus one-standard deviation interval drawn about the mean simulated response.

Appendix C presents the results of 30 realisations for this simulation. The mean simulated drawdowns generally reproduced the timing of the observed drawdowns, but overpredicted the magnitude of the observed drawdowns, such as in KAS05 and KAS08 (Figures 4-1, 4-2, 4-3 and 4-4). This indicates that the upper Noflow boundary may have been too restrictive, resulting in the overprediction of drawdowns. The observed responses generally fell within plus or minus one standard deviation of the simulated responses. This indicates that although any one realisation may not

reproduce the observed response, the ensemble of Monte Carlo simulations has bracketed the true characteristics of the HRL.

Notable exceptions to this are observation sections which are close to the side and bottom Dirichlet boundaries, such as KAS02-2 and KAS03. The simulated drawdowns for these sections have limited drawdowns because they are too close to the boundary. The relatively coarse finite difference grid is also inadequate to predict the large drawdowns near the pumped borehole. For example, the observed drawdowns in sections 2, 5 and 6 of KAS07 (e.g. Figure 4-5) are underpredicted, partly because this borehole is close to KAS06. This is in constrast to section KAS07-4 (Figure 4-6), where the drawdowns are overpredicted but at least within the range of Monte Carlo simulations.

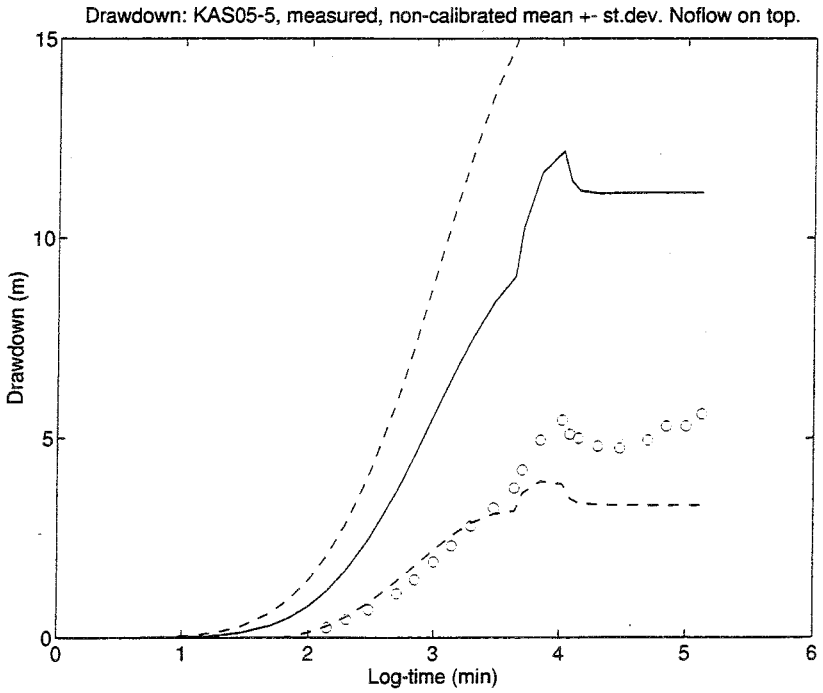

Figure 4-1. *Uncalibrated simulation of drawdowns versus time for KAS05-5: Noflow upper boundary.*

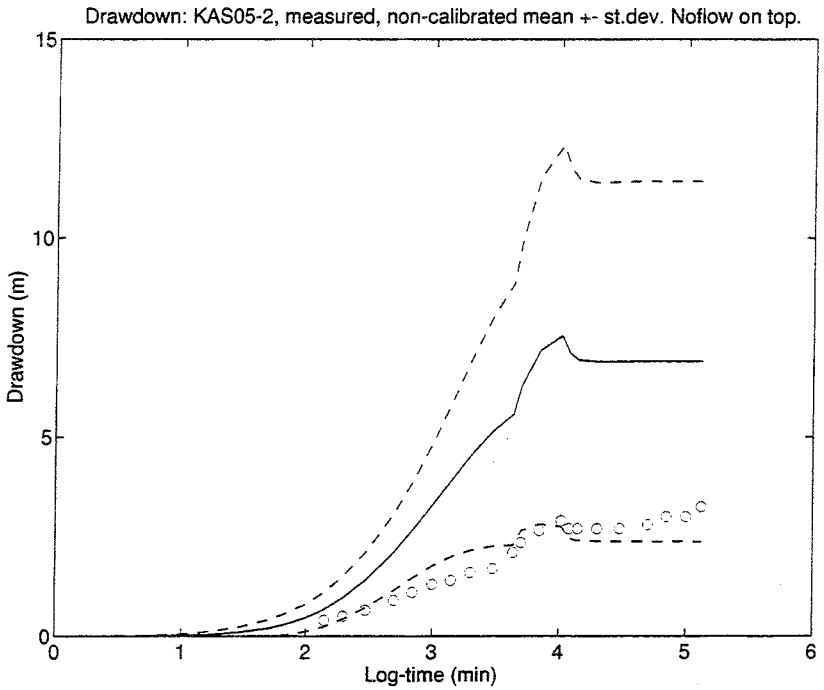

Figure 4-2. *Uncalibrated simulation of drawdowns versus time for KAS05-2: Noflow upper boundary.*

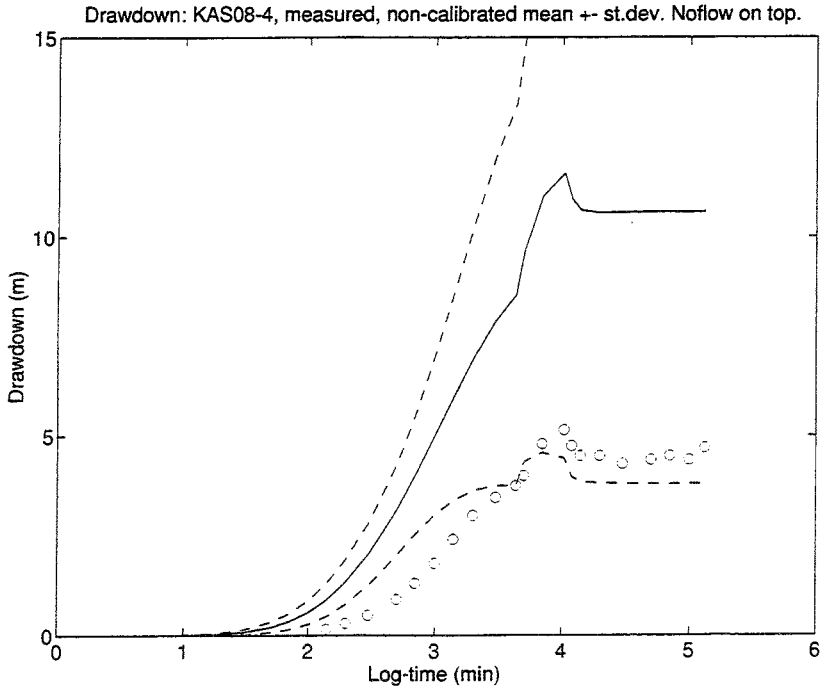

Figure 4-3. *Uncalibrated simulation of drawdowns versus time for KAS08-4: Noflow upper boundary.*

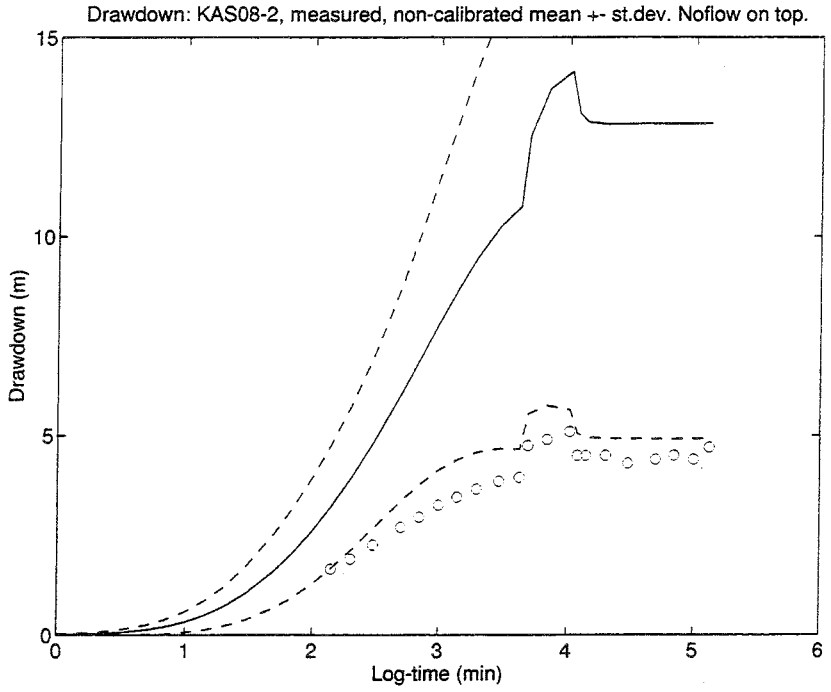

Figure 4-4. *Uncalibrated simulation of drawdowns versus time for KAS08-2: Noflow upper boundary.*

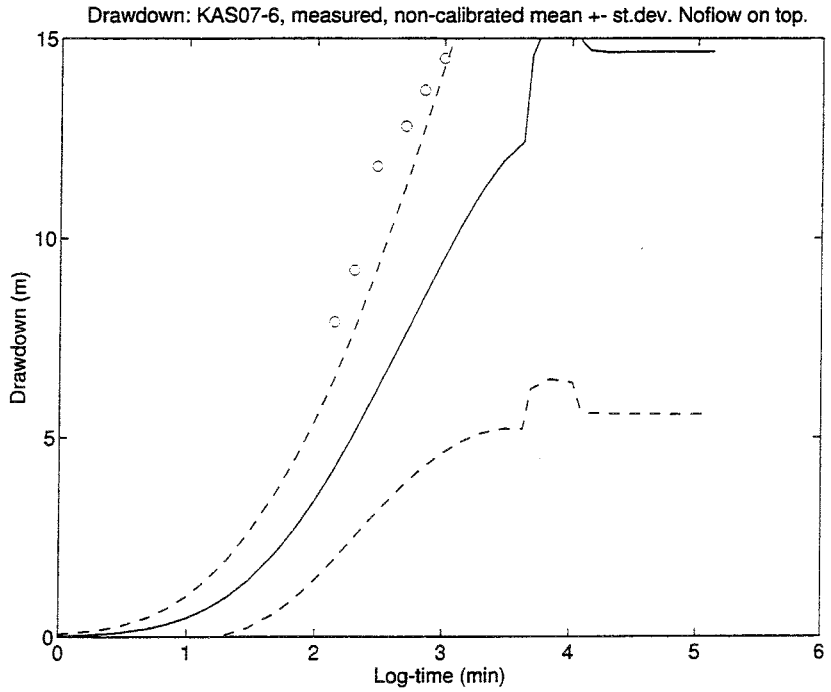

Figure 4-5. *Uncalibrated simulation of drawdowns versus time for KAS07-6: Noflow upper boundary.*

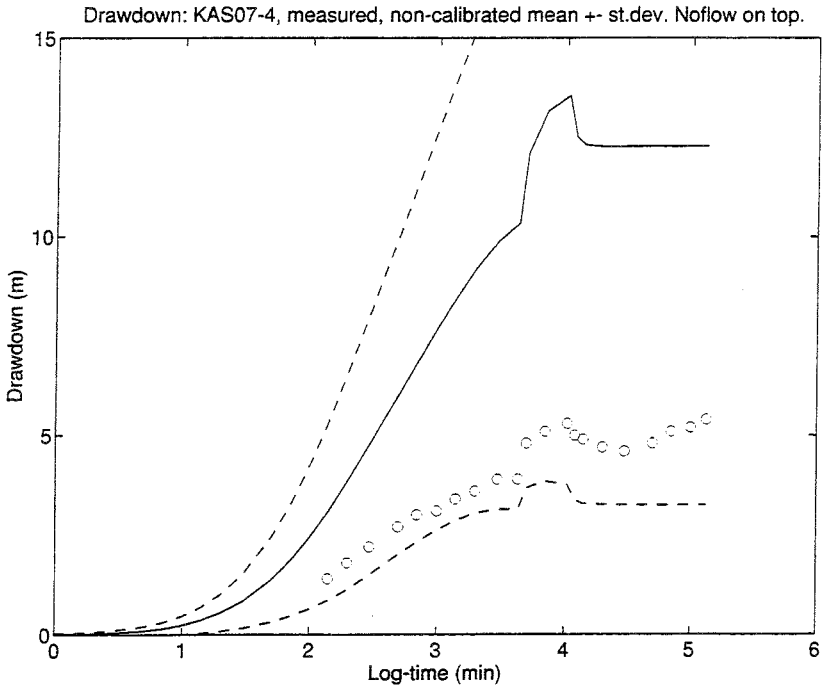

Figure 4-6. *Uncalibrated simulation of drawdowns versus time for KAS07-4: Noflow upper boundary.*

4.2. STEADY-STATE DRAWDOWNS

For the LPT2, steady-state has generally been assumed to exist when the drawdowns have stabilised at the end of the test. An examination of most boreholes shows that the observed drawdowns are approximately stable but show a steady upward trend that persists throughout the latter part of the test (e.g. Figures 4-1 and 4-2). This increase in the observed drawdowns could be due to a variety of causes, including the limited extent of the modelled domain, measurement errors, pumping rate increases, seasonal variations in recharge, etc. Because none of these stresses were included in this HYDRASTAR application, the simulated drawdowns do not reflect this observed trend. The true cause of this trend is unknown and it consequently could not be included in this model. It should be noted, however, that the inclusion of a time-variant model stress (e.g. increased pumping or decreased recharge) is a simple modification of the model and would result in a substantial reduction of the error in simulating the late-time observed drawdowns.

It is difficult to assess the overall accuracy of any one model, and harder still to assess and compare the accuracy of several very different modelling approaches. Gustafson and Ström (1995) chose to compare the various ATFM models using several performance measures (Appendix D) computed for simulation errors at steady-state. The steady-state head was to be the observed head at the end of LPT2 (t = 132595 min.). It should be noted that such a comparison would not necessarily be favourable to HYDRASTAR,

since it fits the late-time data as a whole, rather than at any one time step. As an alternative, one might choose to compute the same performance measures for t = 20000 minutes. Another performance measure could be the same as the optimisation criterion for the pilot point method in HYDRASTAR: the sum of squared errors for all locations. For the purpose of comparison to the previous ATFM studies, this study used performance measures similar to those used by Gustafson and Ström (1995), i.e., the error of observed minus the mean of realisations of simulated head for the last measurement at t = 132595 minutes. The same measures were also computed for t = 20000 minutes for comparison.

Table 4-1 presents the performance measures for this uncalibrated simulation. Note that at either early or late times, the uncalibrated HYDRASTAR simulation overpredicts the drawdowns, as indicated by the positive mean error (dh) and distance weighted mean errors (dh(lnr), dh(r)). These measures are quite different at the later time, and indicate that the model had a better fit at the later time. Table 4-1 also repeats the performance measures reported in Gustafson and Ström (1995) for the ATFM modelling studies. In comparison, the performance of the uncalibrated HYDRASTAR model was slightly below the average performance of the ATFM models.

Table 4-1. Summary of performance measures for HYDRASTAR and ATFM models of LPT2

			Performance Measures (1)						
Model			dh	dh(abs)	dh(lnr)	dh(r)	Dh	Dh(lnr)	Dh(r)
HYDRASTAR	Uncalibrated	early (2)	4.03	4.66	21.81	956.27	3.48	18.75	873.08
		late (3)	3.78	4.04	20.35	876.30	2.72	14.70	762.74
	Calibrated	early (2)	-0.35	1.30	-1.87	-77.71	2.78	15.00	628.46
		late (3)	-0.51	1.17	-2.73	-120.40	2.11	11.32	496.55
ANDRA/BRGM I	4		0.04	1.24	0.03	-52.90	2.08	11.34	534.22
ANDRA/BRGM II	4		-0.23	2.05	-1.77	-278.44	3.11	16.98	931.49
ANDRA/ITACA	4		0.54	1.48	2.89	143.95	2.61	14.46	748.20
CRIEPI	4		0.77	1.56	4.24	198.19	2.52	13.54	613.03
PNC/Golder (mar.)	4		-1.65	2.20	-9.11	-452.45	2.85	15.52	822.80
PNC/Golder (sept.)	4		0.30	1.28	2.42	156.39	2.14	11.54	510.13
PNC/HAZAMA	4		1.22	2.33	6.97	356.52	2.88	14.89	562.04
SKB/CFE	4		0.00	0.96	-0.09	-24.54	1.59	8.85	462.11
SKB/KTH	4		-4.87	5.54	-25.30	-1014.00	4.98	24.20	990.18
TVO/VTT I	4		-0.04	1.10	-0.02	47.24	1.78	9.89	503.89

1) Performance measures defined in Appendix E.
2) Errors in comparison to observed value at t=20000 min.
3) Errors in comparison to observed value at t=132595 min., i.e., comparable to performance measures reported in Gustafson and Ström, 1995.
4) As reported in Gustafson and Strom, 1995, included for comparison.

Gustafson and Ström (1995) also compared the ATFM models using plots of observed and simulated drawdowns versus distance. Figures 4-7 and 4-8 present comparable plots for this uncalibrated simulation at times of 20000 and 132595 minutes, respectively. The mean drawdown for the realizations is plotted versus radial distance of the observed section to the centre of the pumped section in KAS06. All the observations are reasonably simulated, except for the upper sections of KAS07 (these are the two extreme values in Figures 4-7 and 4-8). For this region of the HRL, both the conceptual model and its HYDRASTAR representation are inadequate.

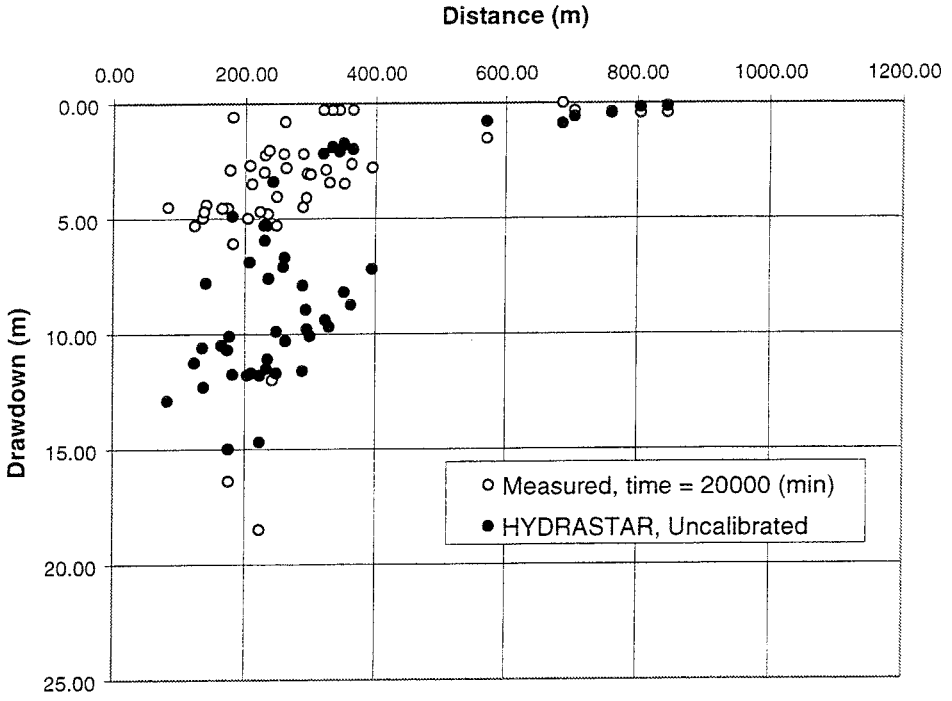

Figure 4-7. Drawdown versus distance for uncalibrated mean simulated drawdowns and observed drawdowns at time = 20000 minutes.

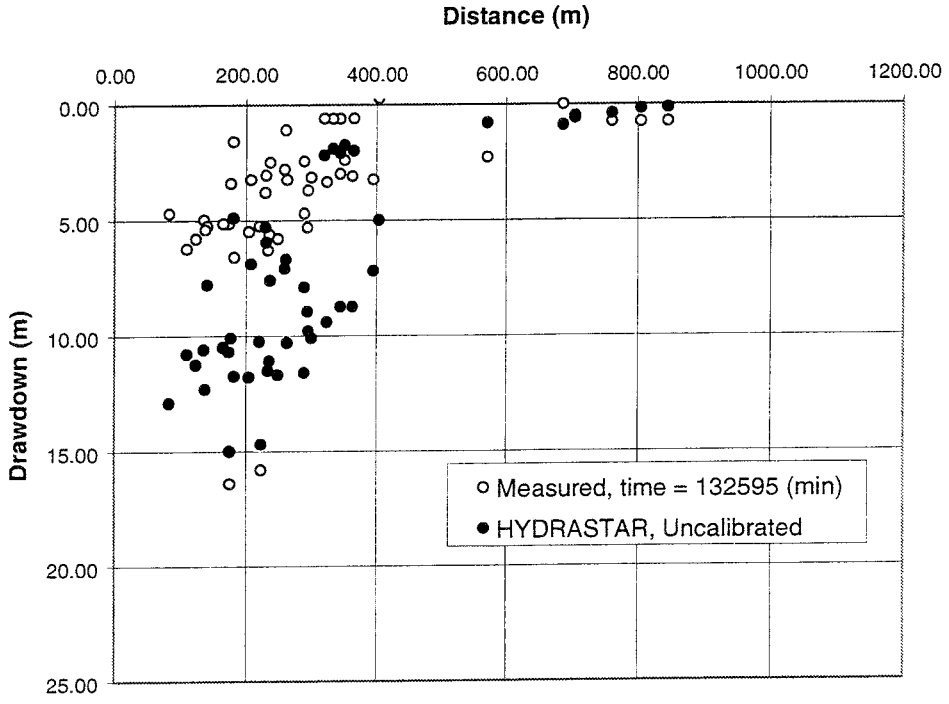

Figure 4-8. Drawdown versus distance for uncalibrated mean simulated drawdowns and observed drawdowns at time = 132595 minutes.

5. CALIBRATED SIMULATION

This HYDRASTAR simulation models the LPT2 pumping test in Monte Carlo fashion for 30 calibrated realisations of the hydraulic conductivity field. It uses the previously described model of the HRL with a Noflow upper boundary and employs the pilot point inverse method of calibrating the hydraulic conductivity fields using the observed heads (Section 1.2). The model results therefore are conditioned on the head measurements observed during LPT2, and should be compared with the uncalibrated simulation of section 4.0.

The head measurements used for calibration were the drawdowns given by Rhén et al. (1992). However, the current version of HYDRASTAR cannot model mixed storage mechanisms and complex boundary conditions, forcing this study to omit several of the observations. The drawdowns in the upper sections of the HAS holes were not used because they are thought to represent unconfined conditions. The upper and lower sections HAS07, HAS14 and HAS18 were not used because they are thought to be directly connected to the Baltic Sea or to areas of strong recharge. Lastly, the observations in the pumped borehole, KAS06, were not used because it was suspected that the relatively coarse finite difference grid would result in large errors at that location.

This simulation used 32 pilot points scattered throughout the model (Figure 5-1).

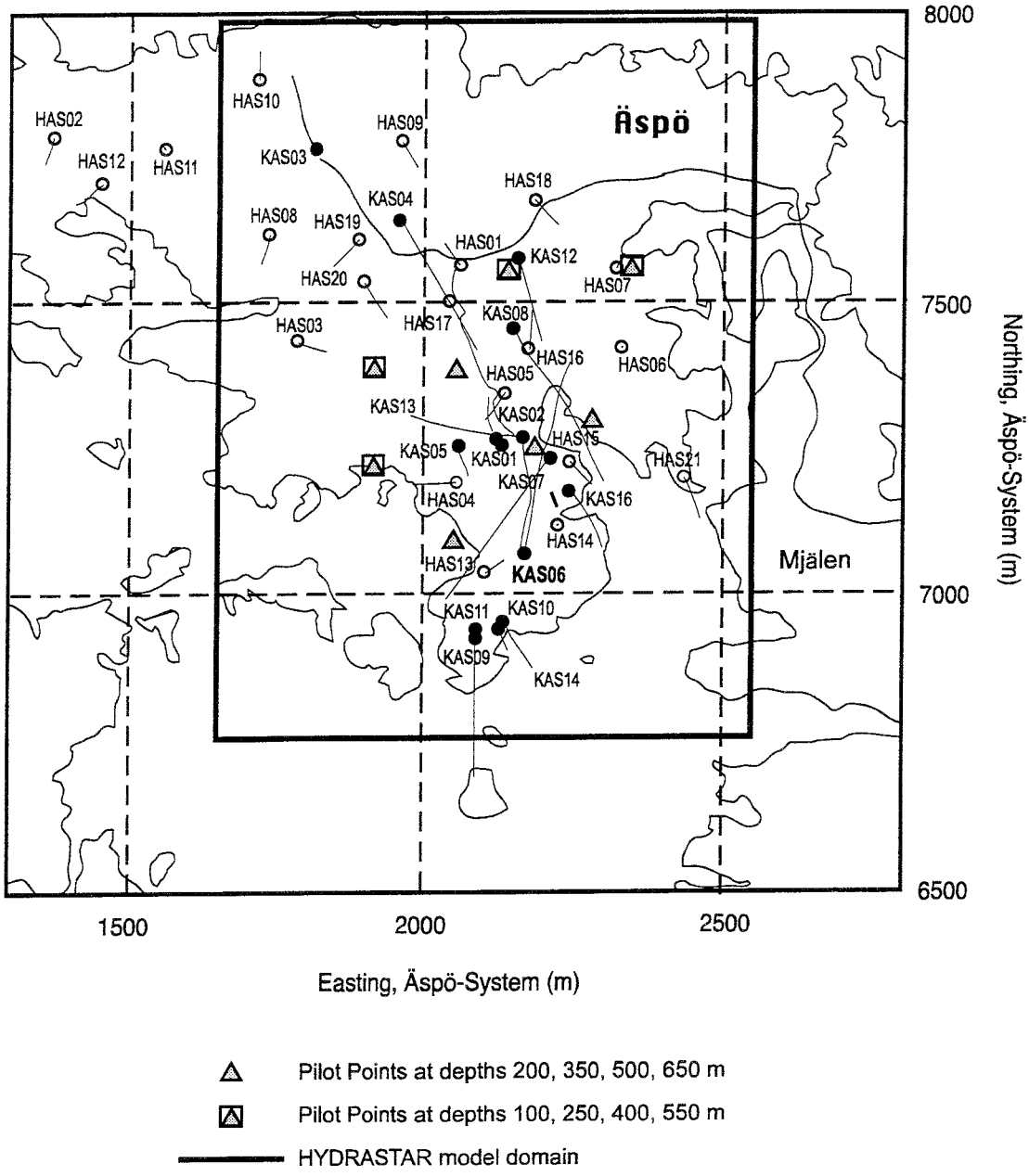

Figure 5-1. *Pilot point locations. Four pilot points are positioned directly beneath the indicated locations..*

Unlike the pilot point algorithm of RamaRao et al. (1995), this algorithm makes no attempt to optimally select the locations of the pilot points but rather spreads them throughout the model similar to de Marsily et al. (1984). The optimal number of pilot points and their locations are not currently understood (Walker, 1997). The results of this set of simulations are therefore somewhat speculative but do provide a test case for the pilot point method. It is the first known application of the pilot point method in 3-dimensions (RamaRao, 1996).

5.1. TRANSIENT RESPONSE AT SELECTED WELLS

As presented in Appendix C, the calibration has been successful in most of the observation sections. In comparison to the uncalibrated simulation described in section 4.0, the means of the simulated drawdowns are noticeably closer to the observed values (e.g. sections of KAS05 or KAS08, shown in Figures 5-2, 5-3, 5-4, and 5-5). The standard deviations of the realisations are noticeably smaller than those of the uncalibrated simulations at comparable observation wells, indicating that calibration reduces the variability of model simulations. As before, KAS02-2, KAS03, and the upper sections of KAS07 cannot be calibrated. Possibly this would change if the discretisation error around the pumping hole were reduced e.g. by mesh refinement. The drawdown in the pumping hole in this case was approximately 12m, i.e. smaller than in the uncalibrated simulation.

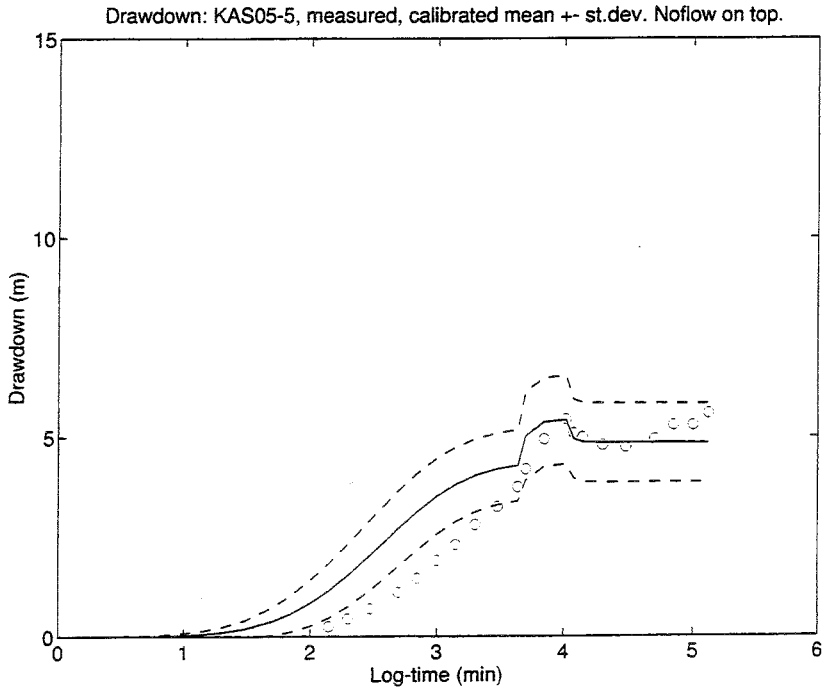

Figure 5-2. *Calibrated simulation of drawdowns versus time for KAS05-5: Noflow upper boundary.*

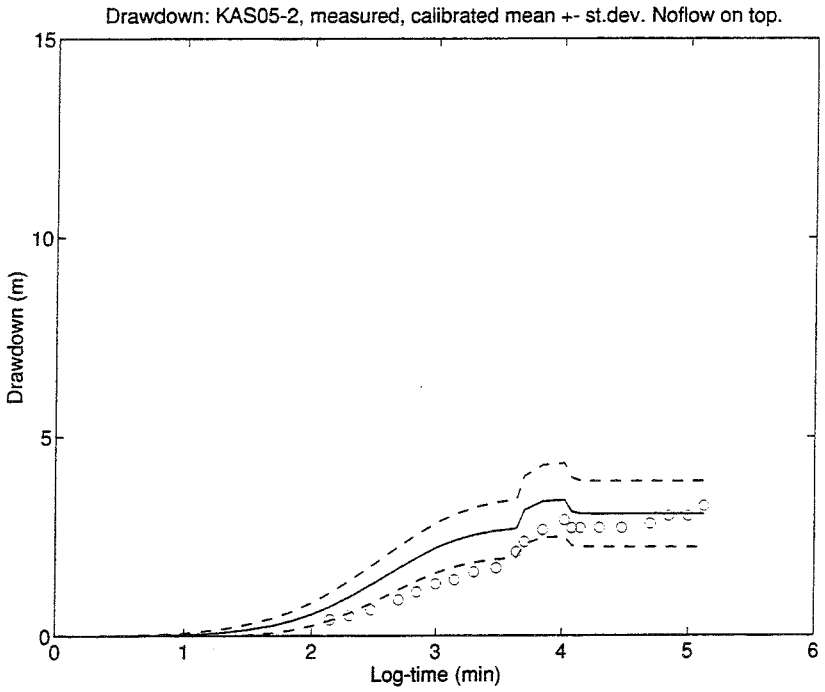

Figure 5-3. *Calibrated simulation of drawdowns versus time for KAS05-2: Noflow upper boundary.*

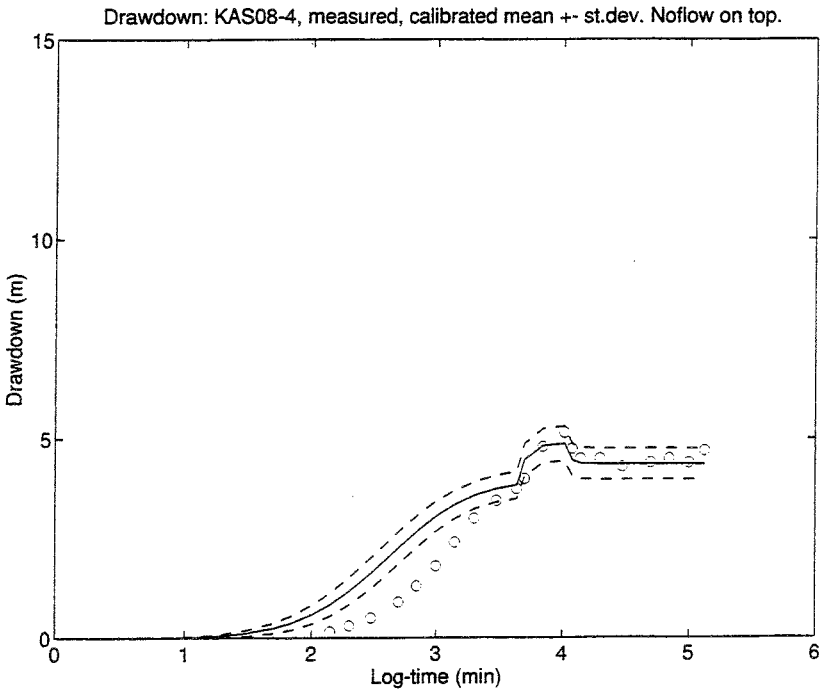

Figure 5-4. *Calibrated simulation of drawdowns versus time for KAS08-4: Noflow upper boundary.*

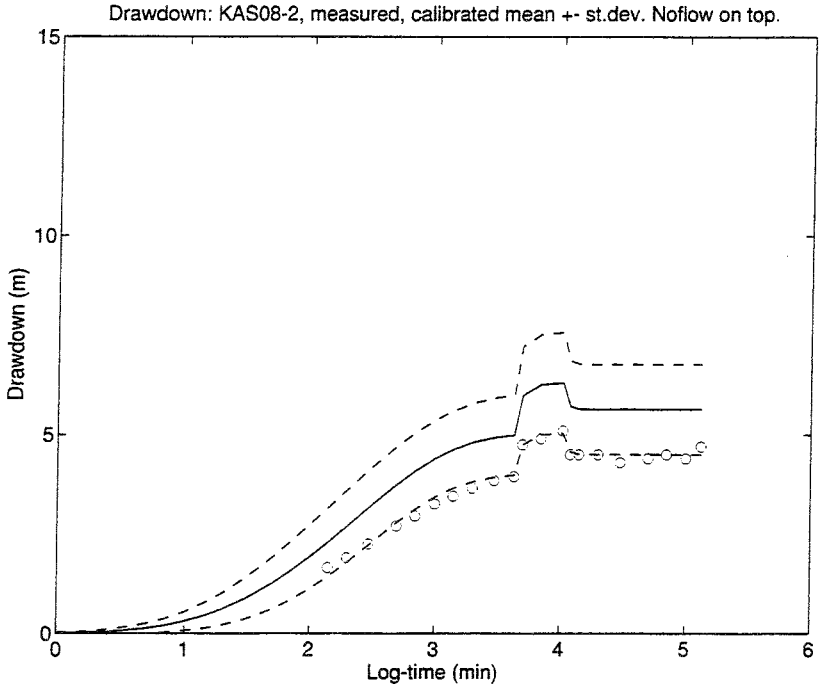

Figure 5-5. *Calibrated simulation of drawdowns versus time for KAS08-2: Noflow upper boundary.*

As noted in Section 3.5.4, the early system response is dominated by the specific storativity, and the late system response by the hydraulic conductivity. Thus, calibration has little effect on the simulated responses in the early phase of the pumping, suggesting that is reasonable to exclude the contributions to the objective function from this time interval. The calibration would then be based essentially only on the values of the drawdowns at the end of pumping, when quasi-stable conditions are attained. This could be achieved with simple modifications to the existing code to allow for spatially and temporally variable weights on the objective function as suggested by RamaRao et al. (1995). This would allow modellers greater flexibility in defining the objective function for each application.

5.2. STEADY-STATE DRAWDOWNS

As previously stated in section 4.2, steady-state has been defined as the relatively stable drawdowns taken at the end of the LPT2. However, given the observed increasing trend in the drawdowns, it is unclear that this is appropriate. This is particularly true for the calibrated simulations which compare these observed drawdowns to the simulated drawdowns in order to adjust the hydraulic conductivity field. Although the model includes no other stresses to account for this trend (ref. to Section 4.2), this study calibrates the hydraulic conductivities to all of the late-time observed drawdowns.

Table 4-1 presents the performance measures for the error of observed minus the mean of the realisations of simulated heads at steady-state. As noted in Section 4.2, these are computed in the same fashion as those performance measures reported in Gustafson and Ström (1995). As expected, the errors are reduced with respect to the uncalibrated model. At both early and late times, HYDRASTAR slightly underpredicts the observed drawdowns, as indicated by the negative mean error (dh) and the distance weighted mean errors (dh(lnr), dh(r)). In comparison to the ATFM modelling studies, the calibrated HYDRASTAR model has slightly better performance than the average of the ATFM models.

Plots of observed and simulated drawdowns versus distance were also prepared for this calibrated simulation. Figures 5-6 and 5-7 present plots at times of 20000 and 132595 minutes, respectively. The mean drawdown for the realisations is plotted versus radial distance of the observed section to the centre of the pumped section in KAS06. In comparison to the uncalibrated model, the simulated values are noticeably closer to the corresponding observed values. All the observations are reasonably simulated, except for the upper sections of KAS07 (the two outliers) which are very close to the pumped borehole, KAS06.

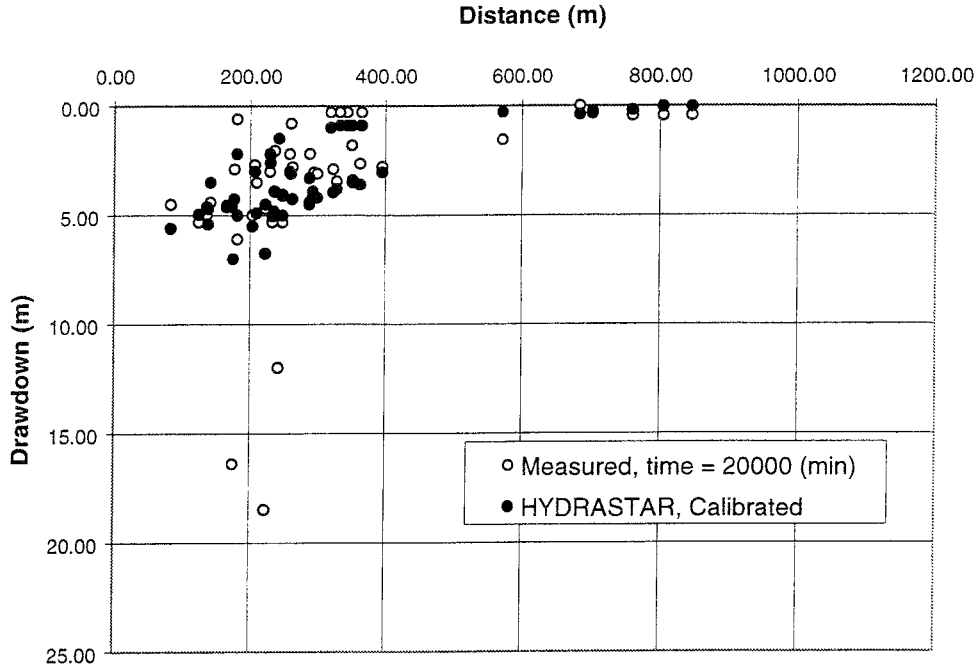

Figure 5-6. Drawdown versus distance for calibrated mean simulated drawdowns and observed drawdowns at time = 20000 minutes.

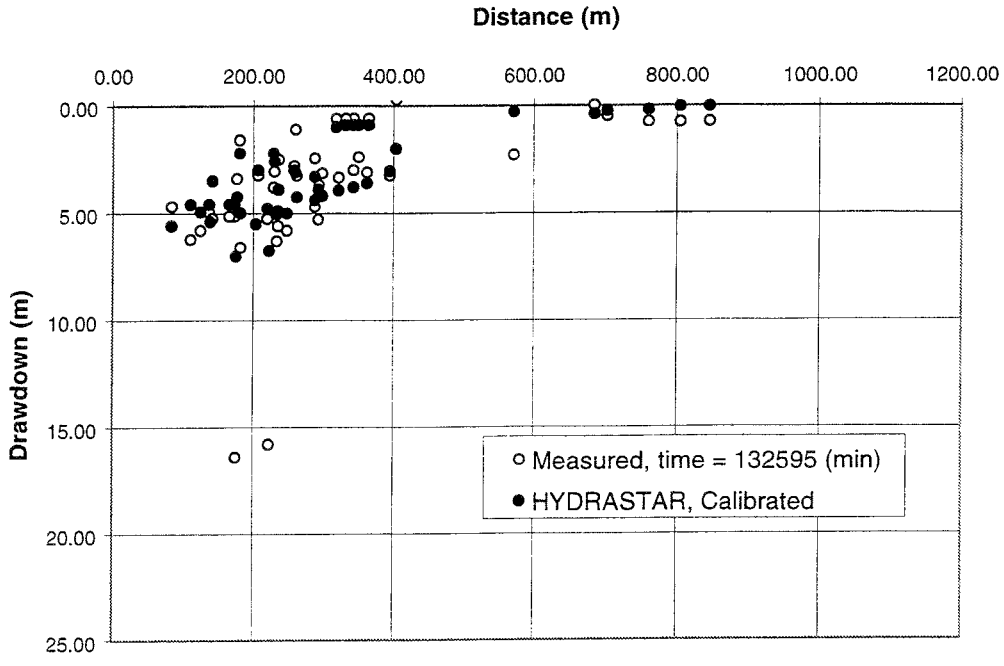

Figure 5-7. Drawdown versus distance for calibrated mean simulated drawdowns and observed drawdowns at time = 132595 minutes.

The performance measures of the calibrated HYDRASTAR model indicate that calibration substantially reduces the bias and improves the accuracy of the model. However, it is not clear from this study that calibration to a single event or single data set is adequate. For example, overcalibrating the model to a single data set might simply bias the model rather than improve the model's simulation of the true system. This suggests that a careful cross-validation of the model or verification using additional data sets would be essential in building confidence in the final model. Such studies are beyond the scope of this project.

5.3. EFFECTS ON THE HYDRAULIC CONDUCTIVITY FIELD

Calibration has two effects on the hydraulic conductivity field, the first of which is the local change at each pilot point. Figure 5-8a presents an example of a realisation of the hydraulic conductivity field before calibration. The figure shows the hydraulic conductivities on a vertical plane passing north-south through the easternmost pilot point locations (see also Figure 3-3 for the cross section location). Figure 5-8b shows the same field after calibrating the hydraulic conductivities at each pilot point. The effects of calibration are more clearly shown in Figure 5-8c, which is a plot through the same plane showing the difference of calibrated minus uncalibrated log hydraulic conductivities. Calibration generally creates small regions of change surrounding each pilot point, each with a radius approximately equal to the range of the variogram (80m).

The second impact of calibration is the change in the field-wide mean. Note that the mean $\log_{10}$ hydraulic conductivity of the entire field in Figure 5-8c has been raised by 0.37. As discussed in Section 3.5.6, the entire field is contained in a single kriging neighbourhood whose mean depends on both the 110 upscaled measurements and the 32 pilot points. Since the pilot point values are calibrated and constitute a large proportion of the data, the calibration algorithm also influences the field-wide mean hydraulic conductivity. Similar effects are noted in Section 3.5.5 with multiple kriging neighbourhoods. Thus the pilot point method can also influence large zones of the hydraulic conductivity in addition to the changes at individual pilot points.

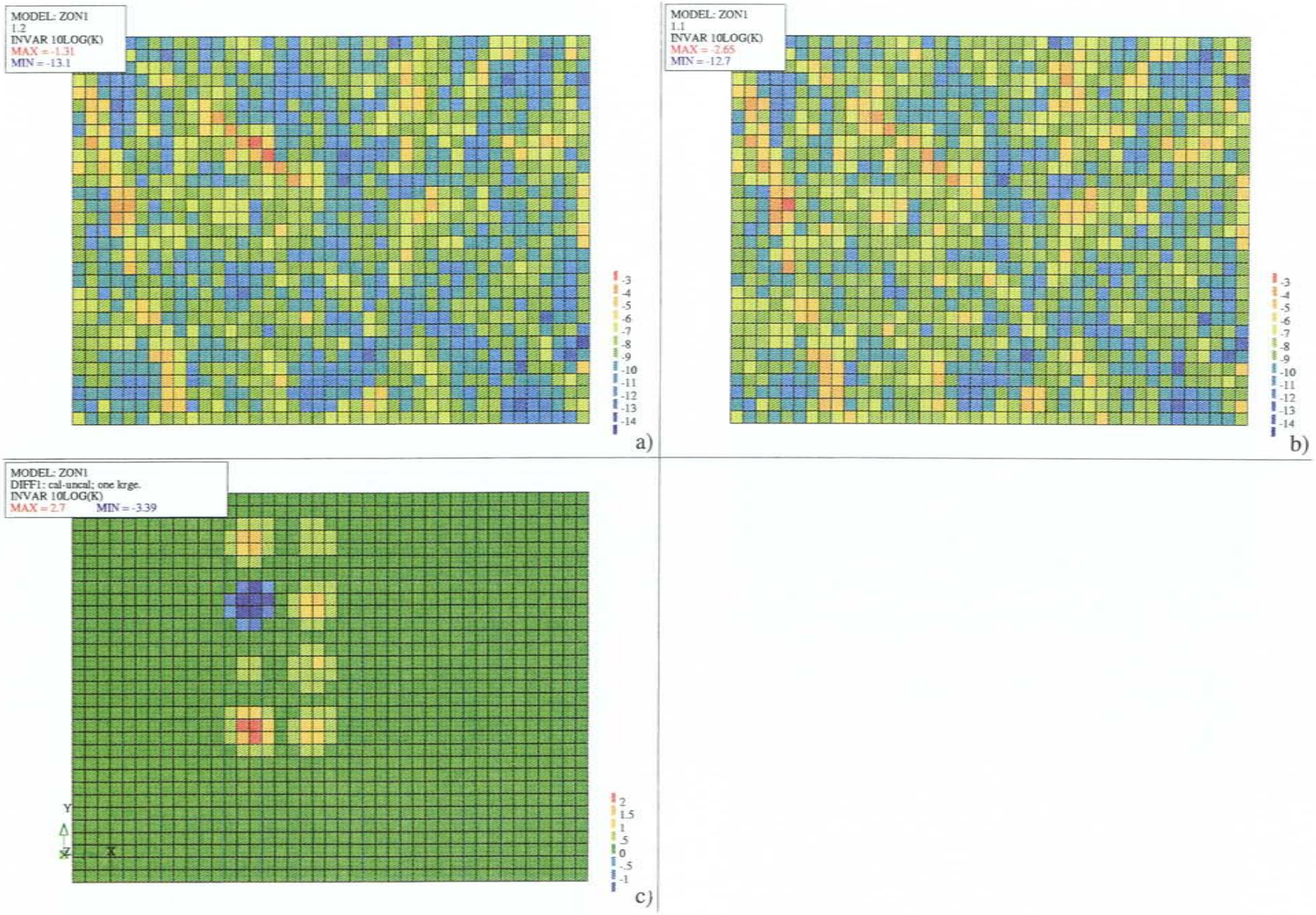

Figure 5-8. *Vertical cross section A-A' through one realisation of a log hydraulic conductivity field (m/s), a) uncalibrated b) calibrated, and c) difference of b minus a.*

6. DISCUSSION AND CONCLUSIONS

This report has presented the application of HYDRASTAR, a stochastic continuum groundwater model, to the Äspö HRL LPT2 pumping test. The main objective of this study has been to provide an additional real-world test case for HYDRASTAR. This study differs from previous LPT2 modelling studies because it uses the inverse modelling capabilities of HYDRASTAR to condition the model results to the observed hydraulic heads. The purpose of this conditioning via inverse modelling is to improve the reliability of input hydraulic conductivity fields and thus minimise the uncertainty of the model predictions. This study also evaluated the Äspö HRL hydrogeologic conceptual model via inverse modelling of the LPT2.

Preliminary simulations evaluated alternative choices of parameters and representations, resulting in a final model of the LPT2 which was successful in simulating the responses observed during the LPT2. Specifically, the mean of the Monte Carlo realisations of simulated drawdowns reproduced the magnitude, timing, and shape of the observed drawdowns. The observed drawdowns generally were bracketed by an interval of plus or minus one standard deviation about the mean of the realisations. Calibration was successful in reducing the variability of the model simulations. Some discrepancies in the magnitude and timing of the observed versus the simulated drawdowns were revealed at several wells. With few exceptions, the model realisations were centred on the observed drawdowns and bracketed the observed responses. This suggests that the ensemble of realisations has bracketed the true characteristics of the HRL, supporting both the conceptual model and its representation by HYDRASTAR.

The following sections discuss the results of this study, followed by a summary of the main conclusions.

6.1. BOUNDARY CONDITIONS

Previous modelling studies of the HRL have been steady state simulations. This allowed such studies to use Dirichlet (constant head) boundary conditions with the head values taken from regional steady state models, using a nested approach. This study examined a transient simulation which required re-evaluating the boundary conditions used on all sides of the HYDRASTAR model. A preliminary simulation of the HRL using Dirichlet boundaries on all surfaces of the model domain showed that such a specification is inappropriate to represent the transient responses to the LPT2 pumping test. It also showed that while most observation sections were not well-modelled with a Dirichlet boundary condition for the upper boundary, a few sections were well-modelled by this upper boundary condition. This indicates that a combination of boundary conditions on the upper surface might provide the best representation of the HRL. However, the current version of HYDRASTAR (version 1.5) does not permit combinations of boundary conditions on a single model surface. Because

precipitation and leakage from the Baltic Sea are thought to add only small amounts of recharge to the upper surface of the model, this study adopted a Neumann condition for the upper boundary (which is equivalent to a Noflow boundary for the purposes of superposition). Subsequent simulations showed this to be an acceptable choice.

The preliminary model simulations also indicated that some observation sections were too close to the Dirichlet boundaries on the sides and bottom of the model. Although one alternative would be to extend the model grid, this would dramatically increase the computational demands of the model. Since the interior of the model was acceptably modelled by Dirichlet boundaries on the sides and bottom of the model, this representation was retained. A Mixed-type boundary condition might be useful in such circumstances but this boundary type is not an option in the current version of HYDRASTAR.

The representation of the pumped borehole without mesh refinement or well indexing leads to underpredicting drawdowns in the vicinity of this borehole. This also influences the ability of the calibrated model to reproduce large drawdowns in observation sections that are close to or well-connected to the pumping hole.

6.2. STORAGE PROPERTIES

As previously stated, most applications of HYDRASTAR have been for steady state simulation, where storage properties of the system are not of interest. One of the preliminary transient simulations indicated that the model is quite sensitive to changes in specific storativity within the range of values reported for the HRL. It further indicated that some observations are well-modelled by one value of specific storativity, while other observations might require another value of specific storativity. Final simulations used a specific storativity of 10^{-7} 1/m, which was the most successful in reproducing the LPT2 responses. Further evaluation of this parameter is beyond the scope of this study.

6.3. KRIGING PARAMETERS

The primary objective of this study was to provide a test case for HYDRASTAR, not to determine the best stochastic model for the hydraulic conductivities. However, several preliminary simulations evaluated the sensitivity of the model to the choice of kriging parameters. These simulations indicated that choice of kriging neighbourhoods can effect both the uncalibrated and calibrated simulations. A preliminary specification of kriging neighbourhoods was used to implicitly include a decreasing trend in $\log_{10}$ hydraulic conductivity. In order to match the observed heads, the calibration algorithm removes this trend, suggesting that such a trend is incompatible with the chosen boundary conditions. Subsequent model simulations used a single kriging neighbourhood for the entire domain, implying no trend with depth. This is consistent with the geostatistical modelling study of Äspö by LaPointe (1994).

6.4. PILOT POINT CALIBRATION

The pilot point method of calibrating hydraulic conductivity was intended to increase the reliability of the hydraulic conductivity fields by utilising transient head measurements during long term interference pumping tests. On a numerical/mathematical level, the calibration method has been shown to decrease the errors of simulated versus observed drawdowns, resulting in more reliable hydraulic conductivity fields. The decrease in model uncertainty is evidenced by the decreased standard deviation of the set of realisations with respect to the corresponding uncalibrated simulation. It is possible that the pilot point method may introduce bias into the model by overcalibrating the model to a single data set. This could be evaluated by cross-validation with the same data set or by verifying the model with additional data sets. The optimal location and number of pilot points has not been evaluated.

For the LPT2 case, the results from the calibration exercises performed can be interpreted as follows: If the conceptual model of the site is not well-represented by the boundary conditions or other model input data (i.e., fracture zones, trends), the calibration algorithm may adjust the conductivity field in an hydrogeologically unrealistic manner, rather than improve the quality of the realisations of the conductivity field. Although this application was restricted to a limited choice of boundary conditions, the results are encouraging for the LPT2. The mean drawdowns over the realisations of the computed drawdowns after calibration are close to the observed final values. The standard deviations are substantially reduced relative to the uncalibrated case.

The early transient response is little affected by changes in the conductivity field. On the other hand, this interval is very sensitive to changes in specific storativity. This suggests that calibration of the hydraulic conductivity field might therefore exclude the contributions to the objective function from this time. This could be achieved with simple modifications in the existing code to allow for spatially and temporally variable weights on the objective function.

Simulated drawdowns for the upper sections of KAS07 and in the pumped borehole were poorly modelled. Calibration was unable to improve the simulated response at KAS07, suggesting that either the conceptual model of fracture zones or its HYDRASTAR representation are inadequate in this region of the model. It is possible that revisions to the conceptual model (e.g. additional fracture zones) or mesh refinement could address these errors. It is not known if the calibration introduces bias or if the fields are excessively calibrated, suggesting that verification with multiple data sets should be considered. Pilot point calibration appears to be an important tool for improving the performance of stochastic hydrogeologic simulation.

6.5. SUMMARY OF CONCLUSIONS

In qualitative terms, the HYDRASTAR model simulations and the observed data have fair agreement, and is comparable to the ATFM modelling results

summarised by Gustafson and Ström (1995). This suggests that both the conceptual model and its HYDRASTAR representation are adequate characterisations of the Äspö area and the LPT2. In general, the modelling study suggests the following:

- The land surface and surrounding Baltic Sea is better represented by a Neumann (Noflow) boundary condition than a Dirichlet (constant head) boundary condition
- The relatively small model domain required to reduce computational demand may be restrictive, limiting the accuracy of the simulation near the boundaries.
- The simulations are very sensitive to specific storativity within the range of values reported for the site.
- Mesh refinement or well indexing is needed to improve simulation of the drawdowns near the pumped boreholes.

The study revealed several important aspects of the use of the pilot point method of inverse modelling for calibrating groundwater models. These are:

- Calibration to observed heads can reduce the uncertainty of model simulations.
- The early-time response of the LPT2 is dominated by specific storativity, and is unaffected by calibration of hydraulic conductivity.
- The site conceptual model, geostatistical model and boundary conditions should be chosen prior to calibration to avoid unrealistic calibration results.
- A validation against additional pumping tests to confirm the calibration and check on bias is recommended.

The HYDRASTAR code itself appears to be adequate for modelling the LPT2, but several enhancements have been indicated for future code development. These include, but are not limited to:

- Allowing specification of spatially and temporally variable boundary conditions.
- Including an option for a third-type (Mixed) boundary conditions.
- Adding options for nested variogram structures (e.g., including a nugget).
- Allowing a more refined representation of pumped boreholes to represent the extreme drawdowns near wells, such as well indexing.
- Modification of the calibration method to include spatially and temporally variable weights on the objective function.

ACKNOWLEDGEMENTS

This study was funded by the Swedish Nuclear Waste Management Company (SKB), under the supervision of Mr. Anders Ström.

The authors would like to acknowledge the assistance and patience of Mr. Anders Ström (SKB) throughout this study, and for his comments on this report. We would also like to acknowledge the helpful comments of Mr. Daniel Sundström (Starprog), Mr. Geoff Freeze (INTERA), Mr. Ingvar Rhén (VBB/Viak), Mr. Gregory Ruskauff (INTERA), and Mr. Hans Widén (Kemakta). Finally, we would like to thank Ms. Lydia Biggs (INTERA) for her illustrations, Mr. Bryan Bullard (INTERA) for his compilation of the error statistics, Ms. Christina Skårman and Mr. Marcus Laaksoharju for their assistance in translation, and Mrs. Izabella Hallberg (INTERA) for her assistance in the preparation of the final report.

REFERENCES

Barthélémy Y, Schwartz J, Sehti K, 1994. Äspö Hard Rock Laboratory - Hydrodynamic modelling of the original steady state and LPT2 experiments - MARTHE and SESAME codes. SKB International Cooperation Report ICR 94-16, Stockholm, Sweden.

Birgersson L, Boghammar A, Grundfelt B, Lindbom B, Lundström P, Widén H, 1995. SR 95 Hydrogeological Modelling of Äspö: Comparison of Pre-Investigation Phase Data and Construction Phase Data. SKB Working report AR 95-33, Stockholm, Sweden.

Carrera J, Neuman S P, 1986. Estimation of Aquifer Parameters Under Transient and Steady State Conditions, 2, Uniqueness, stability, and solution algorithms, Water Resour. Res., 22(2), 211-227.

Eriksson L O, Oppelstrup J, 1994. Calibration with respect to hydraulic head measurements in stochastic simulation of groundwater flow - A numerical experiment using MATLAB. SKB Technical Report TR 94-30 Stockholm, Sweden.

Freeze R A, Cherry J A, 1979. Groundwater, Prentice-Hall.

Geier J, 1993a. Verification of the geostatistical inference code INFERENS, Version 1.1, and demonstration using data from Finnsjön. SKB Technical Report TR 93-09, Stockholm, Sweden.

Geier J, 1993b. Version 1.0 User's Guide to INFERENS 1.1. SKB AR 93-24.

Gustafson G, Ström A, 1995. The Äspö Task Force on Modelling of Groundwater Flow and Transport of Solutes: Evaluation report on Task No. 1, the LPT2 large scale field experiments. SKB International Cooperation Report ICR 95-05, Stockholm, Sweden.

Hodgkinson D P, Barker J, 1985. Specification of a Test Problem for HYDROCOIN Level 1 Case1: Transient Flow from a Borehole in a Fractured Permeable Medium, Report AERE R-11574, UK Atomic Energy Authority, Harwell Laboratories, UK.

Indelman P, Dagan G, 1993. Upscaling of permeability of anisotropic heterogeneous formations, 1, The general framework, Water Resour. Res. 29(4), pp.917-924.

Journel A G, Huijbregts Ch J, 1978. Mining Geostatistics, Academic Press.

Kipp K, 1986. Adaptation of the Carter-Tracy Water influx calculation to groundwater flow simulation, Water Resour. Res., 22(3), pp. 423-428.

Lovius L, Eriksson L, 1993. Verification of HYDRASTAR version 1.4. SKB Working report AR 93-46, Stockholm, Sweden.

Lovius L, Eriksson L, 1994. Development of a Transient Version of HYDRASTAR. SKB Working report AR 94-12, Stockholm, Sweden..

de Marsily G, Lavedan C, Boucher M, Fasanino G, 1984. Interpretation of Interference Tests in a Well Field Using Geostatistical Techniques to Fit the Permeability Distribution in a Reservoir Model, in Geostatistics for Natural Resources Characterization. Second NATO Advanced Study Institute, GEOSTAT 1983, Tahoe City, California. Edited by G Verly, M David, A G Journel, and A Marachal, pp. 831-849, D Reidel, Hingham, Mass,USA.

Morris S T, Cliffe K A, 1994. Verification of HYDRASTAR: Analysis of hydraulic conductivity fields and dispersion. SKB Technical Report TR 94-21, Stockholm, Sweden.

Norman S, 1991. Verification of HYDRASTAR - A code for stochastic continuum simulation of groundwater flow. SKB Technical Report TR 91-27, Stockholm, Sweden.

Norman S, 1992a. Statistical inference and comparison of stochastic models for the hydraulic conductivity at the Finnsjön-site. SKB Technical Report TR 92-08, Stockholm, Sweden.

Norman S, 1992b. HYDRASTAR - A code for stochastic simulation of groundwater flow. SKB Technical Report TR 92-12, Stockholm Sweden.

OECD, 1983. The International HYDROCOIN Project: Groundwater hydrology modelling strategies for performance assessment of nuclear waste disposal. Level: Code verification.

Peaceman D W, 1978. Interpretation of Well Block Pressure in Numerical Reservoir Simulation, Soc. Pet. Eng. J., pp 183-194.

RamaRao B S,1996. personal communication, INTERA Inc.

RamaRao B S, Lavenue A M, de Marsily G, Marietta M G, 1995. Pilot Point Methodology for Automated Calibration of an Ensemble of Conditionally Simulated Transmissivity Fields: Part 1 - Theory and Computational Experiments, Water Resour. Res., 31(3), pp. 475-493.

Rhén I, Svensson U, Anderson J, Andersson P, Eriksson C, Gustafsson E, Ittner T, Nordqvist R, 1992. Äspö Hard Rock Laboratory: Evaluation of the combined longterm pumping and tracer test (LPT2) in borehole KAS06. SKB Technical Report TR 92-32, Stockholm, Sweden.

Rhén I, 1995. SR-95: Compilation of Geohydrological Data for Äspö. SKB Arbetsrapport AR 95-12, Stockholm, Sweden.

Rubin Y, Gómez-Hernández J, 1990. A stochastic approach to the problem of upscaling of conductivity in disordered media: Theory and

unconditional numerical simulations, Water Resour. Res., 26(4), pp. 691-702.

SKB, 1992. SKB 91: Final disposal of spent nuclear fuel. Importance of bedrock for safety. SKB Technical Report TR 92-20, Stockholm, Sweden.

SKB, 1996. User's Guide to HYDRASTAR 1.5 (Draft), 1996. SKB, Stockholm, Sweden.

Uchida M, Doe T, Dershowitz W, Thomas A, Wallmann P, Sawada A, 1994. Discrete-fracture modelling of the Äspö LPT-2, large-scale pumping and tracer test, SKB International Cooperation Report ICR 94-09, Stockholm, Sweden.

Walker D, 1997. Verification of HYDRASTAR v.1.5 Inverse Modelling. In preparation.

Ward D, Buss D, Mercer J, Hughes S, 1987. Evaluation of a groundwater corrective action at the Chem-Dyne hazardous waste site using a telescopic mesh refinement modeling approach, Water Resour. Res., 23(4), pp. 603-617.

Wikberg P, Gustafson G, Rhén I, Stanfors R, 1991. Äspö Hard Rock Laboratory: Evaluation and conceptual modelling based on the pre-investigations 1986-1990, SKB Technical Report TR 91-22, Stockholm, Sweden.

Yeh W W-G, 1986. Review of Parameter Identification Procedures in Groundwater Hydrology: The Inverse Problem, Water Resources Research, Vol. 22, No. 2, pp. 95-108.

APPENDIX A. PRELIMINARY SIMULATION RESULTS: DIRICHLET UPPER BOUNDARY CONDITION

This appendix presents 30 uncalibrated realisations in comparison to 11 calibrated realisations of the LPT2 model using a Dirichlet (constant head) upper boundary condition. Three angled kriging neighbourhoods were used in the geostatistical simulation of the hydraulic conductivity fields, as described in section 3.5.5. These simulations are described in detail in sections 3.5.1 and 3.5.2 of this report.

Note: The packed-off sections of the boreholes are numbered from the bottom of the hole to the top (i.e., KAS05-5 is the uppermost section in KAS05, and KAS05-1 is the lowest section). Wells designated HAS are shallow percussion-drilled boreholes with only one observation section each. The observed data reported here are taken from Rhén et al. (1992), without modification. No measurements were given for section KAS03-6, and only the final measurement of 4.97m of drawdown was given for KAS05-4.

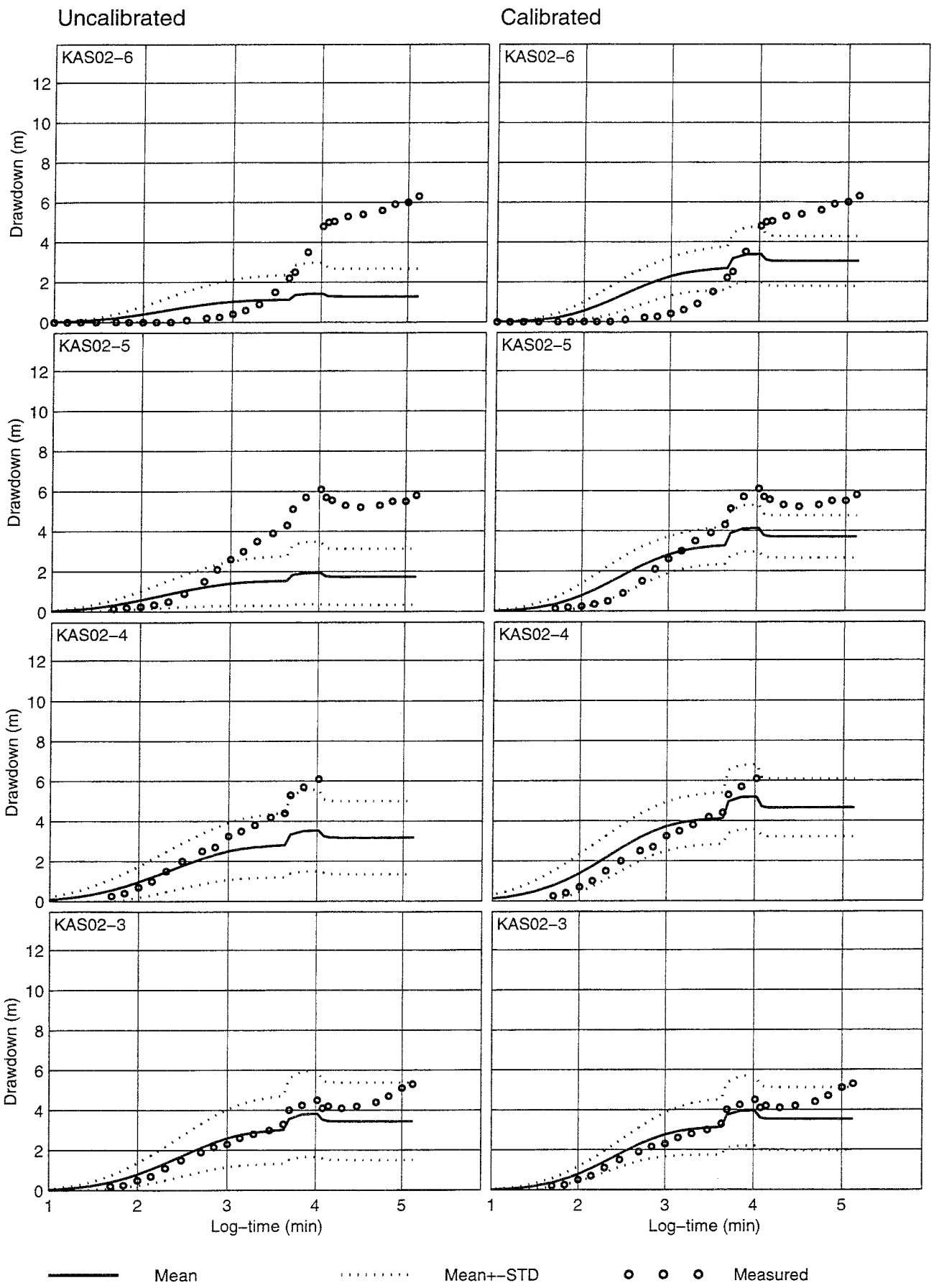

Dirichlet boundary condition on top

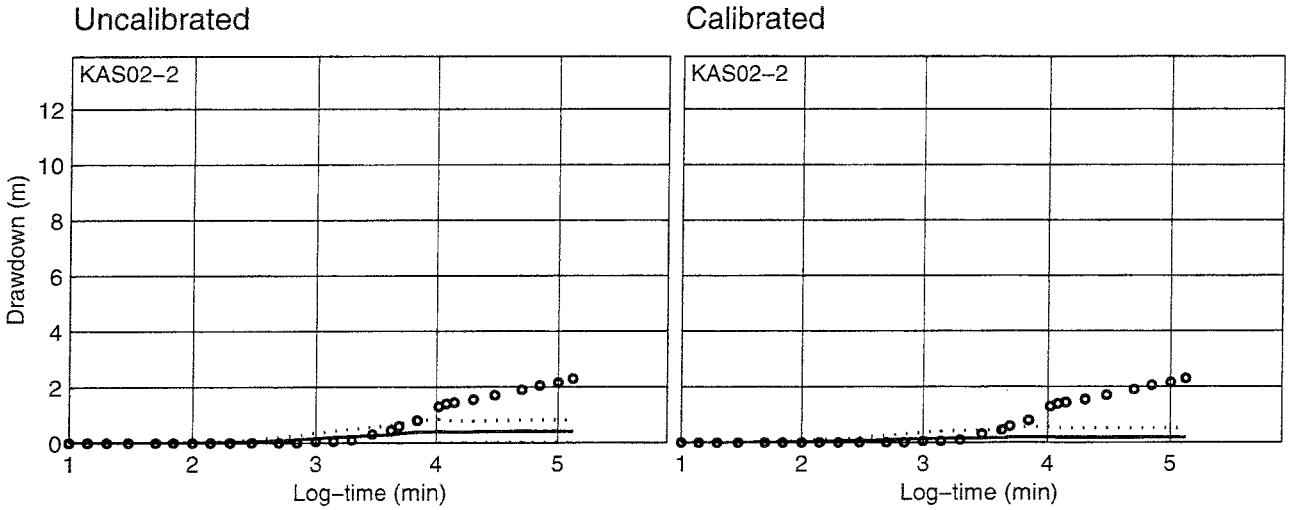

Mean Mean+–STD Measured

Dirichlet boundary condition on top

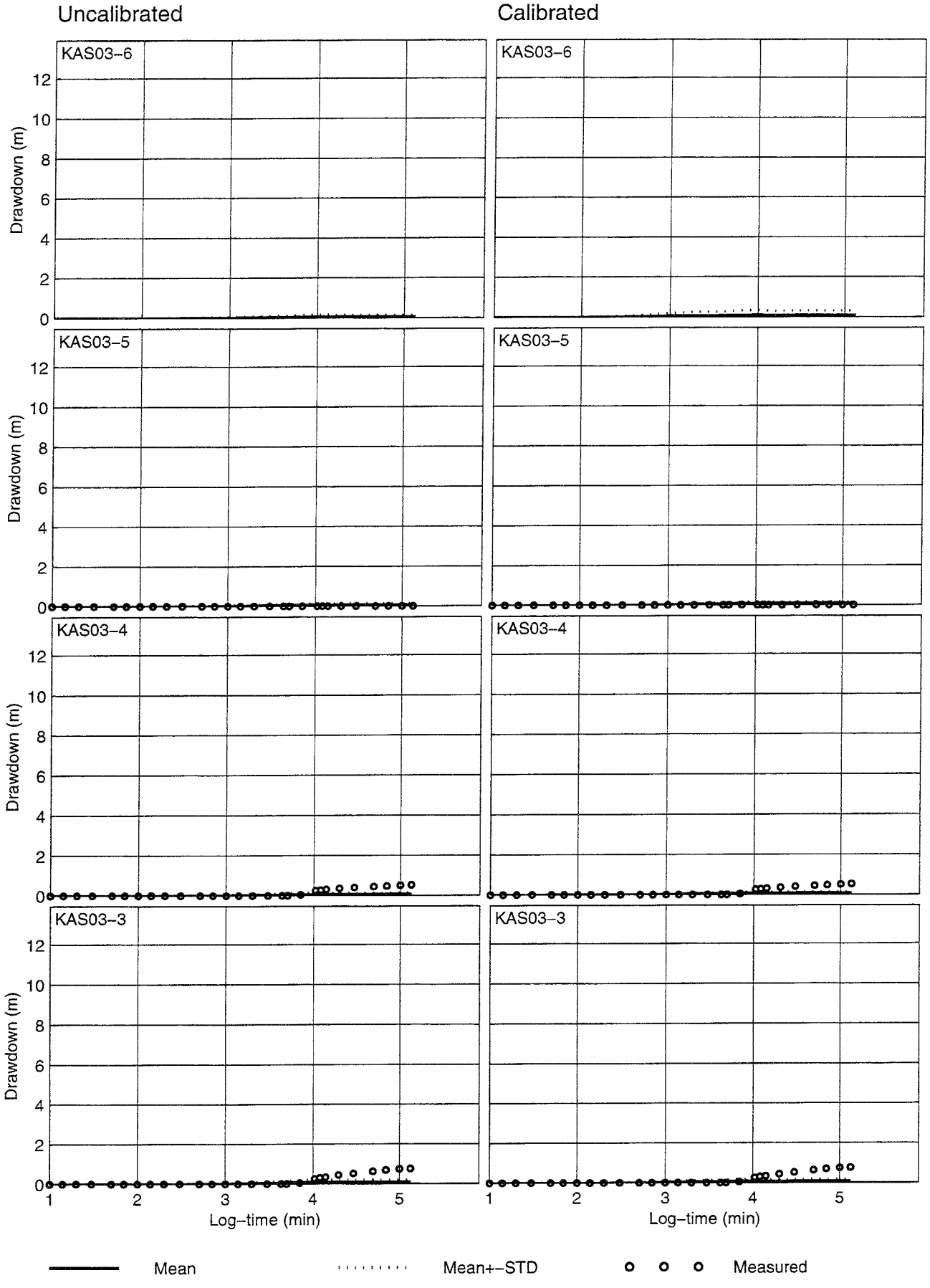

Dirichlet boundary condition on top

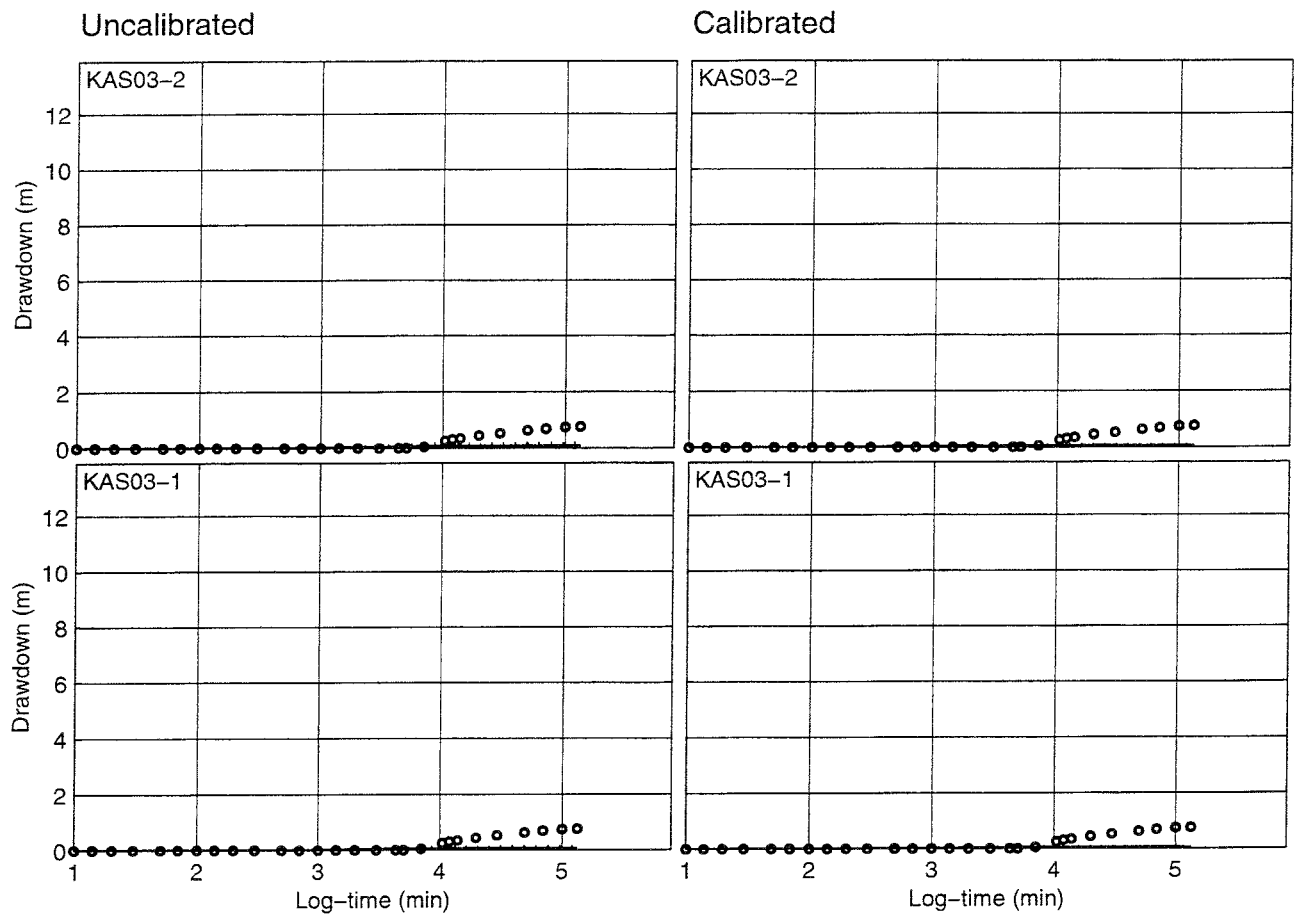

Dirichlet boundary condition on top

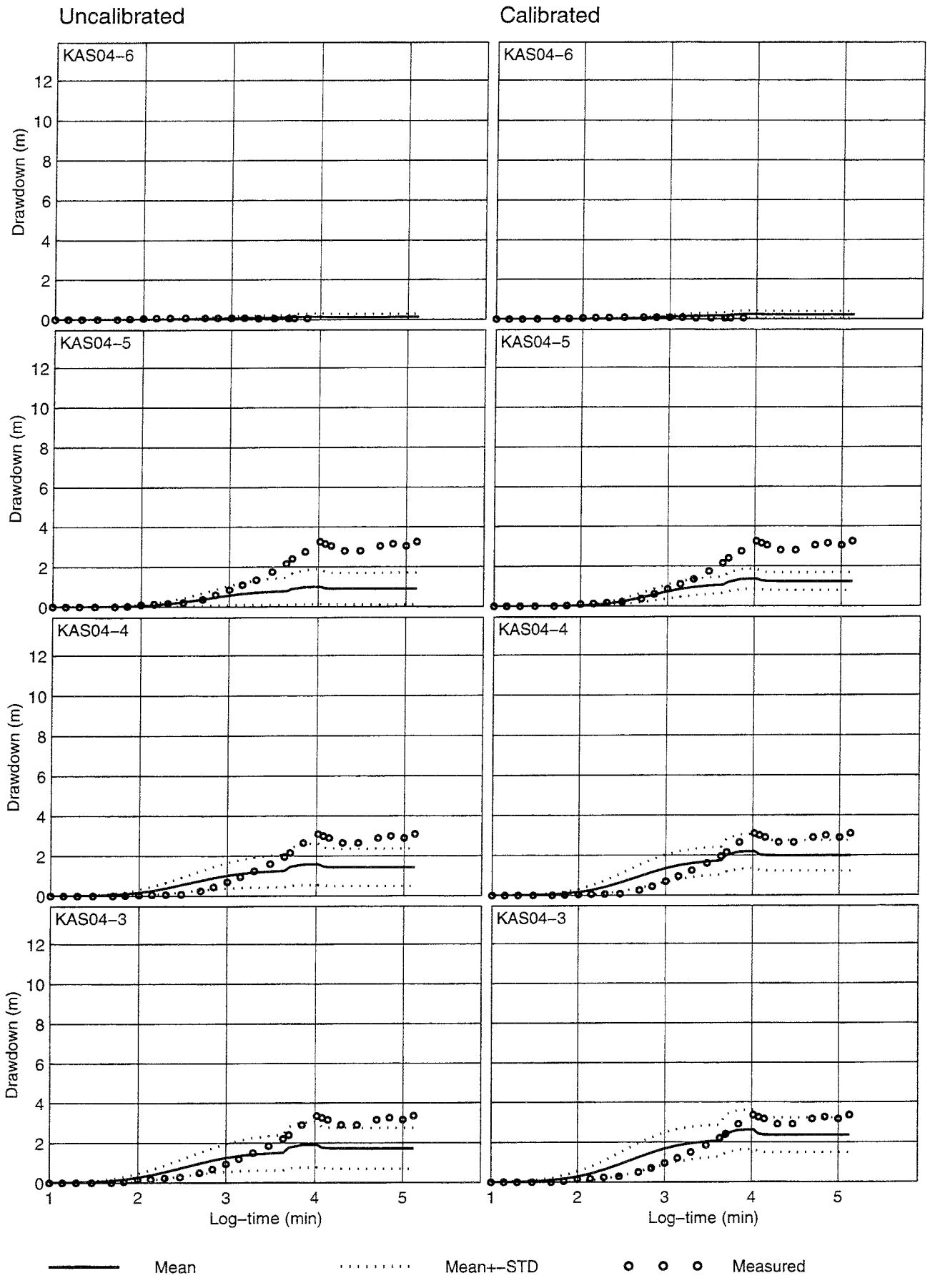

Dirichlet boundary condition on top

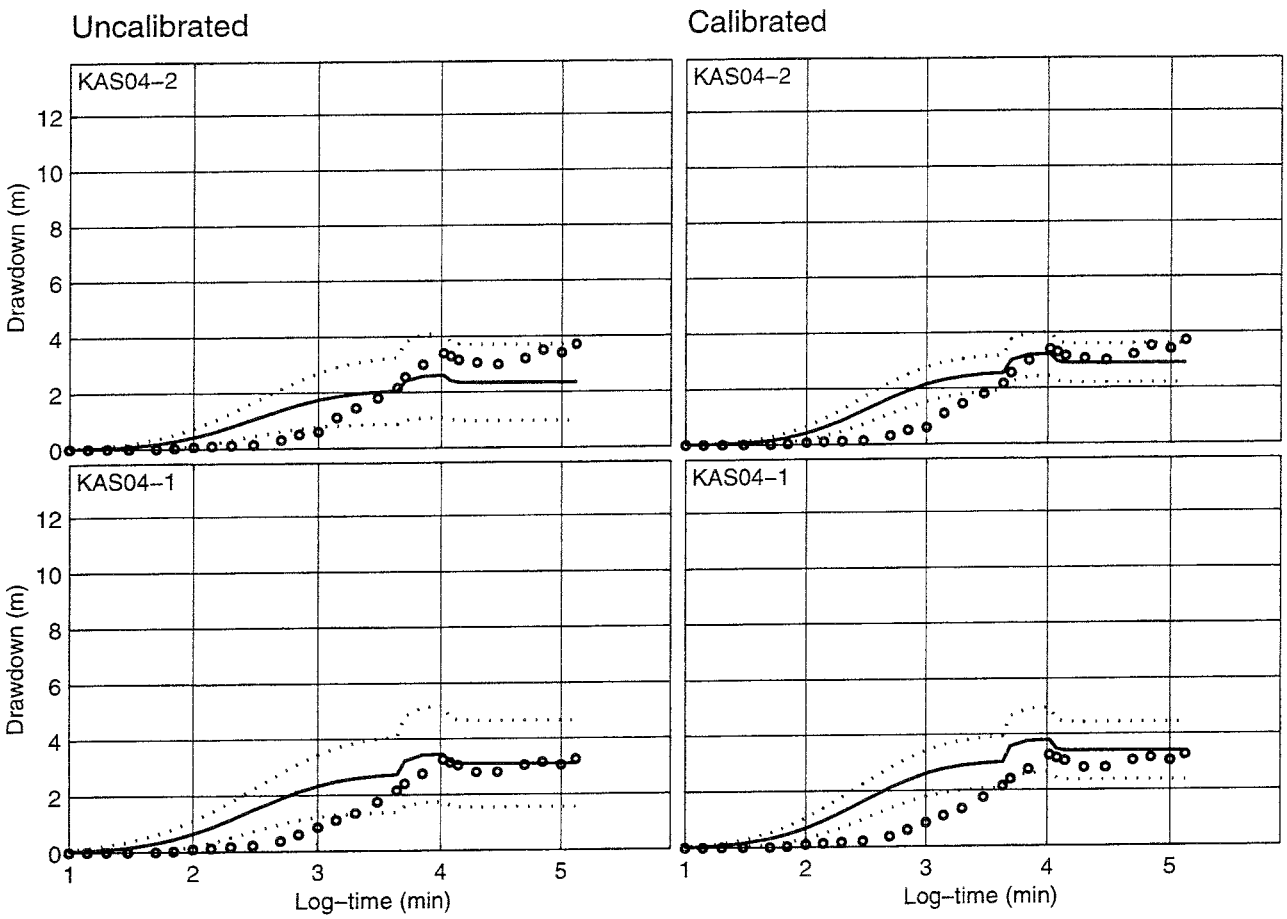

Dirichlet boundary condition on top

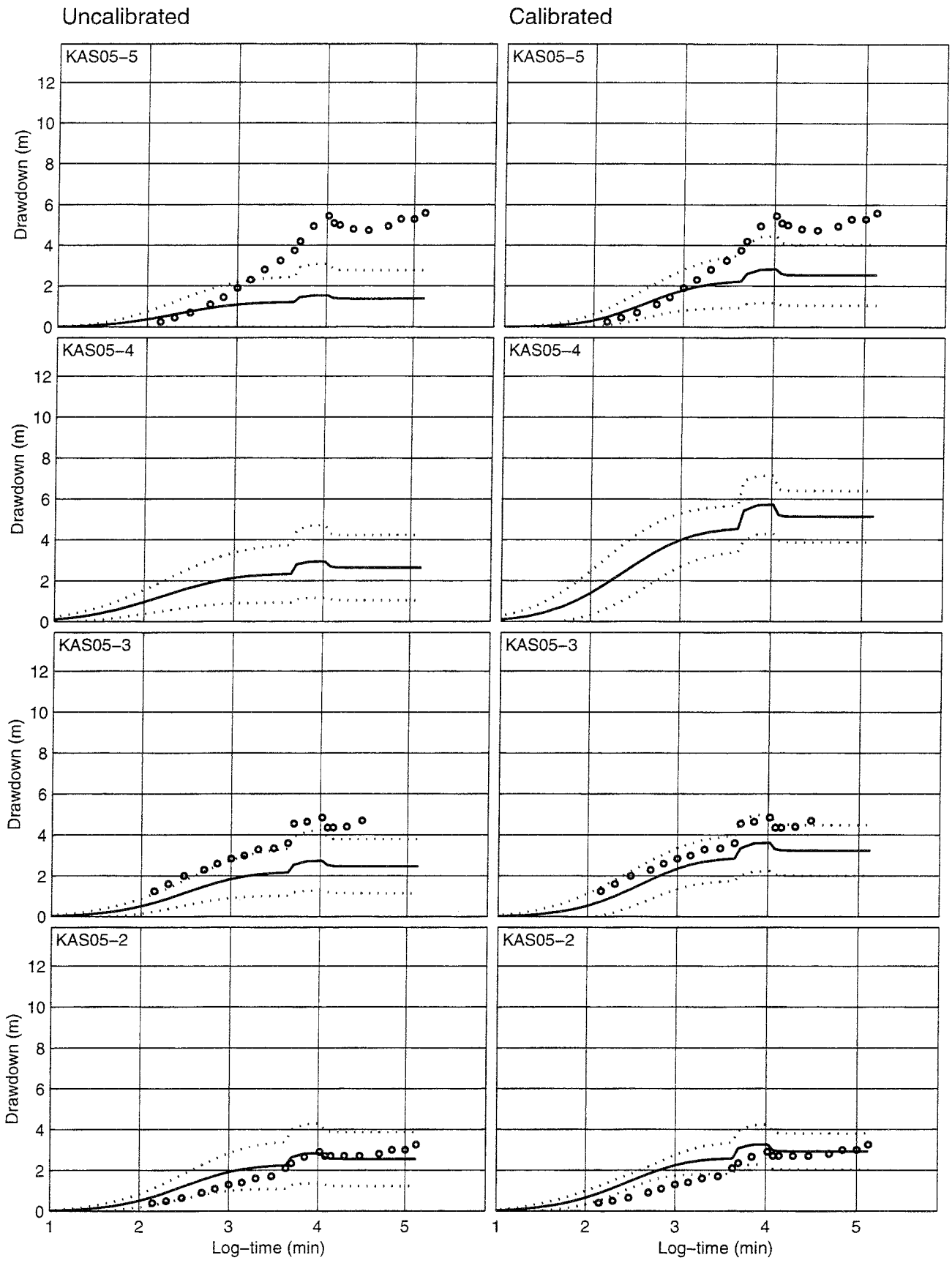

Dirichlet boundary condition on top

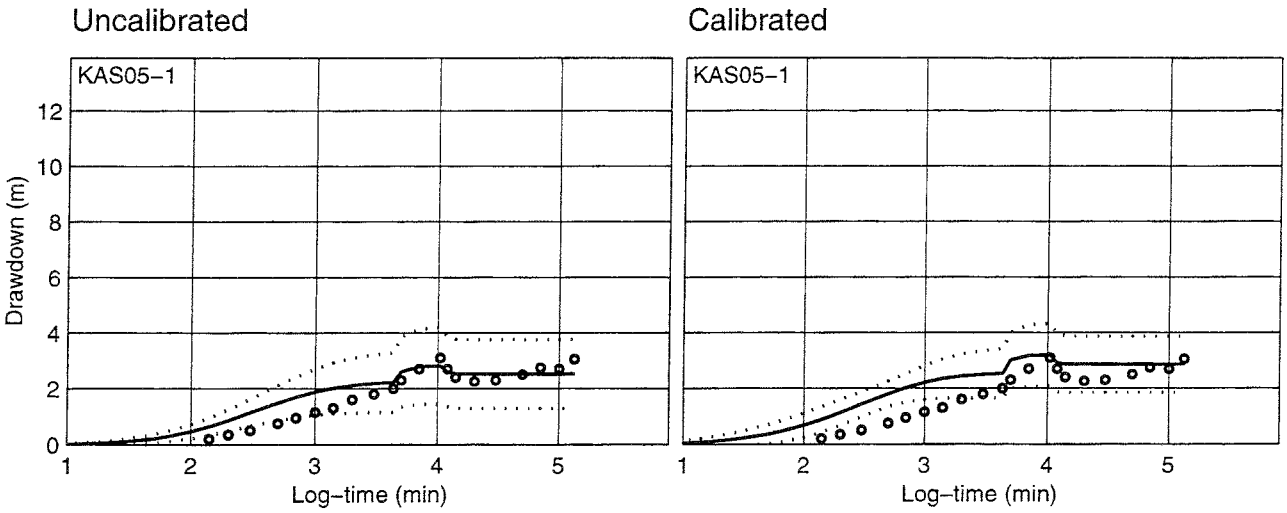

Mean Mean+–STD Measured

Dirichlet boundary condition on top

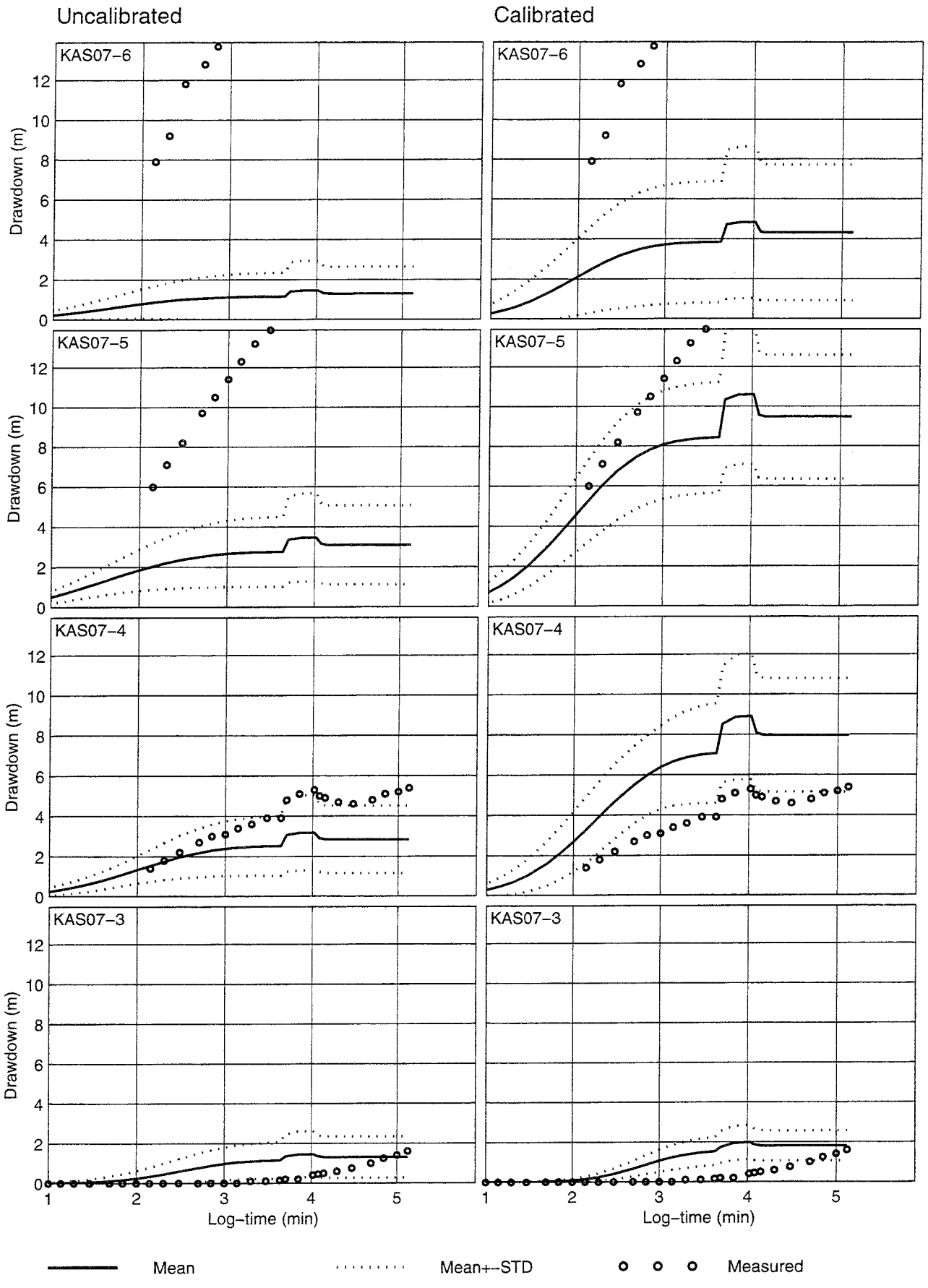

Dirichlet boundary condition on top

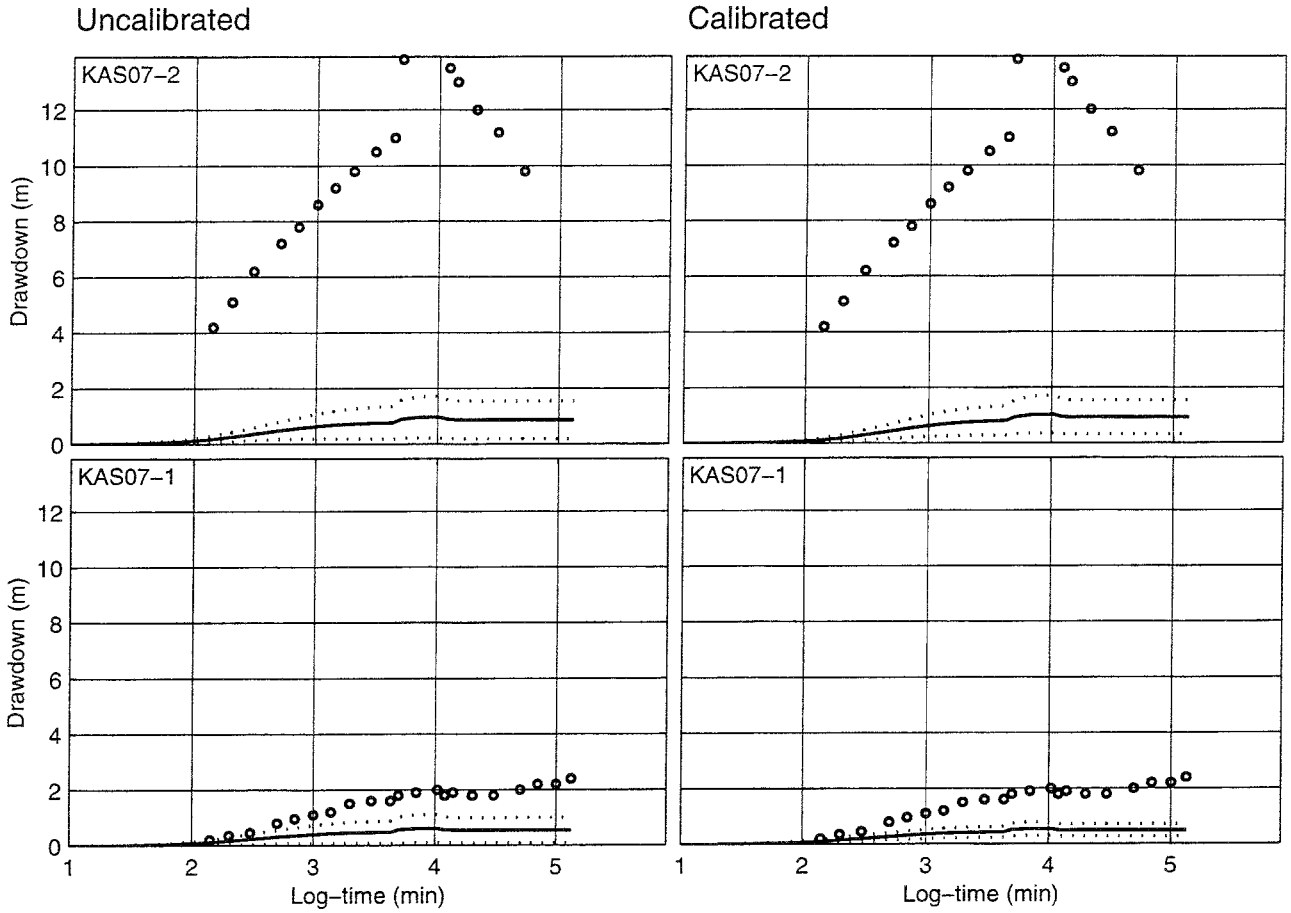

Mean Mean+–STD Measured

Dirichlet boundary condition on top

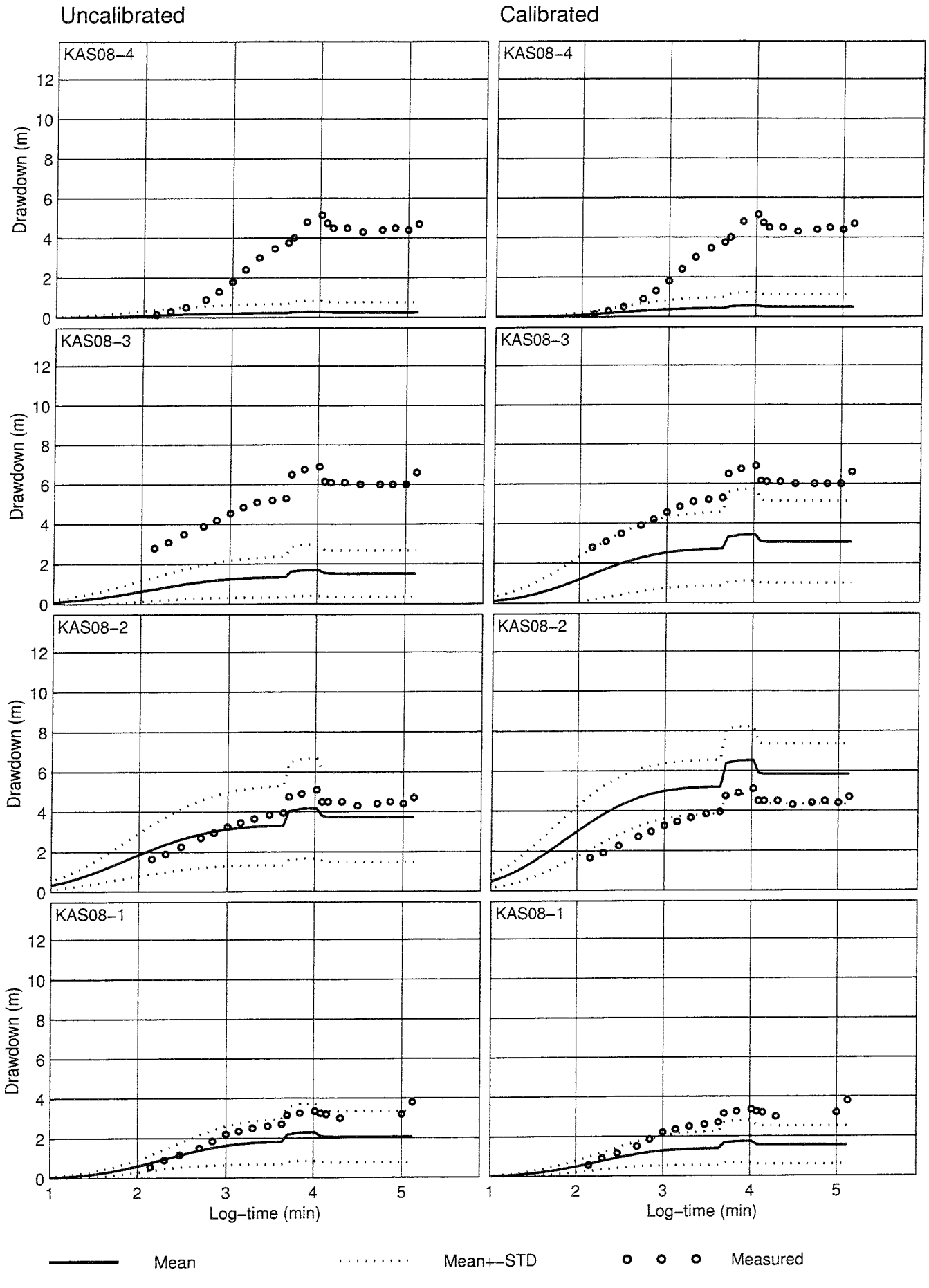

Dirichlet boundary condition on top

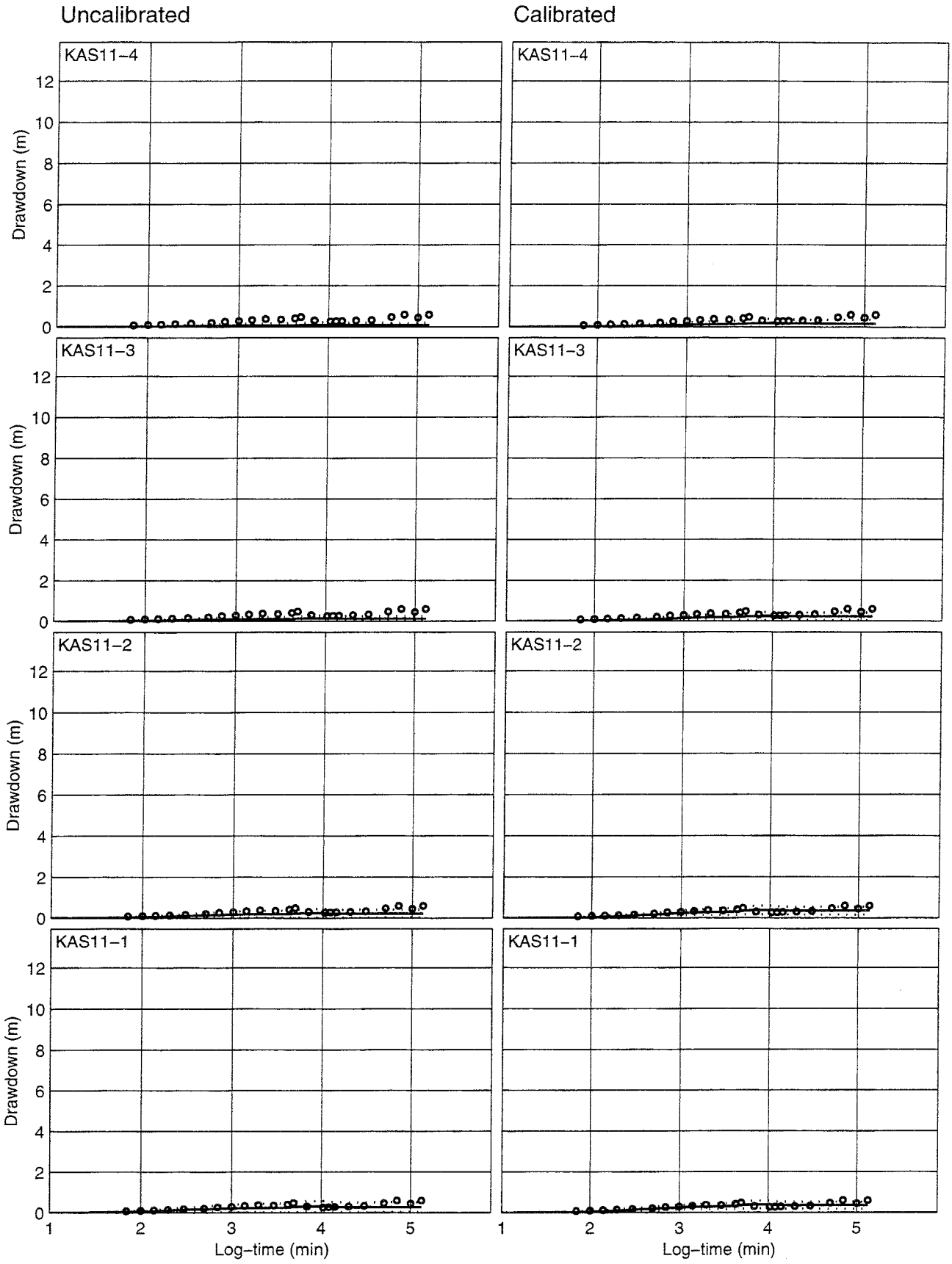

Dirichlet boundary condition on top

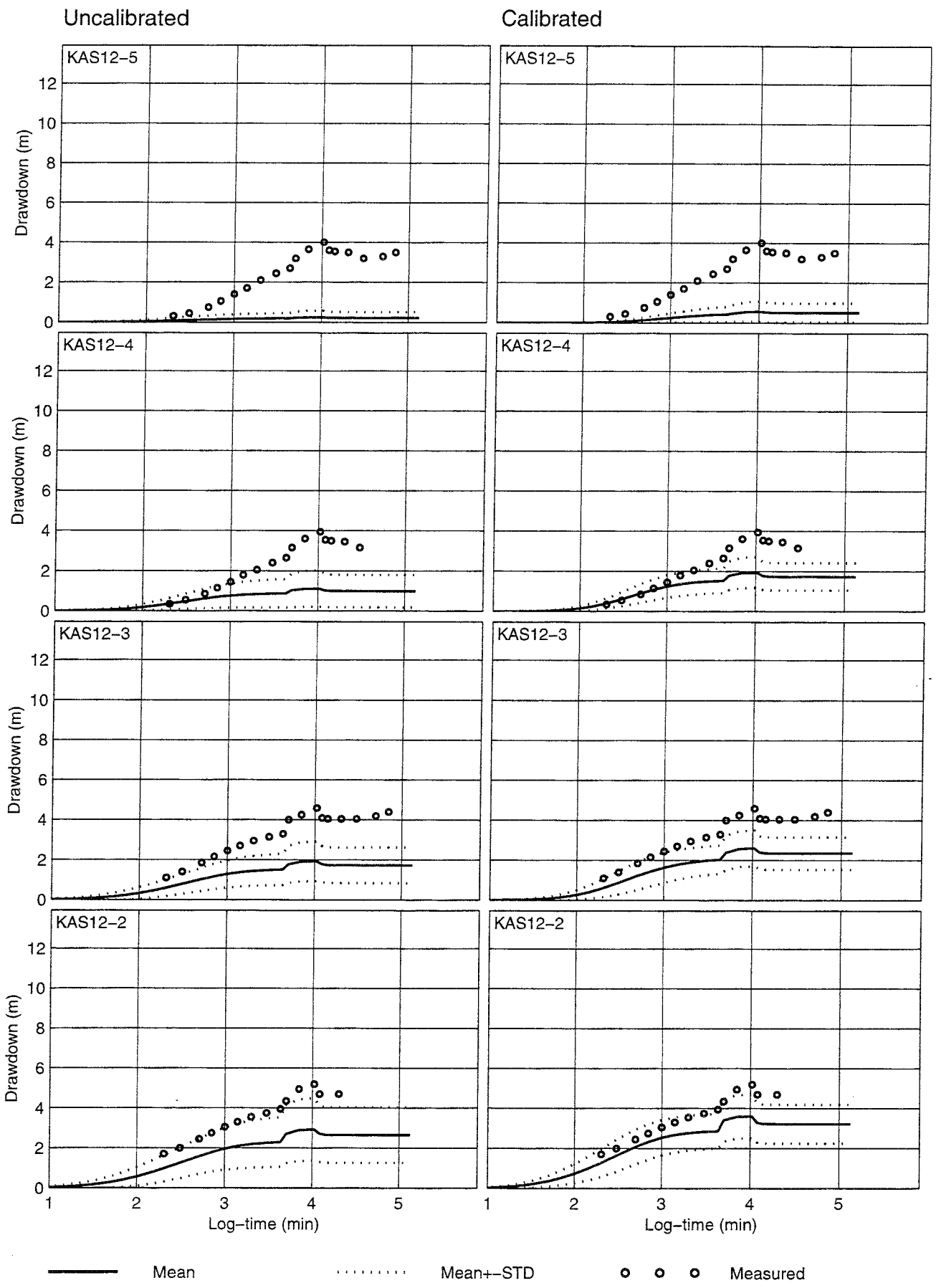

Dirichlet boundary condition on top

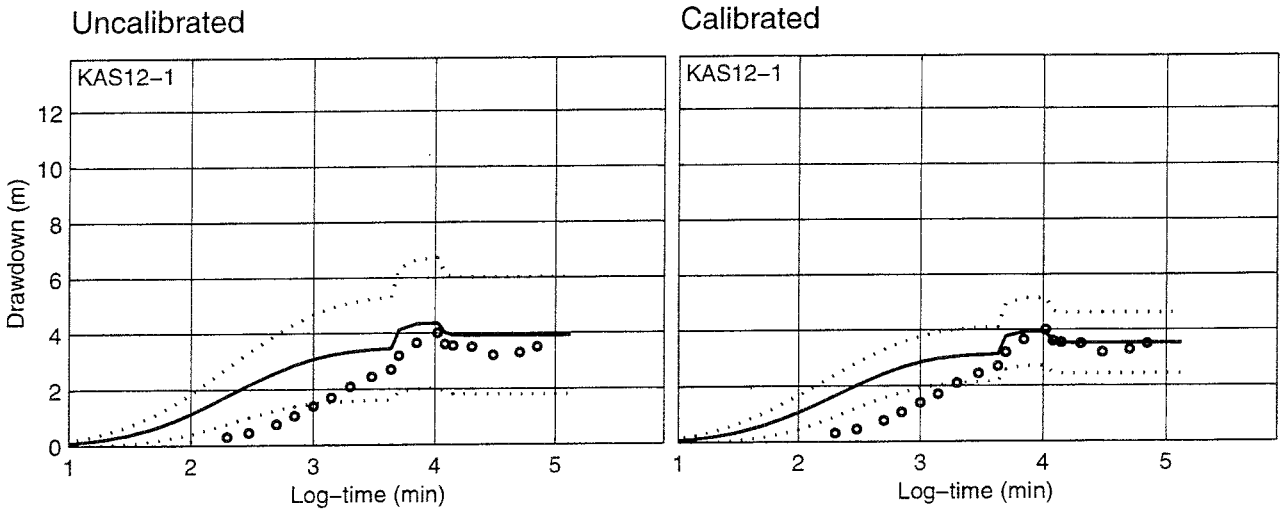

Mean Mean+-STD Measured

Dirichlet boundary condition on top

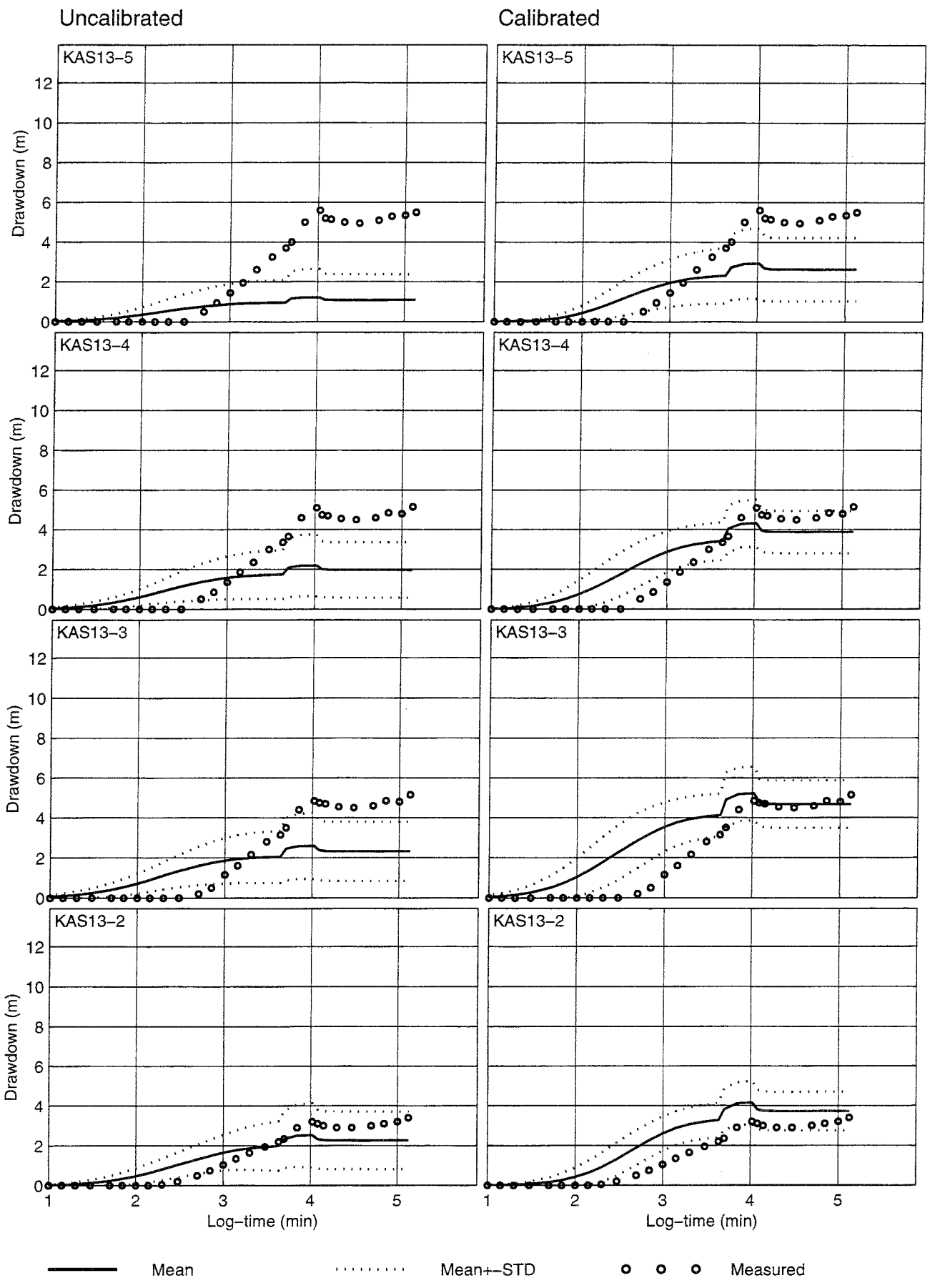

Dirichlet boundary condition on top

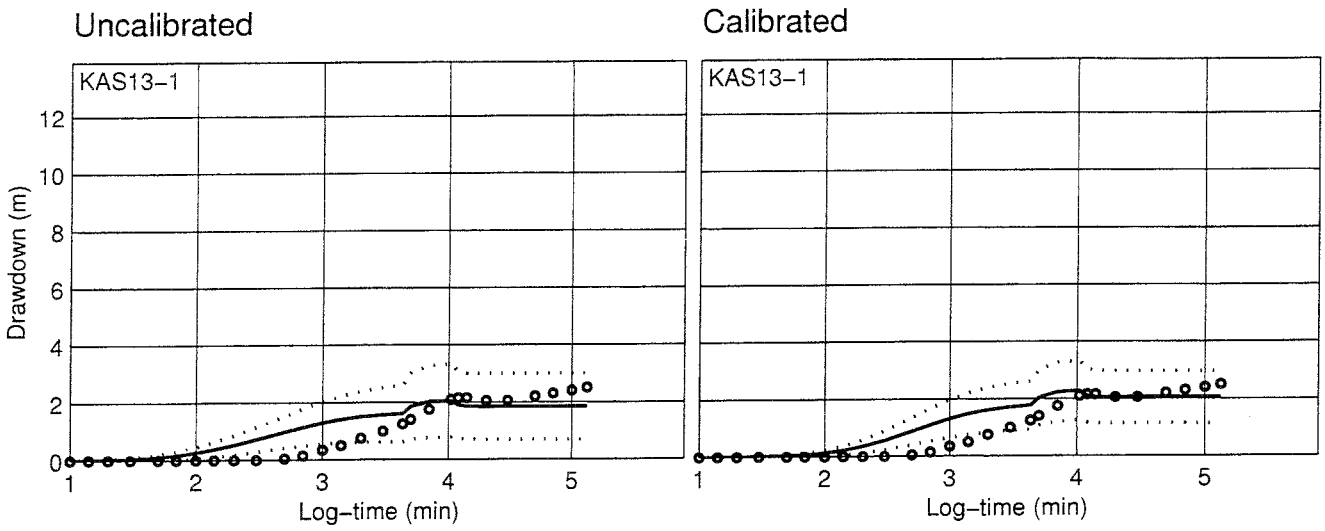

Mean Mean+-STD Measured

Dirichlet boundary condition on top

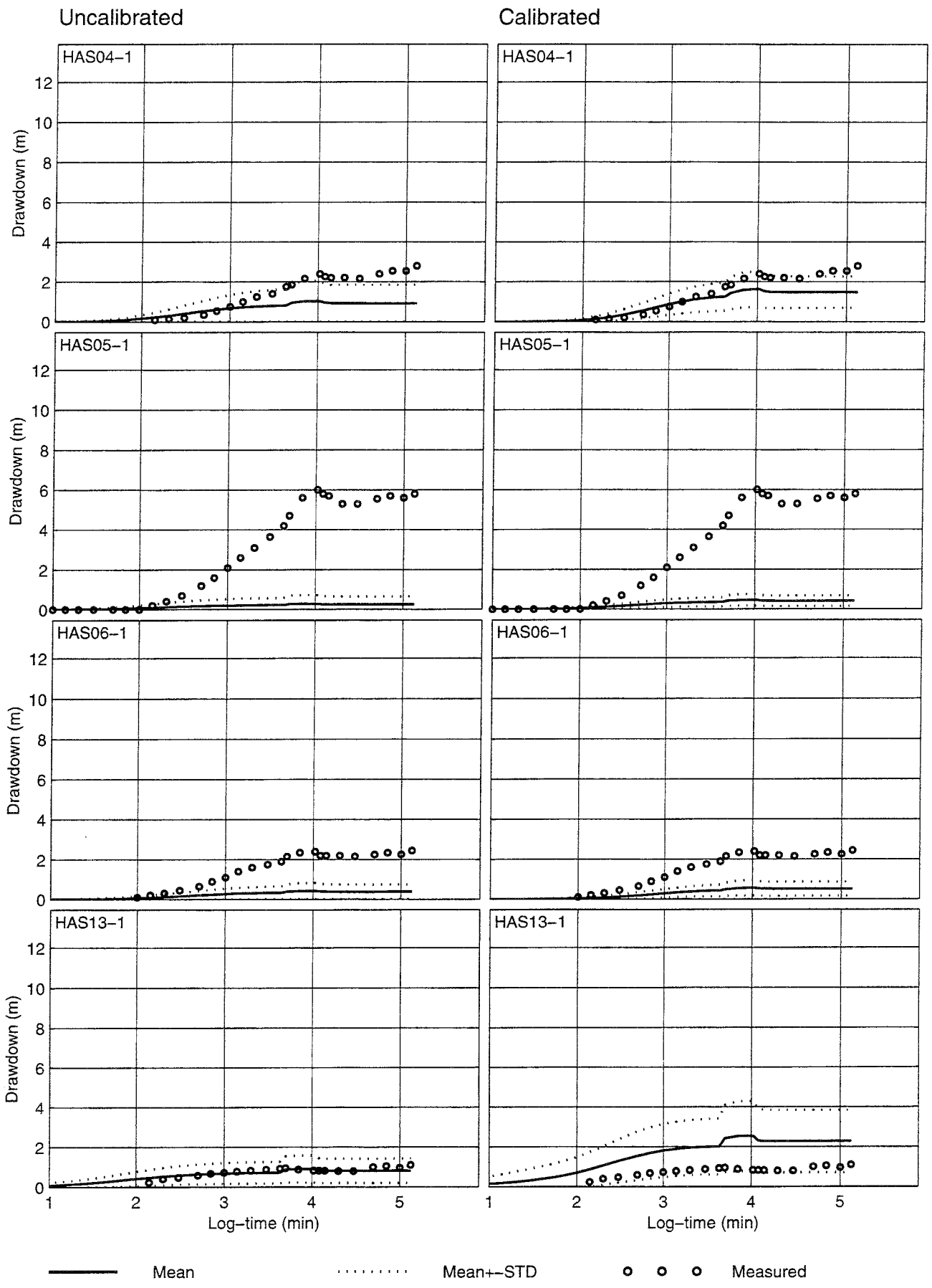

Dirichlet boundary condition on top

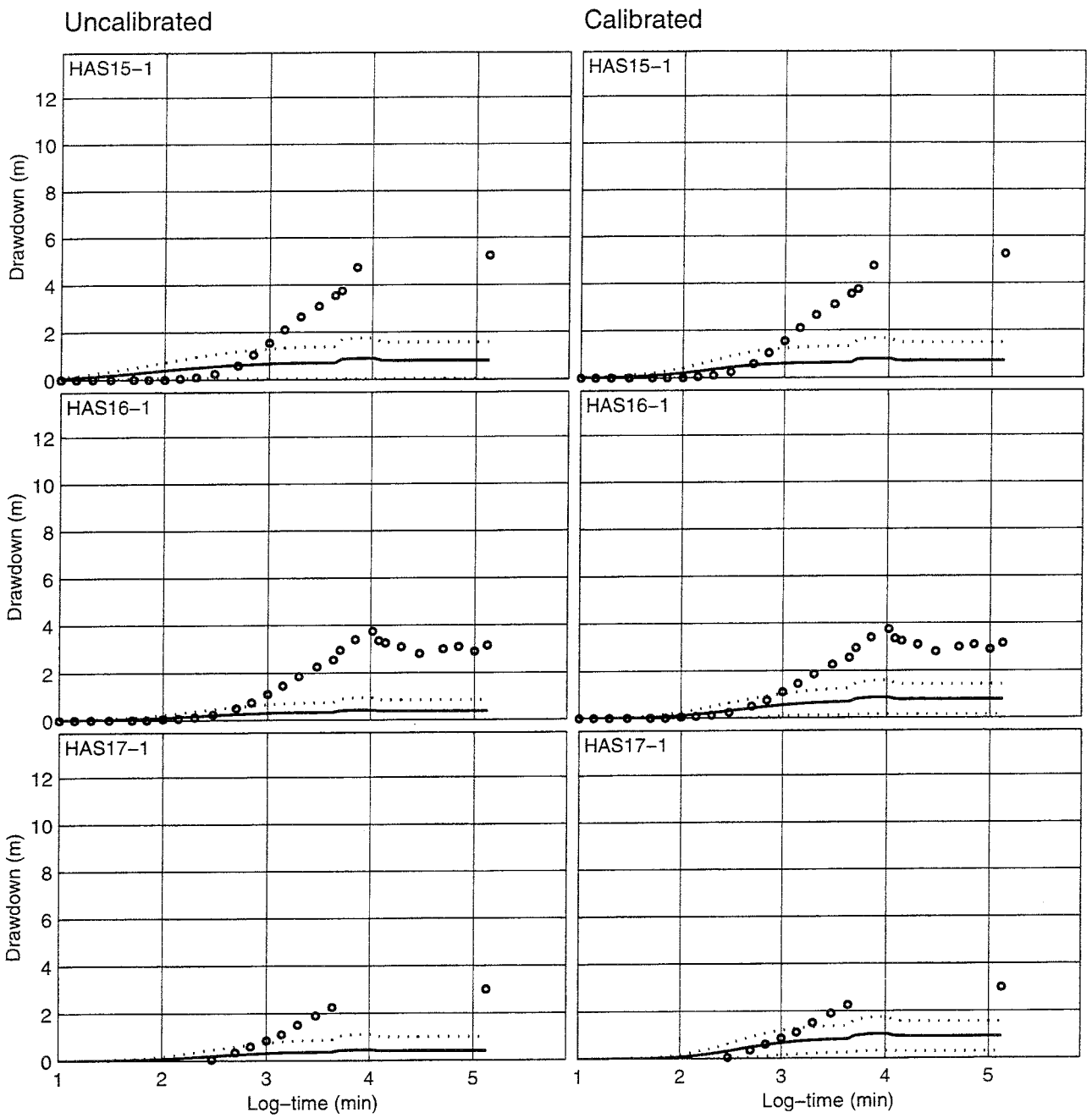

Dirichlet boundary condition on top

APPENDIX B. PRELIMINARY SIMULATION RESULTS: NEUMANN UPPER BOUNDARY CONDITION

This appendix presents 30 uncalibrated realisations in comparison to 39 uncalibrated realisations of the LPT2 model using a zero flux Neumann (Noflow) upper boundary condition. Three angled kriging neighbourhoods were used in the geostatistical simulation of the hydraulic conductivity fields, as described in Section 3.5.5. These simulations are described in detail in Section 3.5.5 of this report.

Note: The packed-off sections of the boreholes are numbered from the bottom of the hole to the top (i.e., KAS05-5 is the uppermost section in KAS05, and KAS05-1 is the lowest section). Wells designated HAS are shallow percussion-drilled boreholes with only one observation section each. The observed data reported here are taken from Rhén et al. (1992), without modification. No measurements were given for section KAS03-6, and only the final measurement of 4.97m of drawdown was given for KAS05-4.

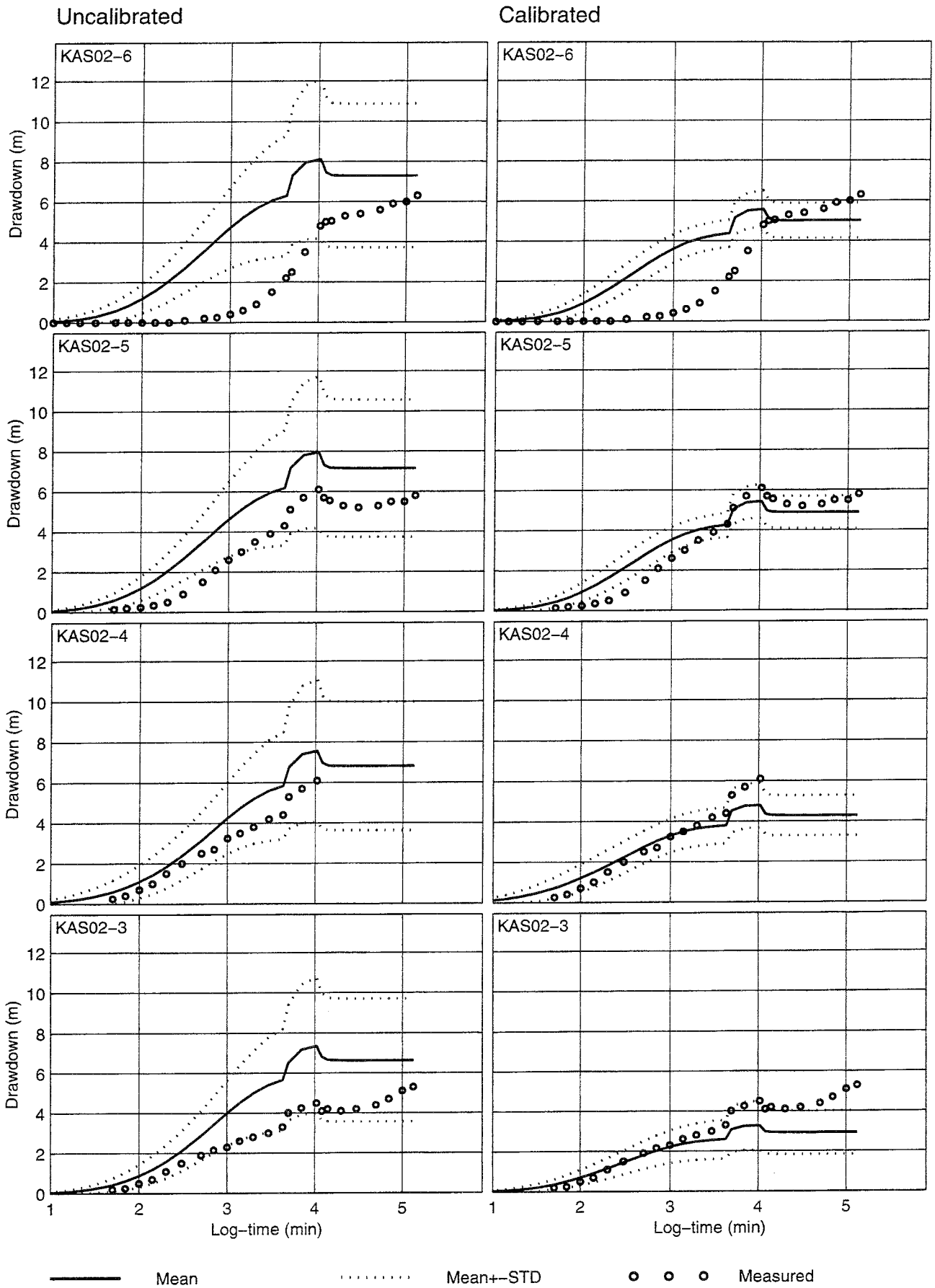

Noflow boundary condition on top

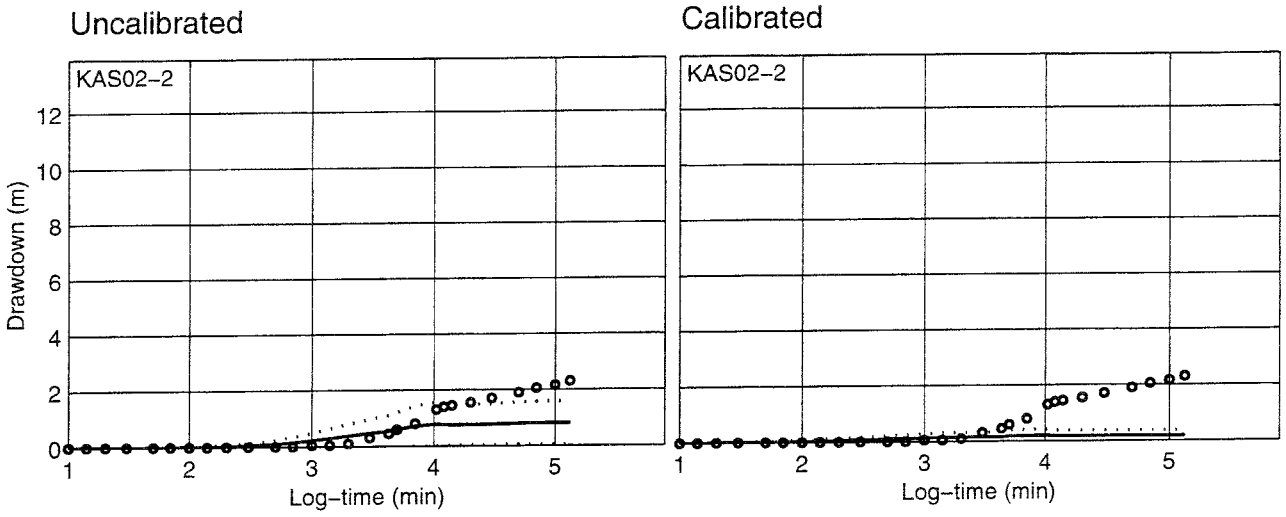

——— Mean ····· Mean+-STD o o o Measured

Noflow boundary condition on top

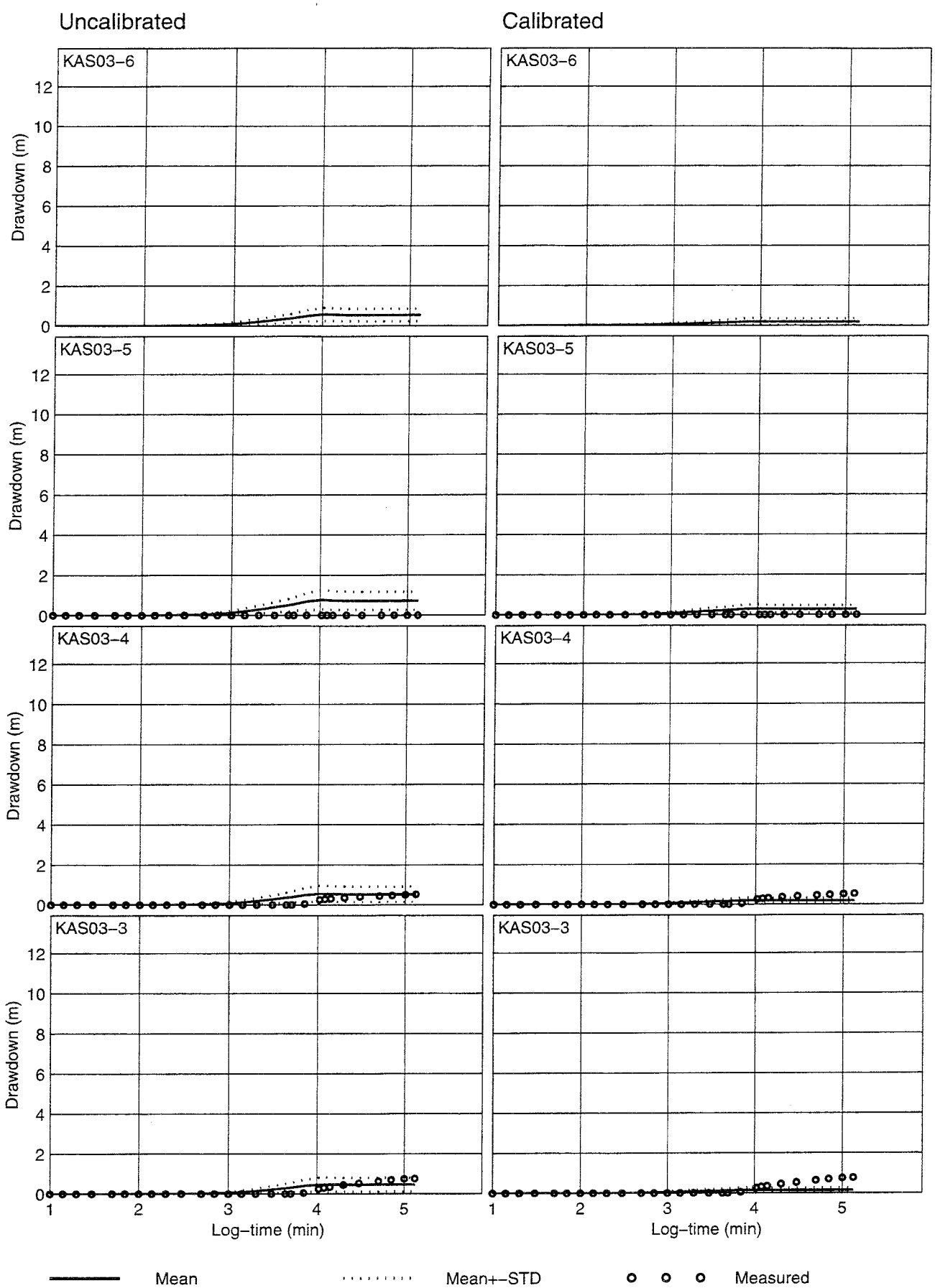

Noflow boundary condition on top

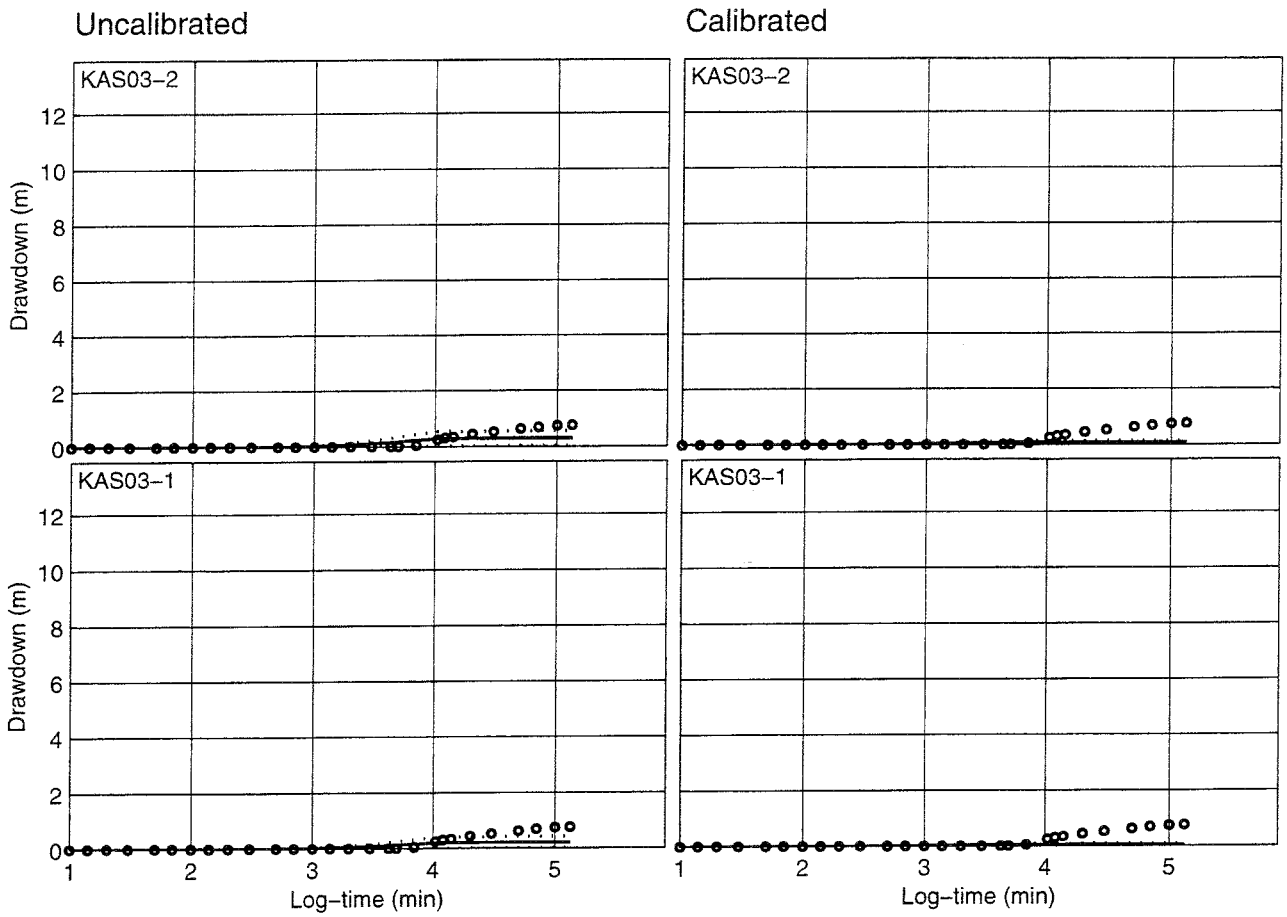

Mean Mean+–STD Measured

Noflow boundary condition on top

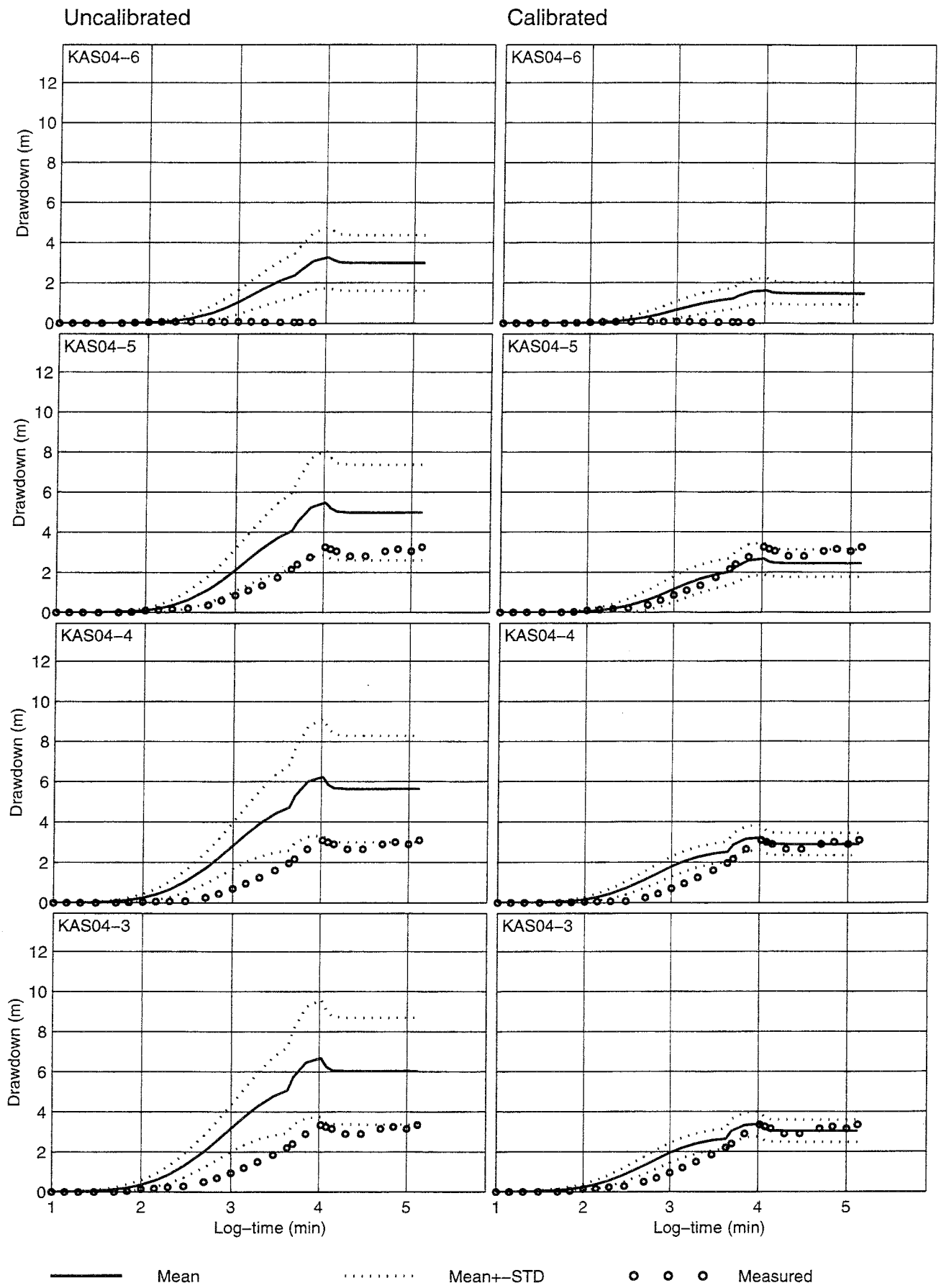

Noflow boundary condition on top

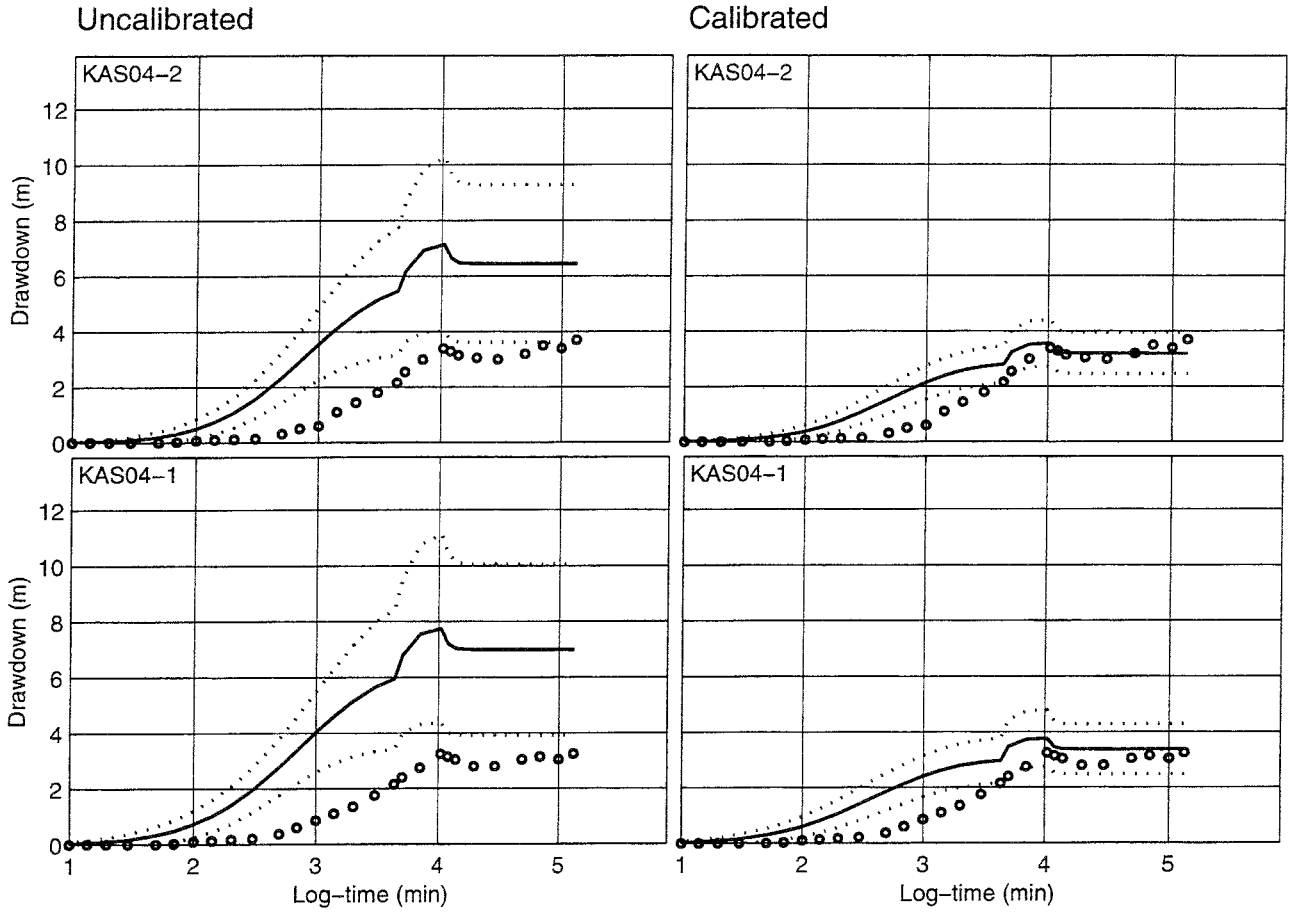

Mean Mean+–STD Measured

Noflow boundary condition on top

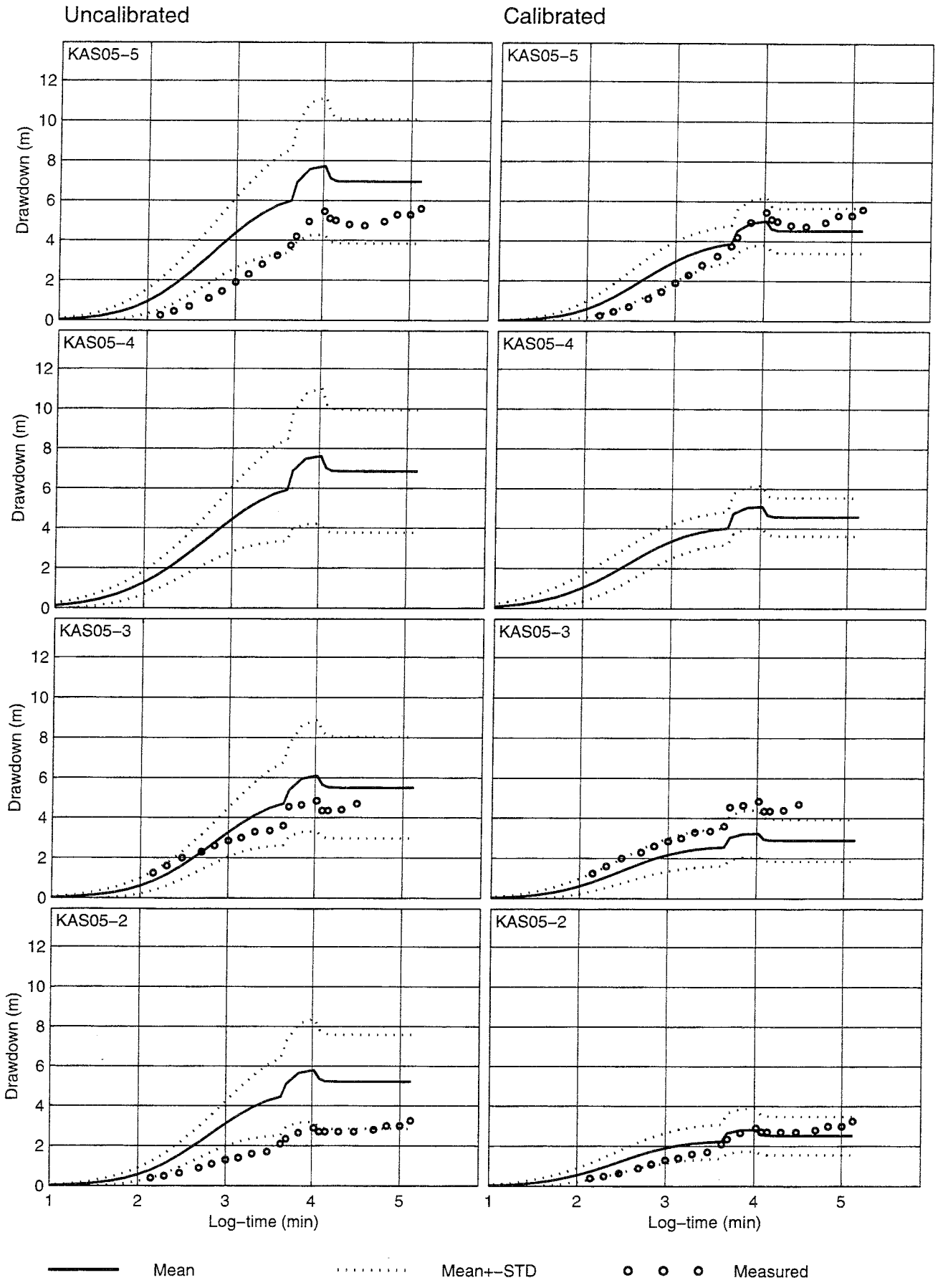

Noflow boundary condition on top

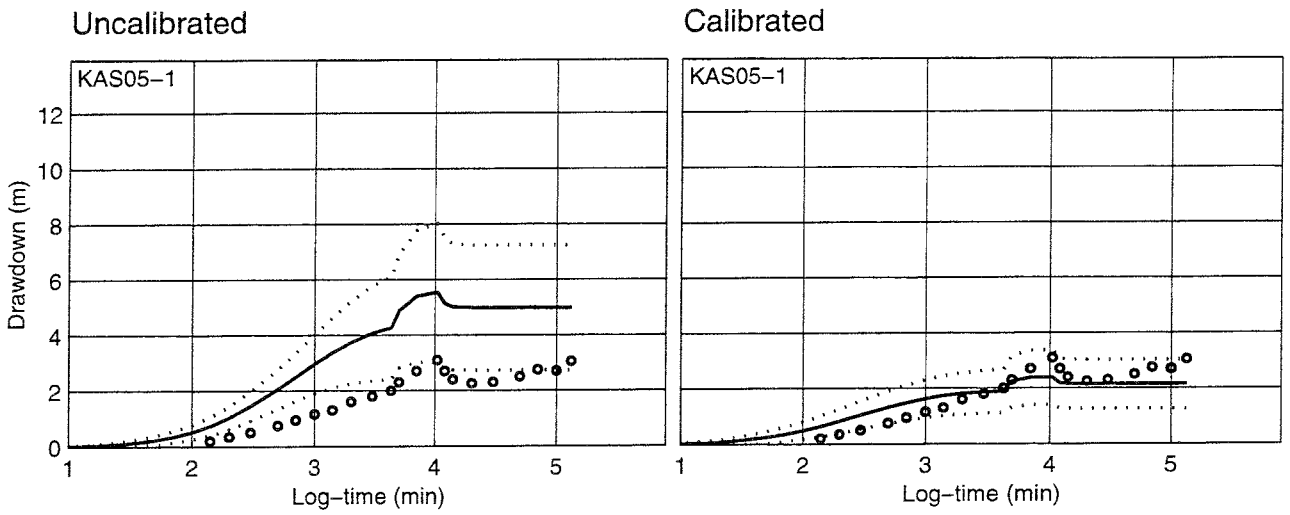

Mean Mean+–STD Measured

Noflow boundary condition on top

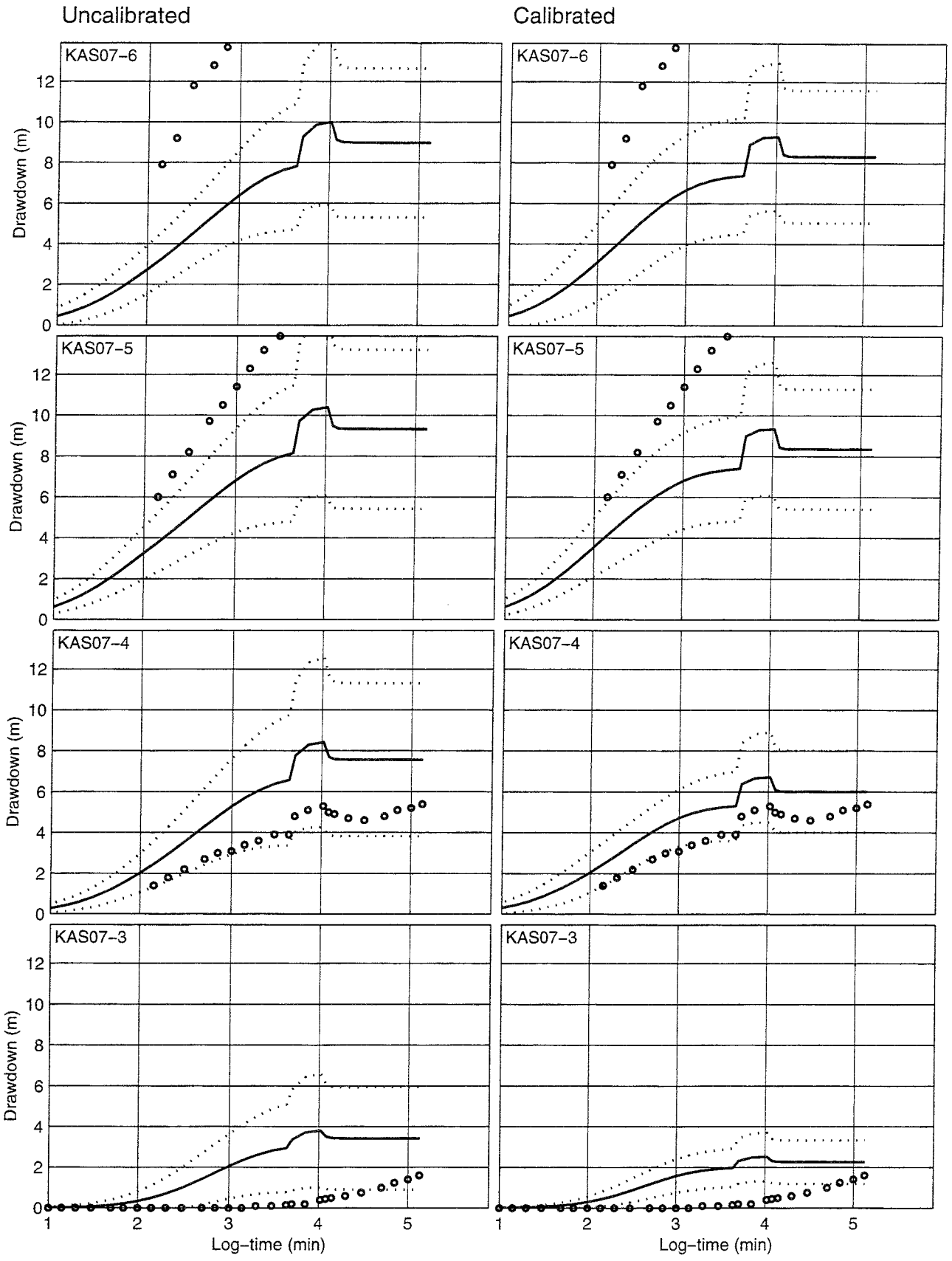

Noflow boundary condition on top

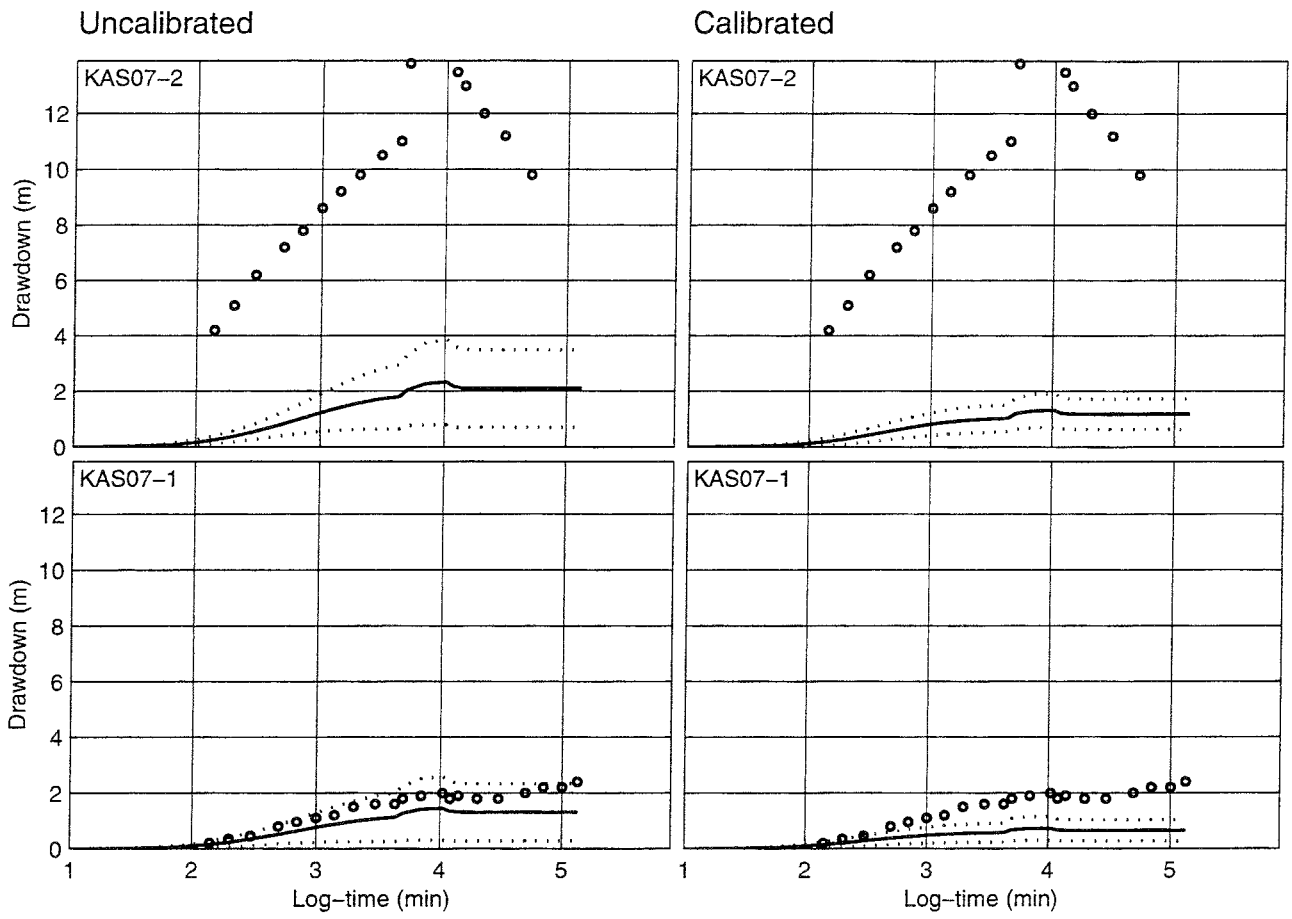

Mean Mean+–STD Measured

Noflow boundary condition on top

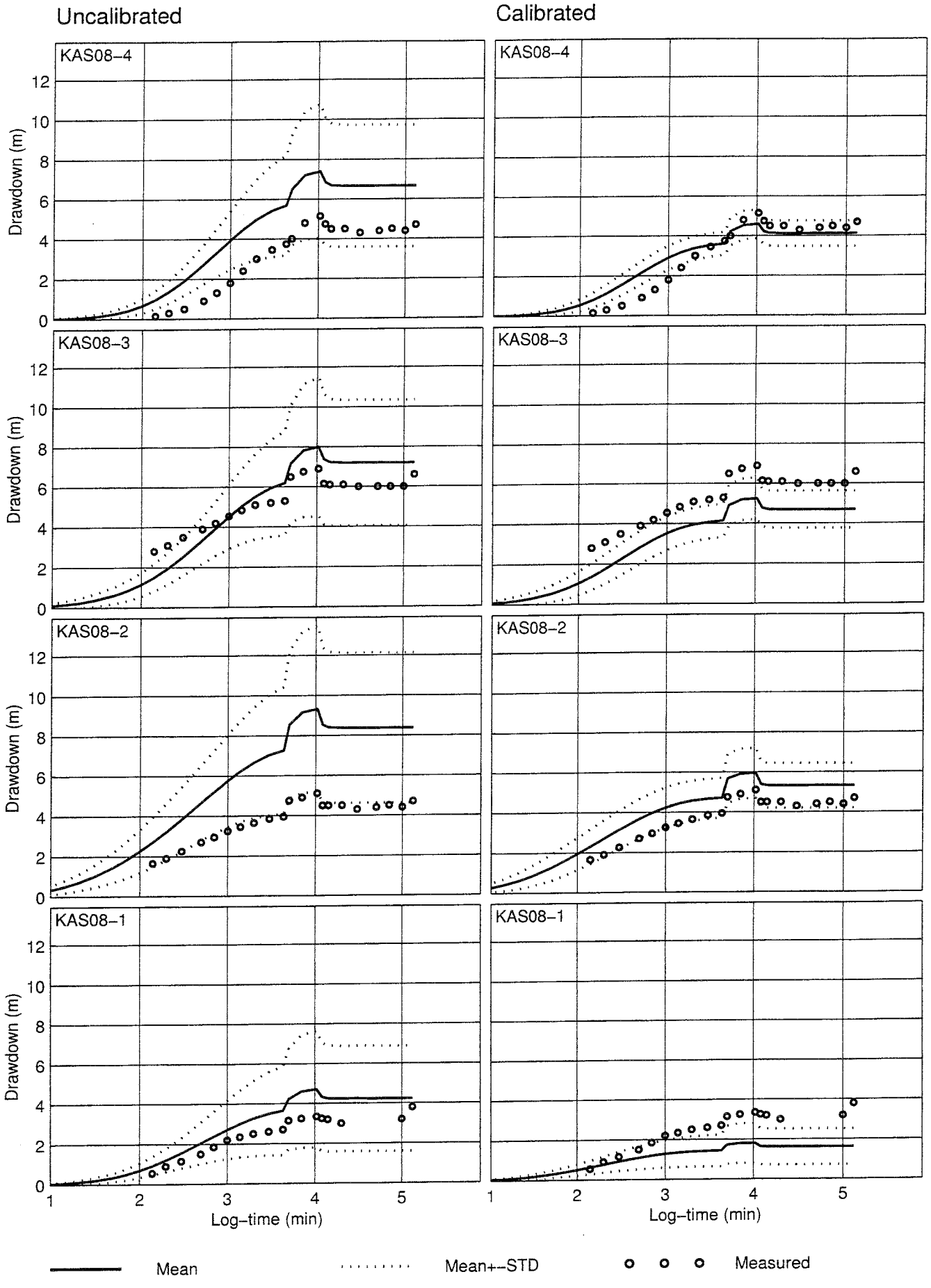

Noflow boundary condition on top

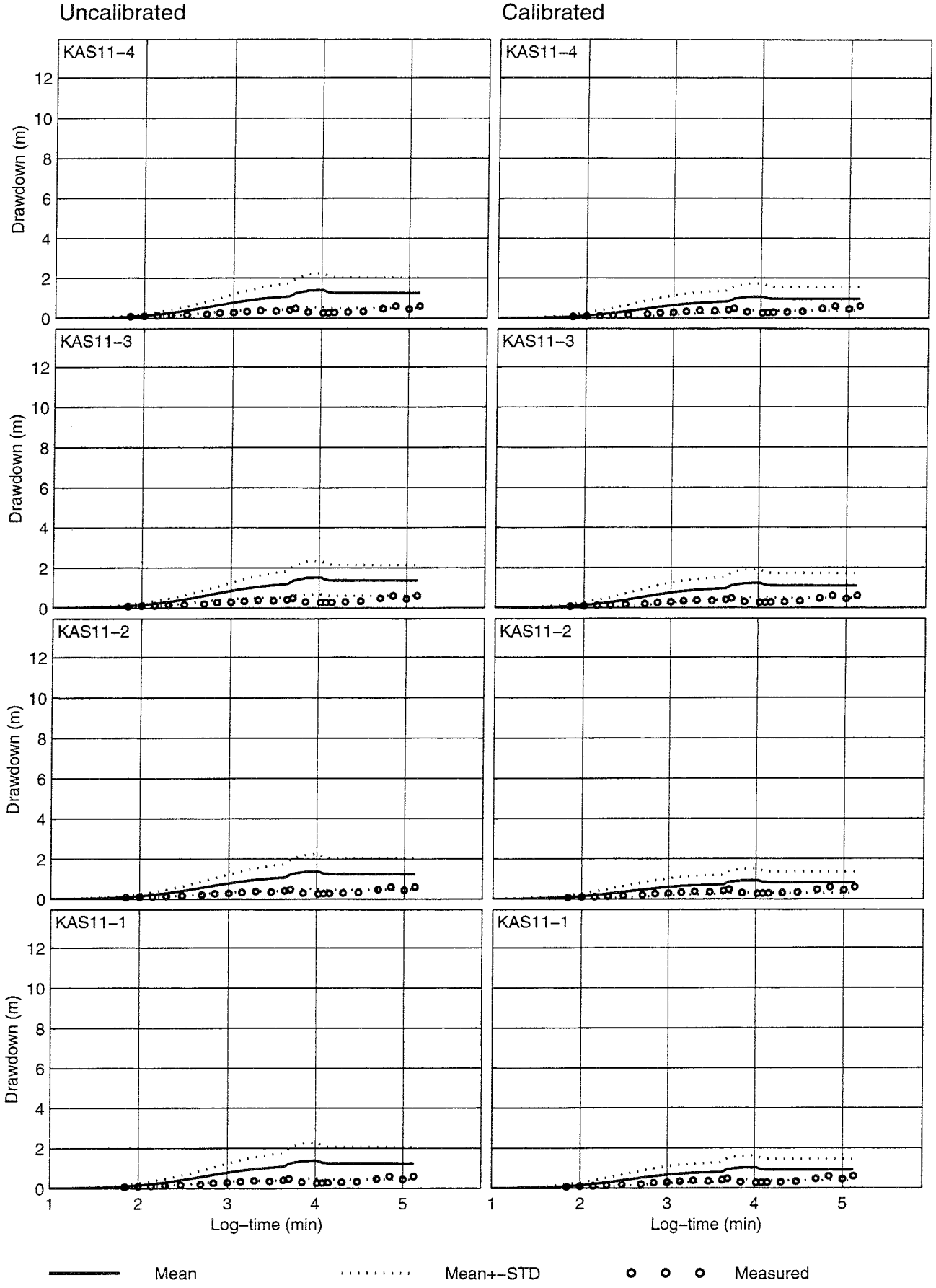

Noflow boundary condition on top

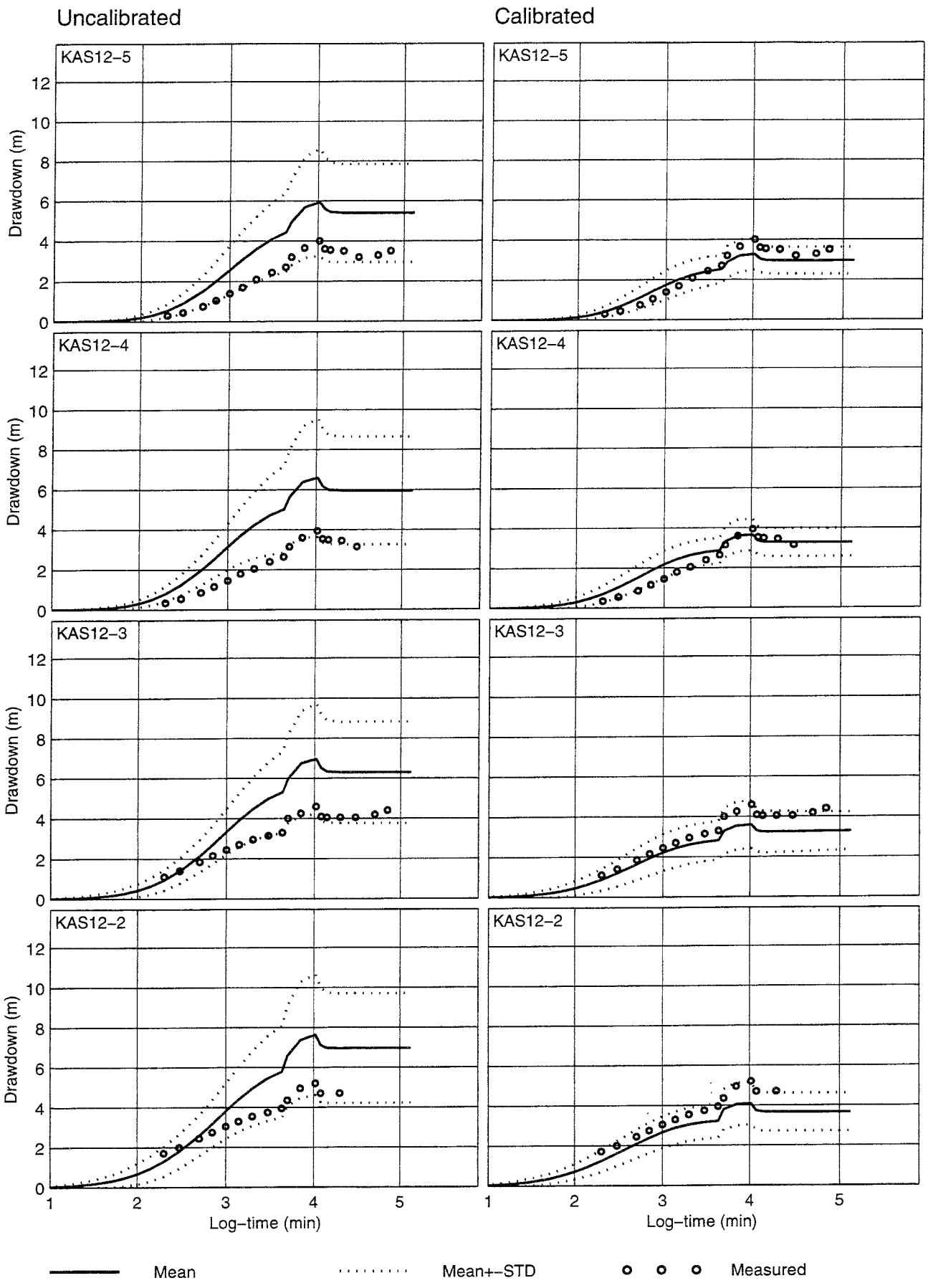

Noflow boundary condition on top

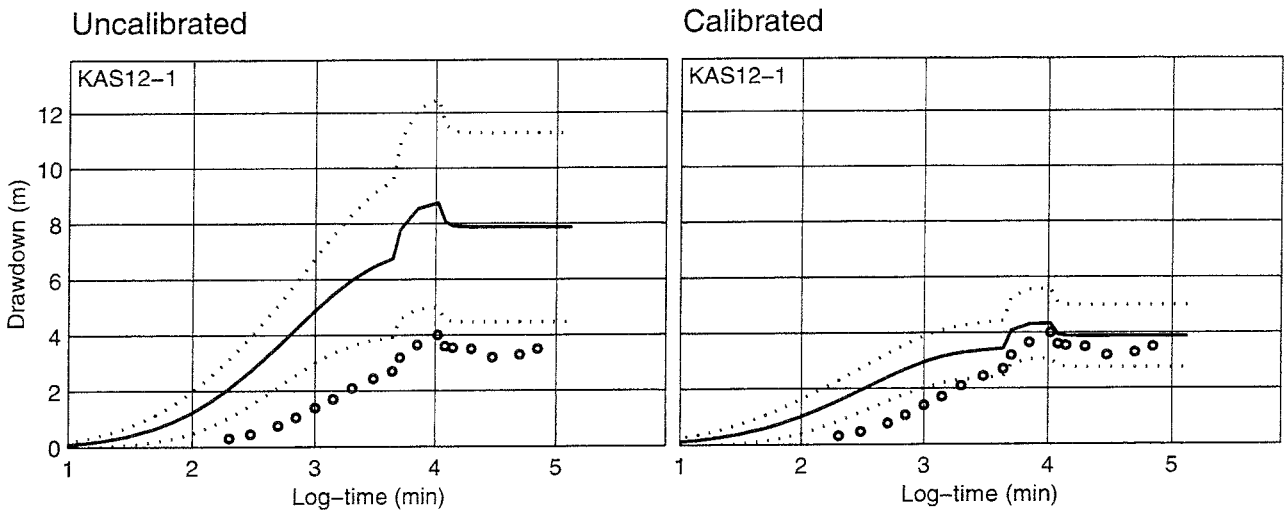

Mean Mean+-STD Measured

Noflow boundary condition on top

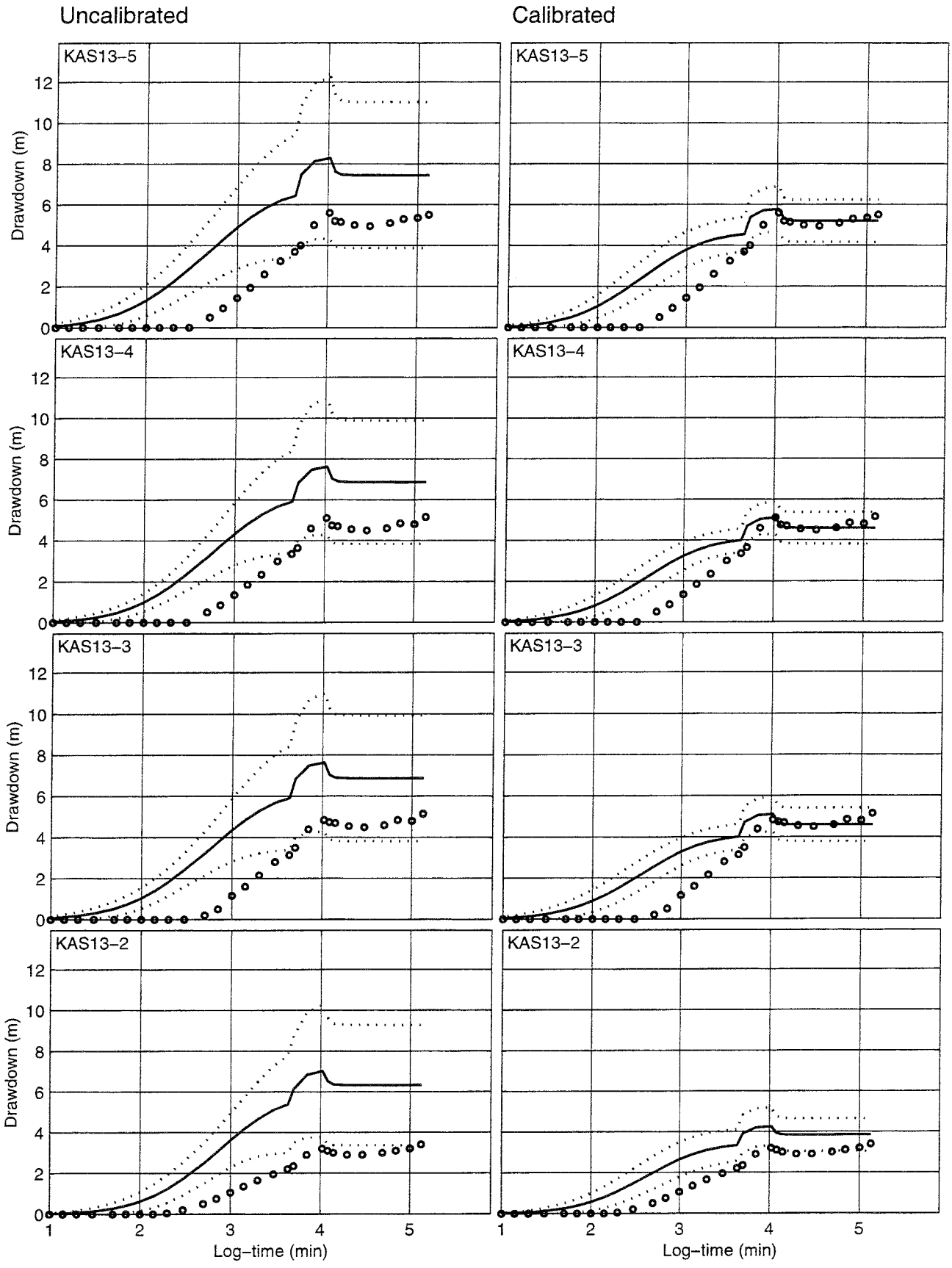

Noflow boundary condition on top

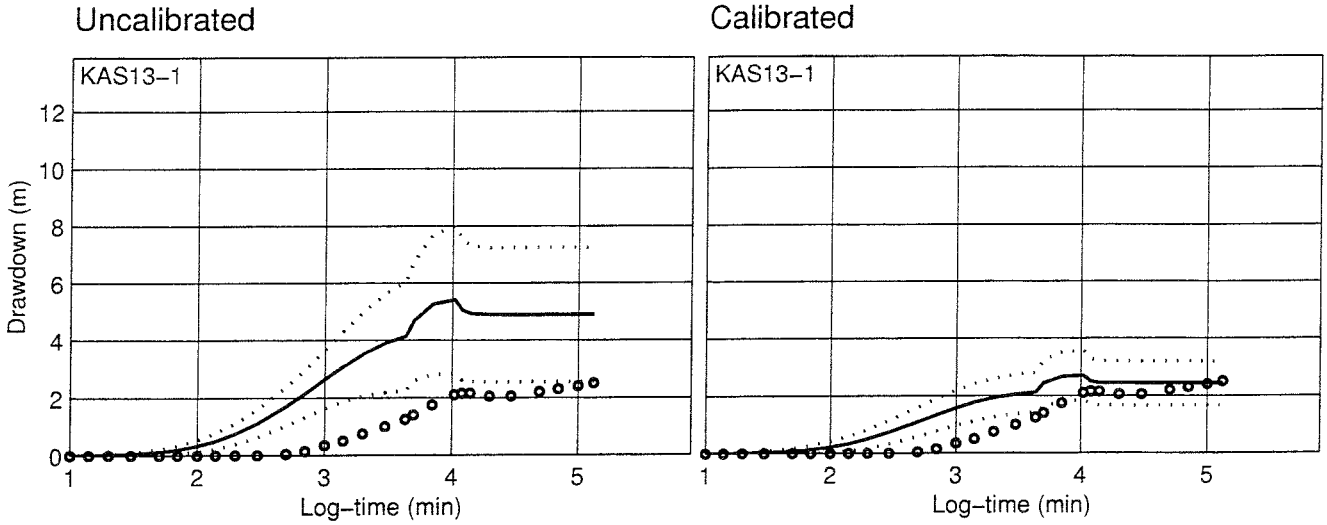

Mean Mean+–STD Measured

Noflow boundary condition on top

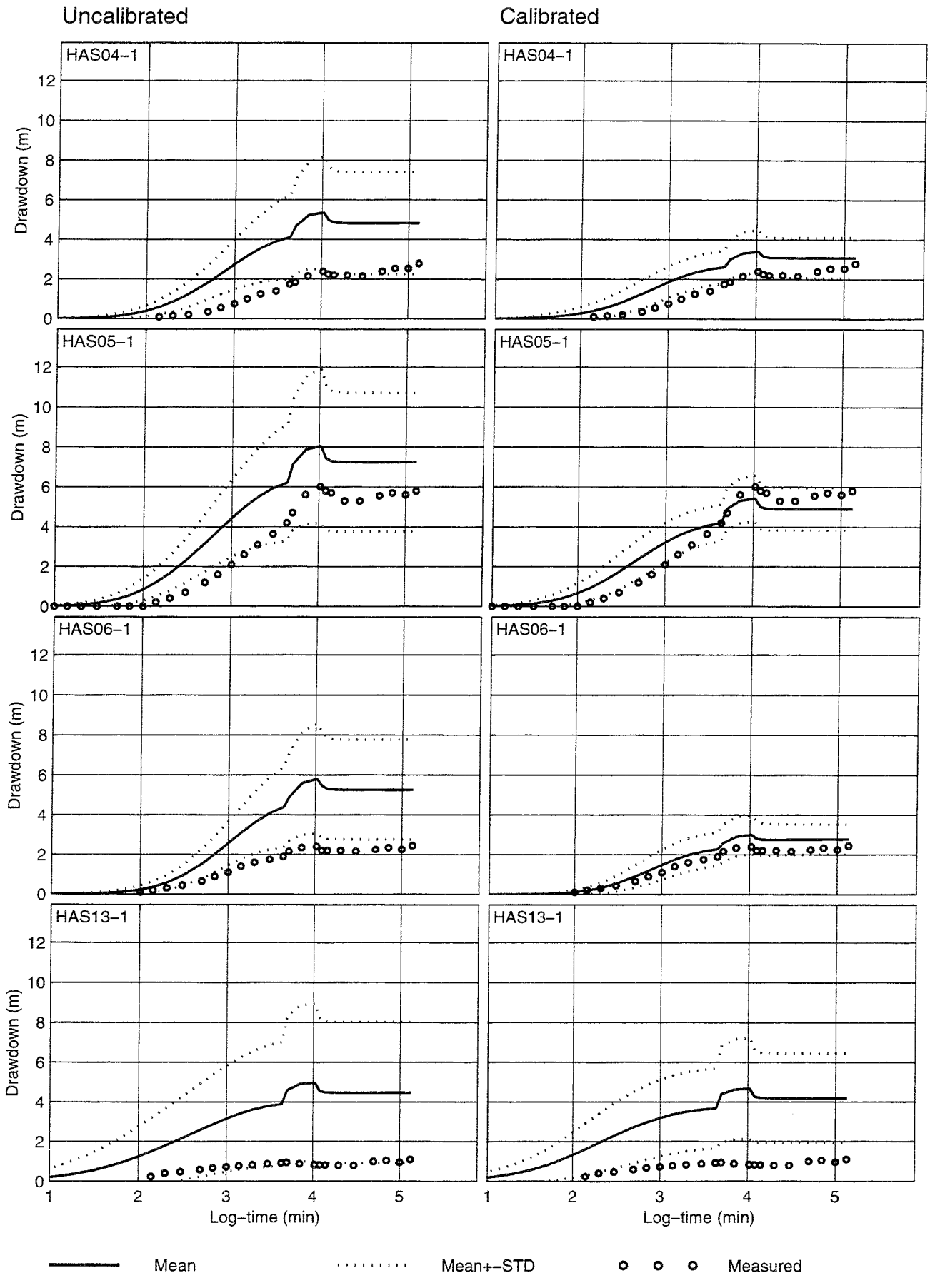

Noflow boundary condition on top

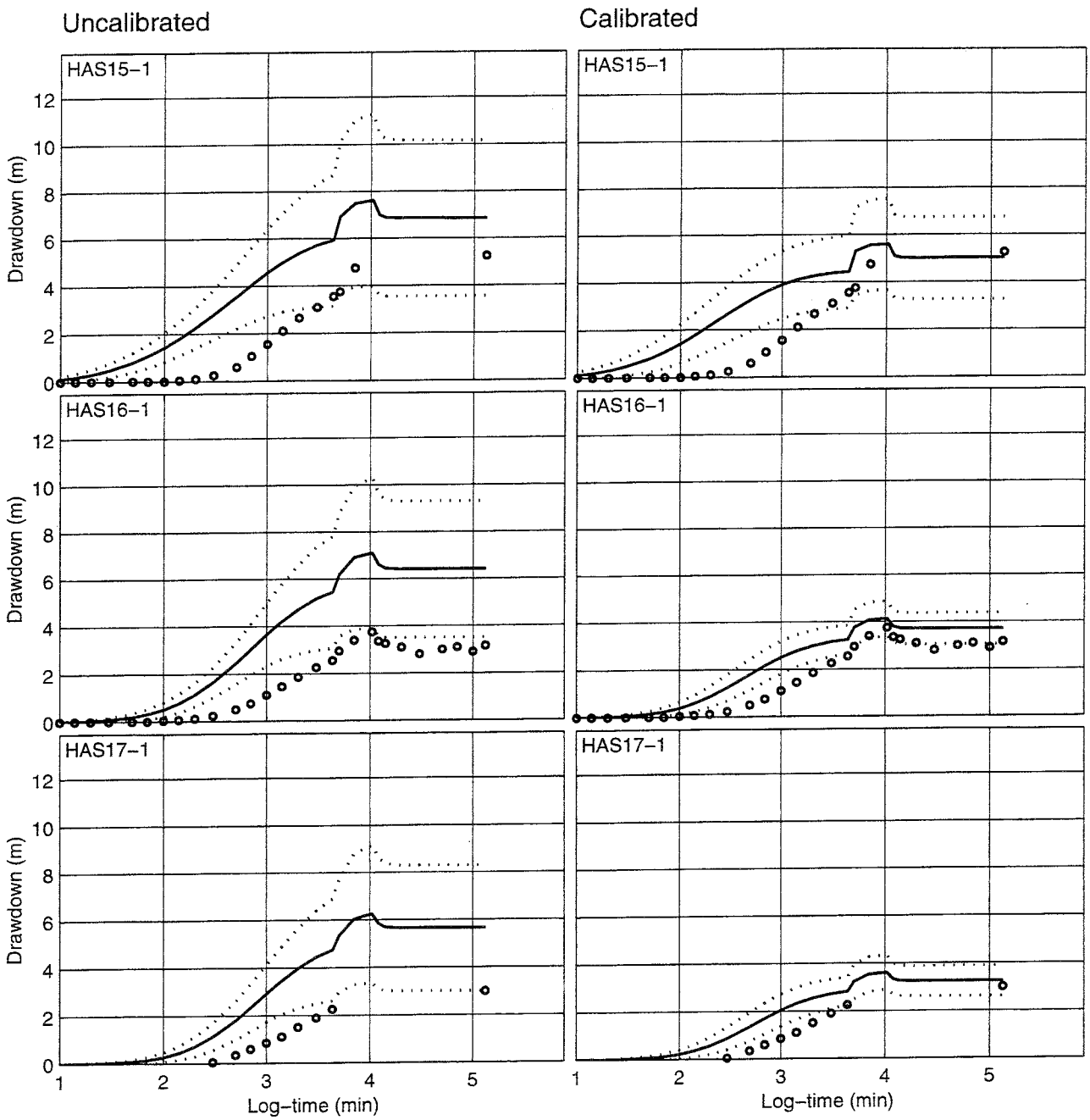

Noflow boundary condition on top

APPENDIX C. UNCALIBRATED VS. CALIBRATED SIMULATION RESULTS

This appendix presents 30 uncalibrated realisations in comparison to 30 calibrated realisations of the LPT2 model using a zero flux Neumann (Noflow) upper boundary condition. One kriging neighbourhood was used in the geostatistical simulation of the hydraulic conductivity fields, as described in Section 3.5.5. These simulations are described in detail in Sections 4 and 5 of this report.

Note: The packed-off sections of the boreholes are numbered from the bottom of the hole to the top (i.e., KAS05-5 is the uppermost section in KAS05, and KAS05-1 is the lowest section). Wells designated HAS are shallow percussion-drilled boreholes with only one observation section each. The observed data reported here are taken from Rhén et al. (1992), without modification. No measurements were given for section KAS03-6, and only the final measurement of 4.97m of drawdown was given for KAS05-4.

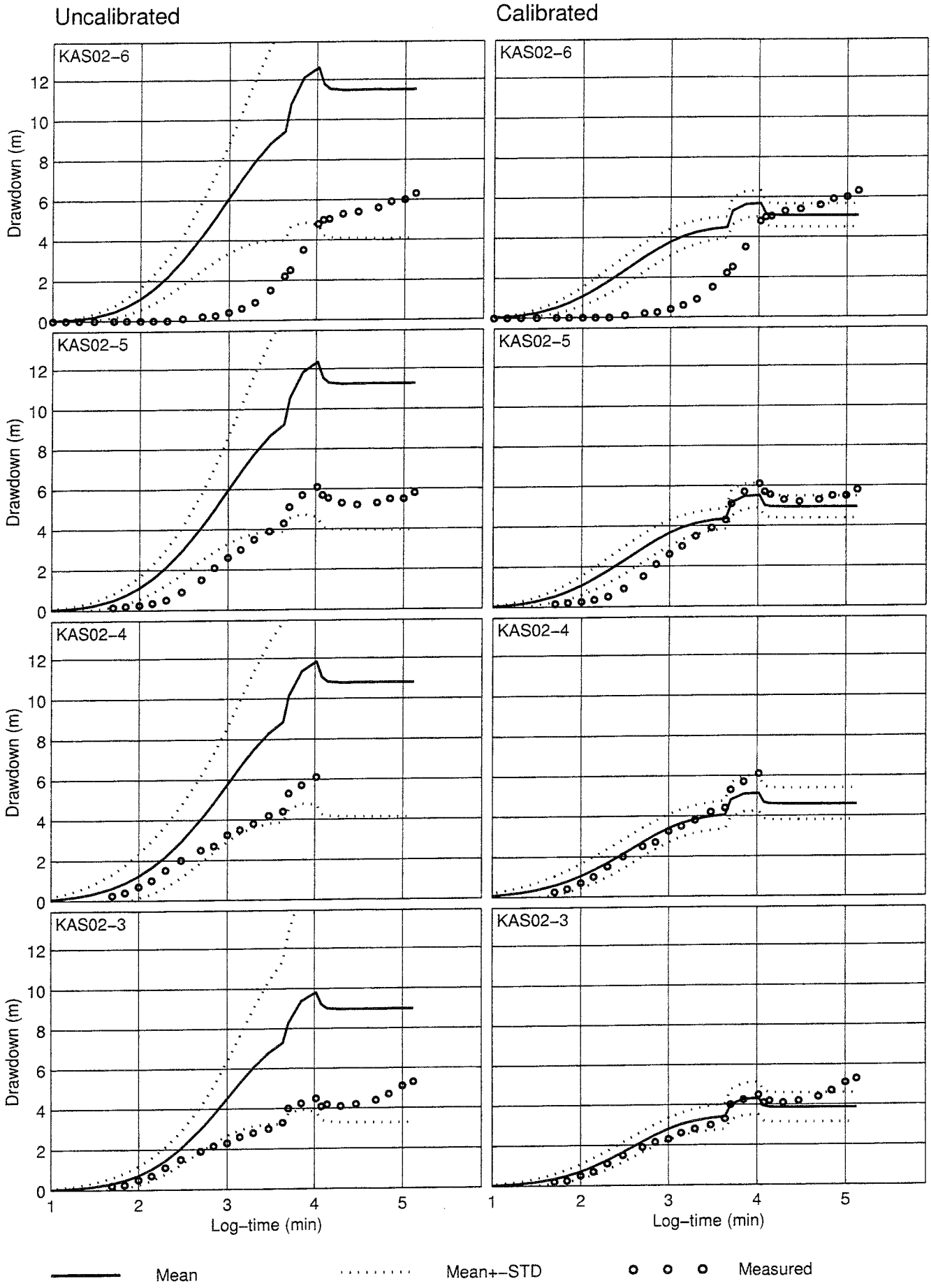

Noflow boundary condition on top, one kriging neighbourhood

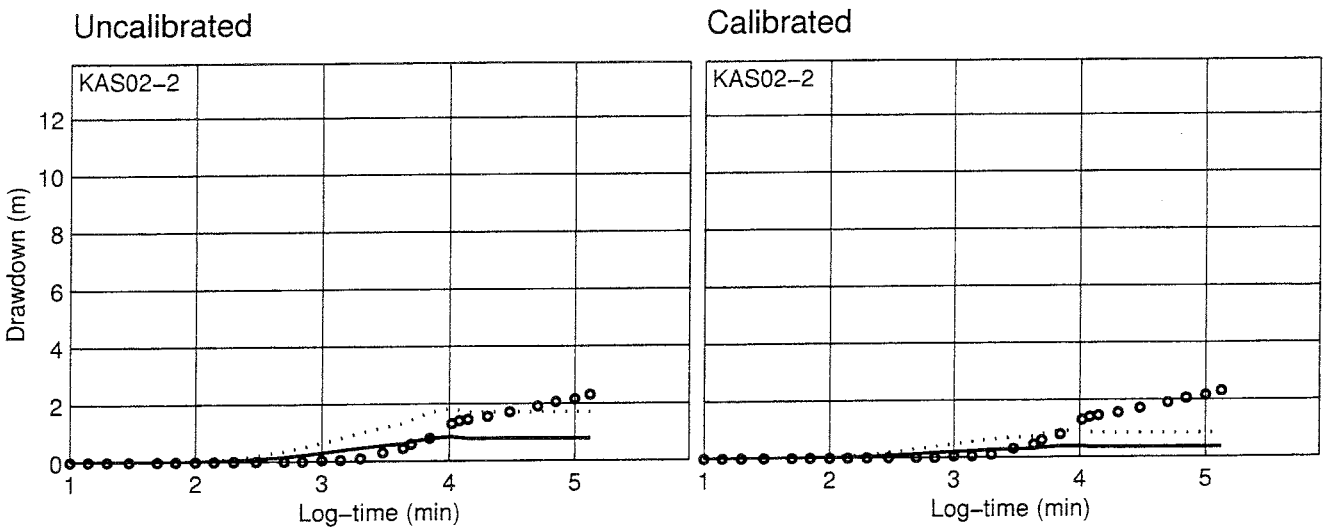

Mean Mean+-STD Measured

Noflow boundary condition on top, one kriging neighbourhood

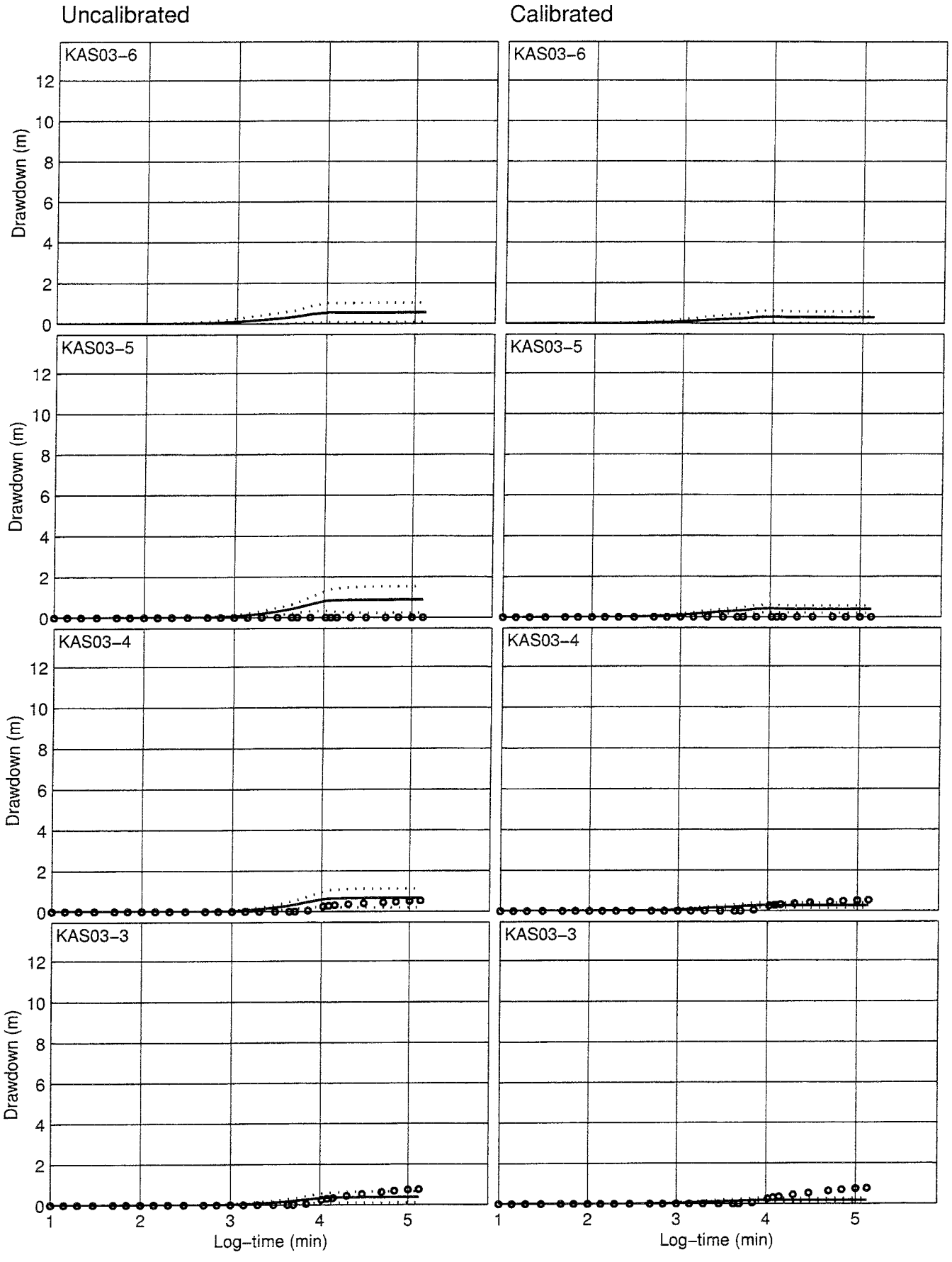

Noflow boundary condition on top, one kriging neighbourhood

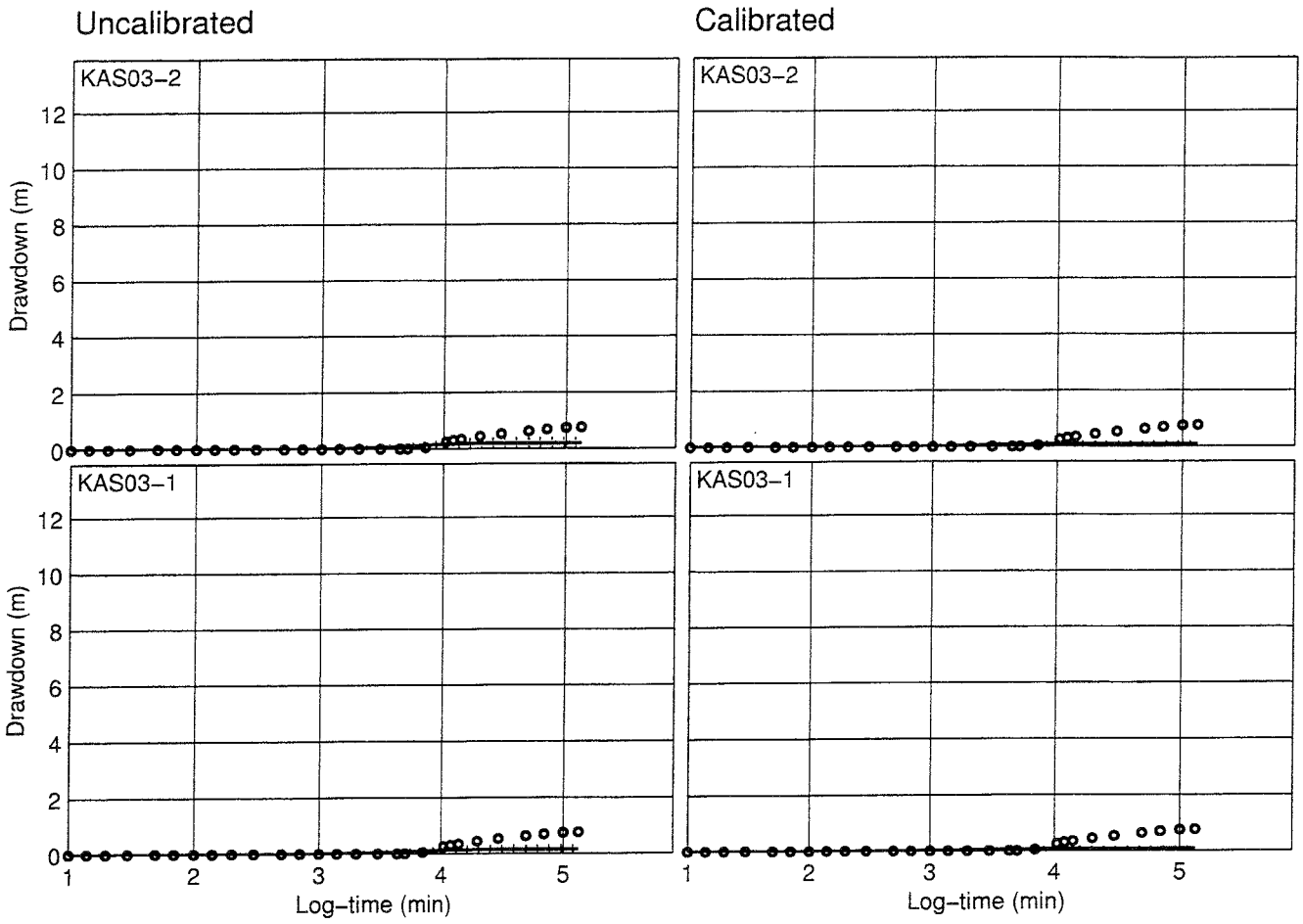

Mean Mean+–STD Measured

Noflow boundary condition on top, one kriging neighbourhood

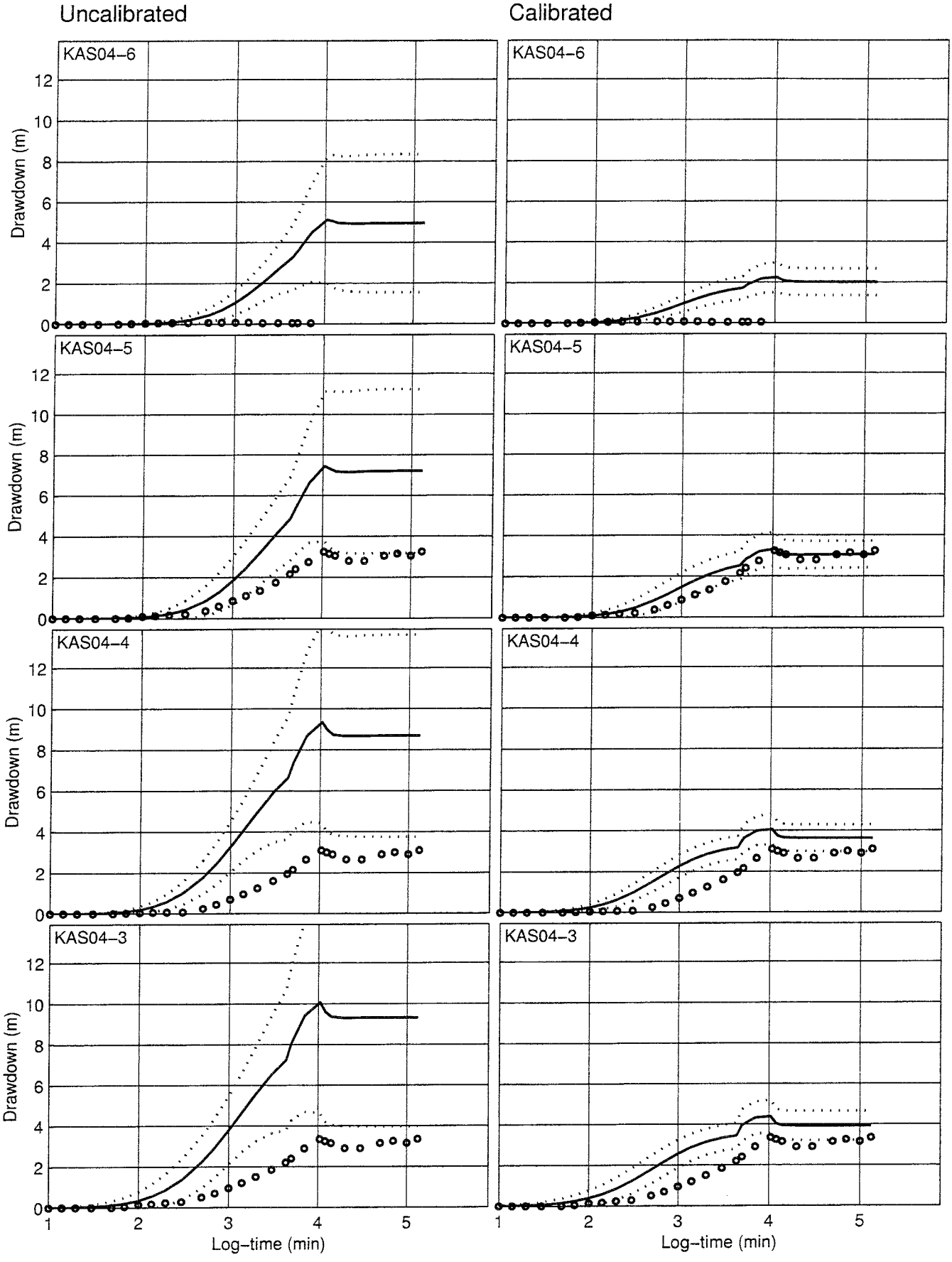

Noflow boundary condition on top, one kriging neighbourhood

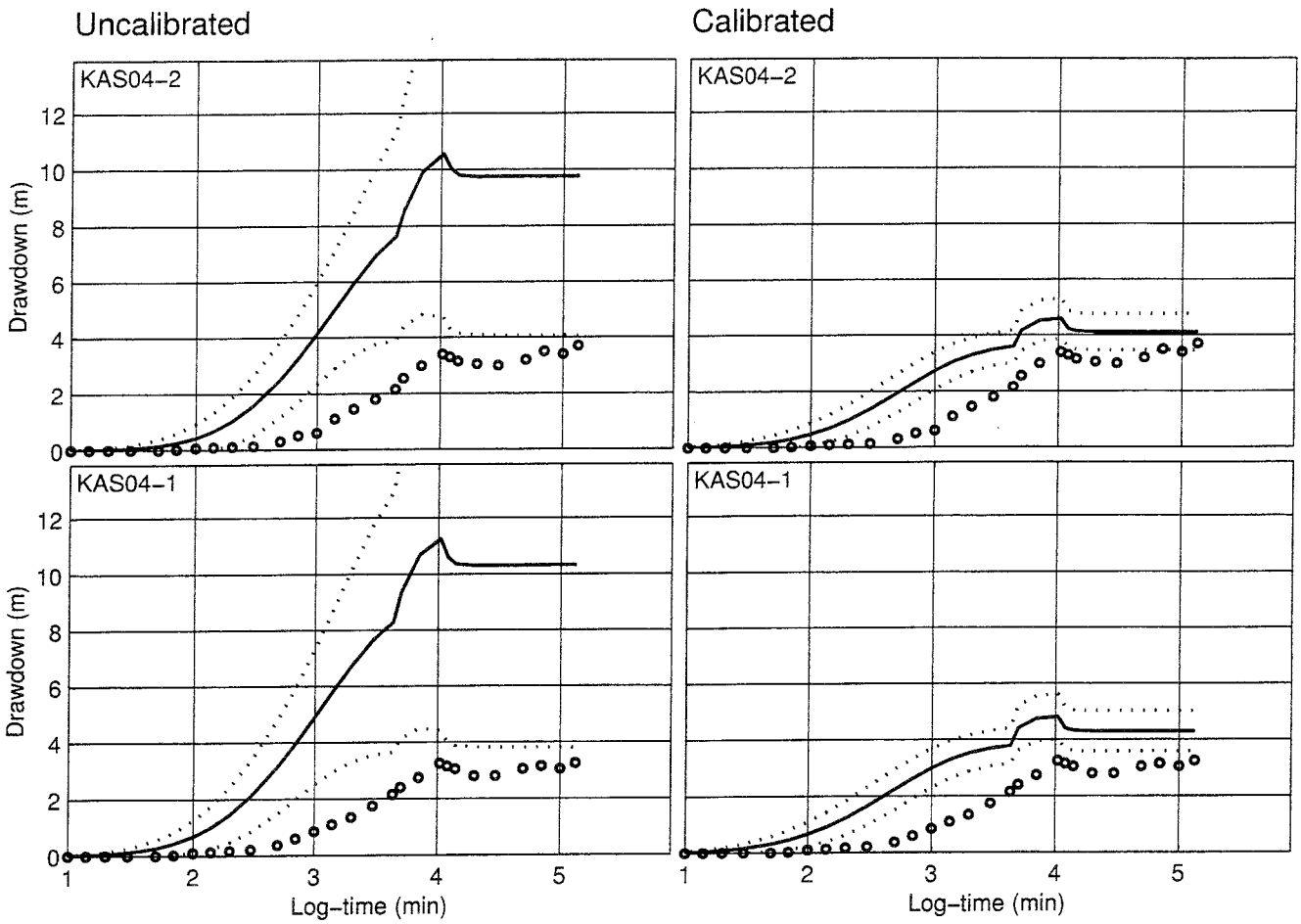

Mean Mean+–STD Measured

Noflow boundary condition on top, one kriging neighbourhood

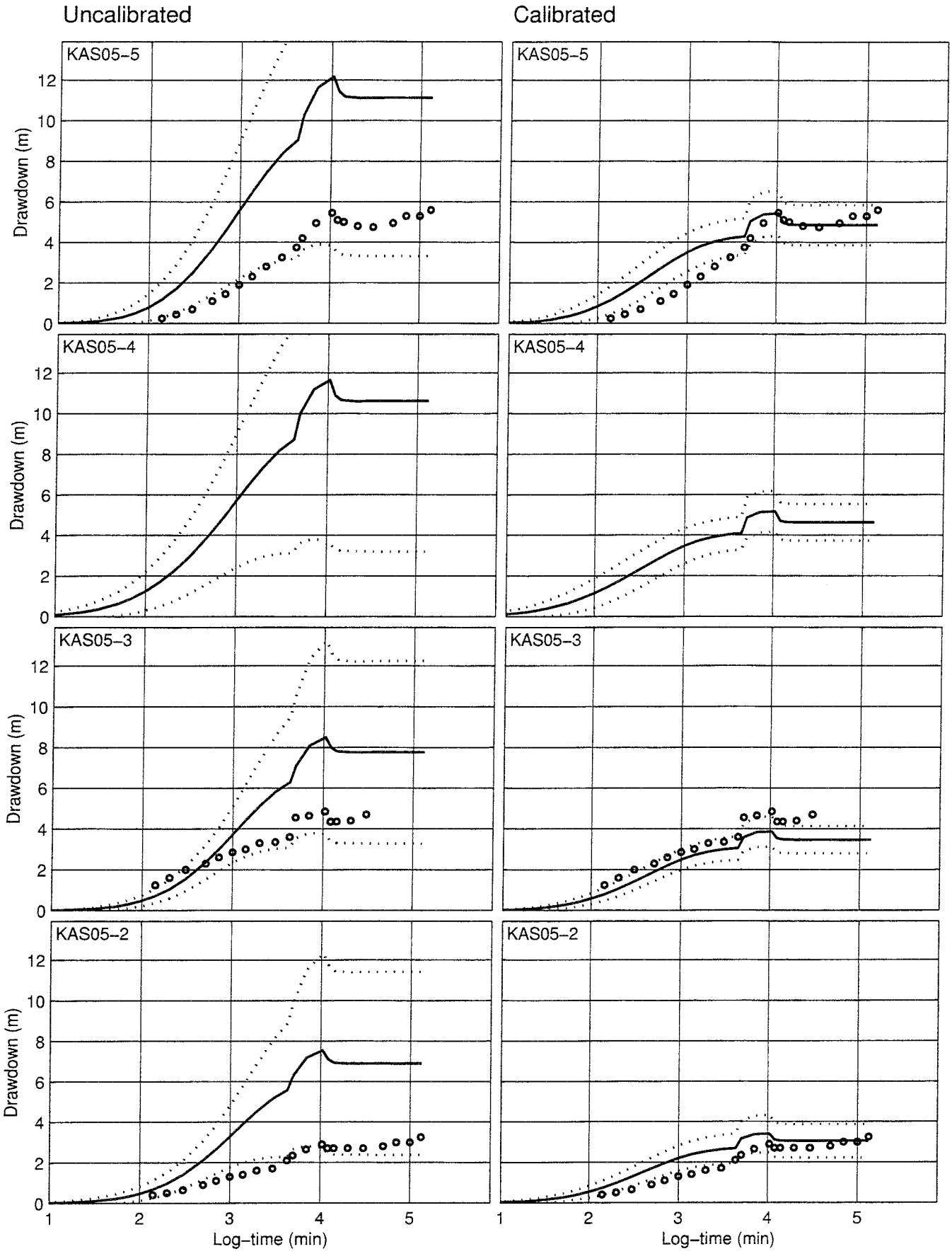

Noflow boundary condition on top, one kriging neighbourhood

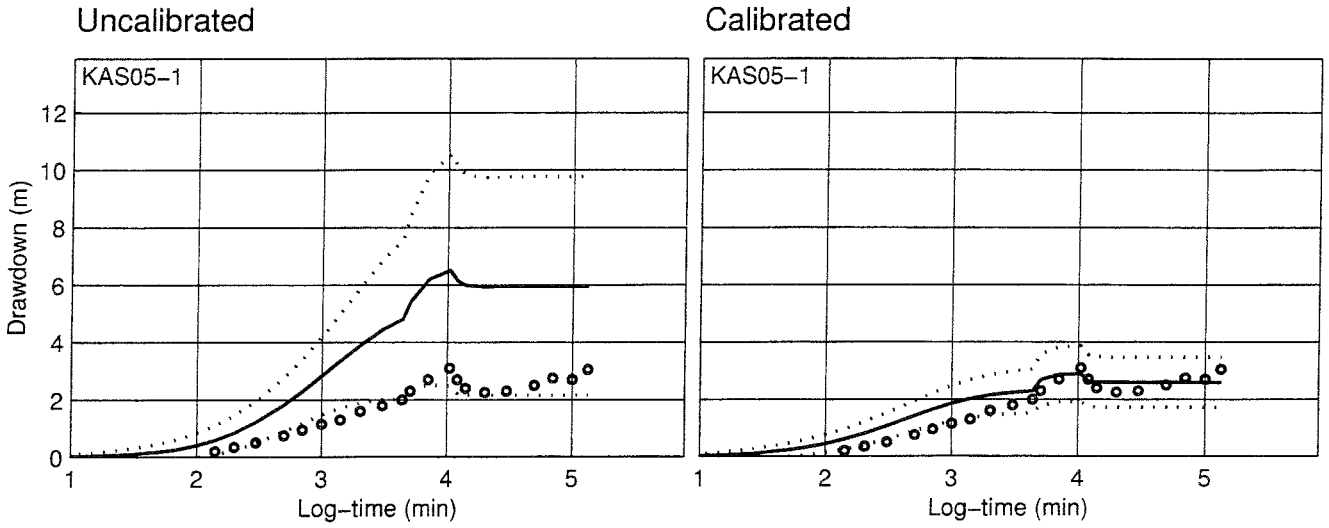

Mean Mean+–STD Measured

Noflow boundary condition on top, one kriging neighbourhood

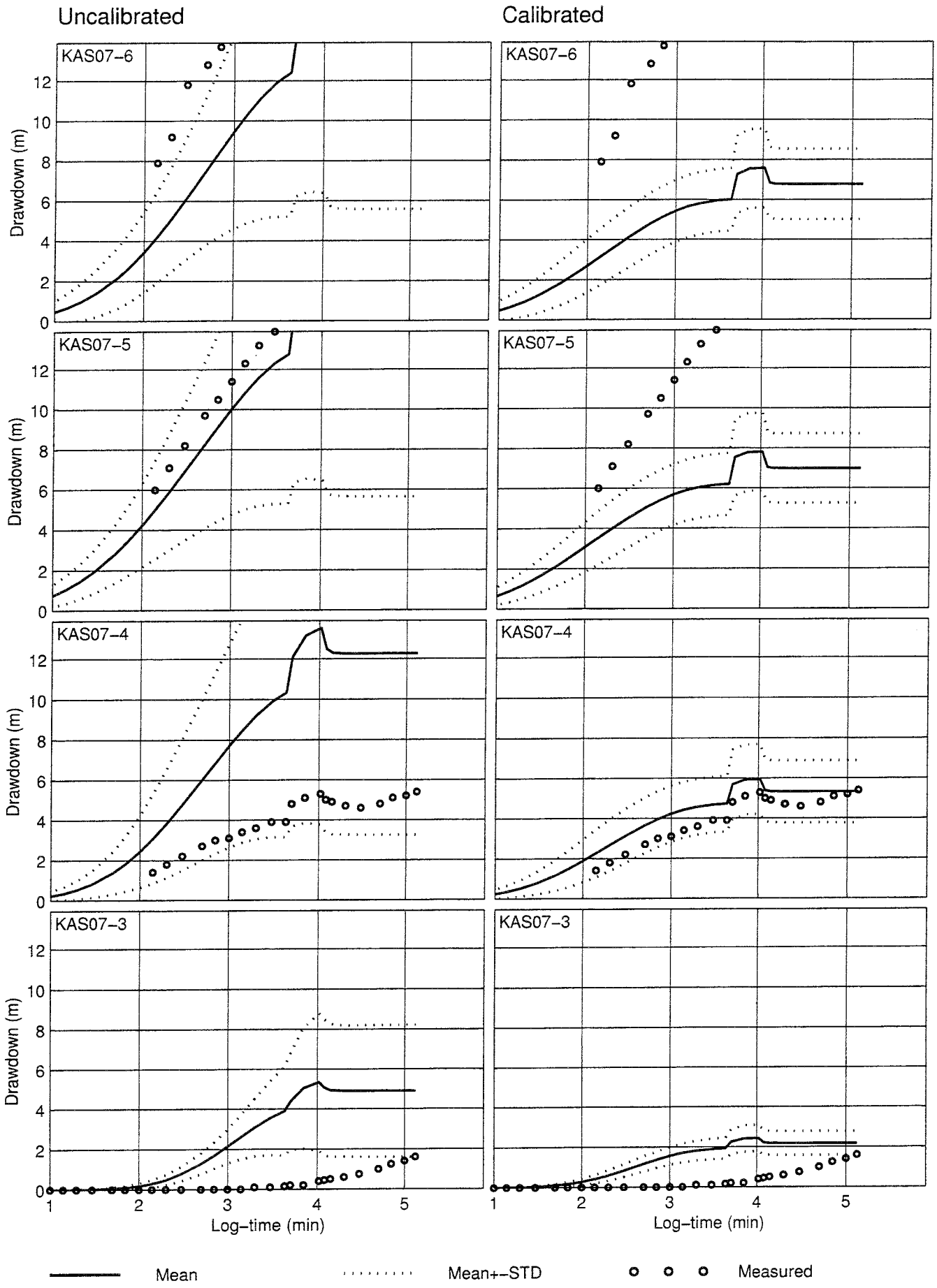

Noflow boundary condition on top, one kriging neighbourhood

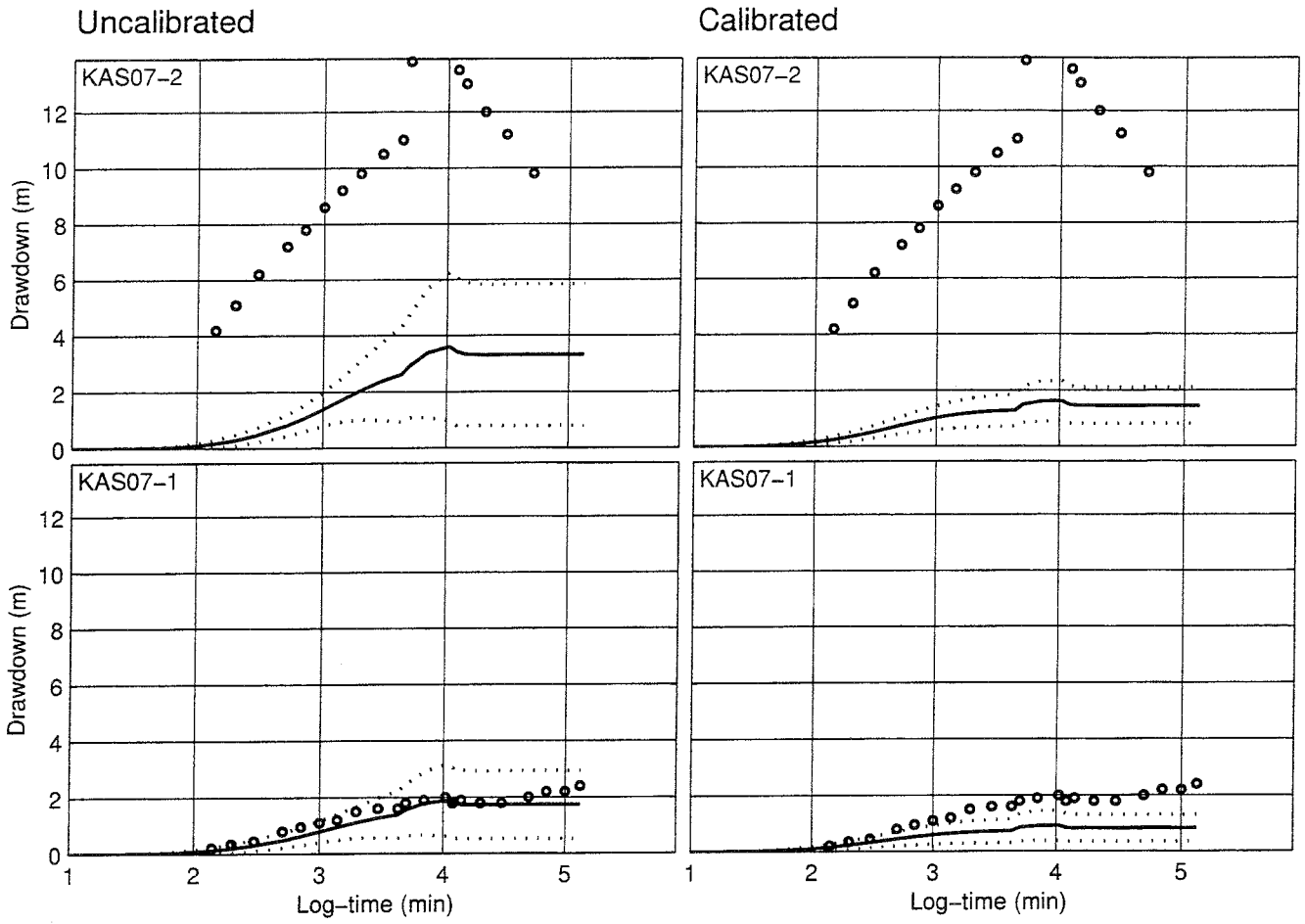

Noflow boundary condition on top, one kriging neighbourhood

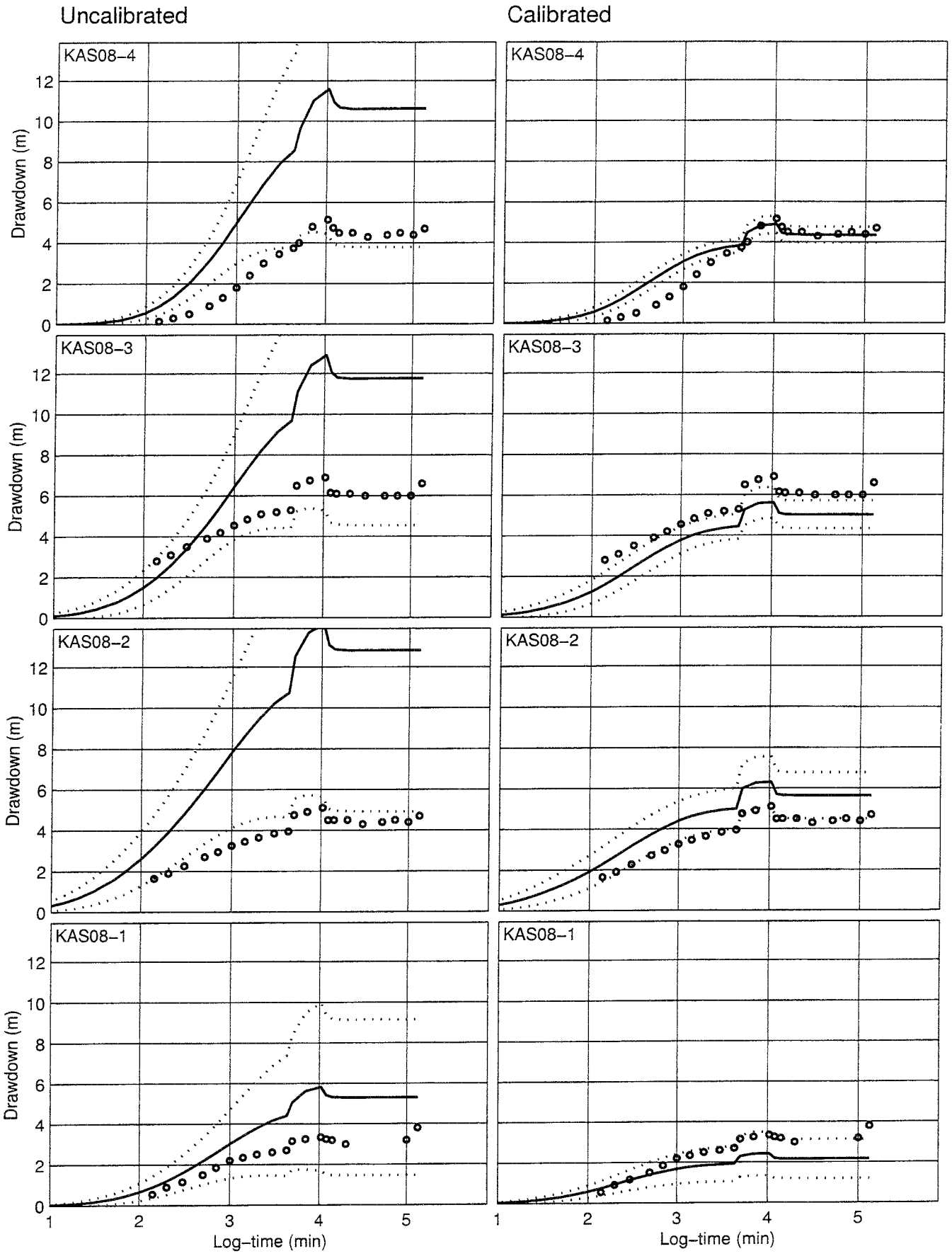

Noflow boundary condition on top, one kriging neighbourhood

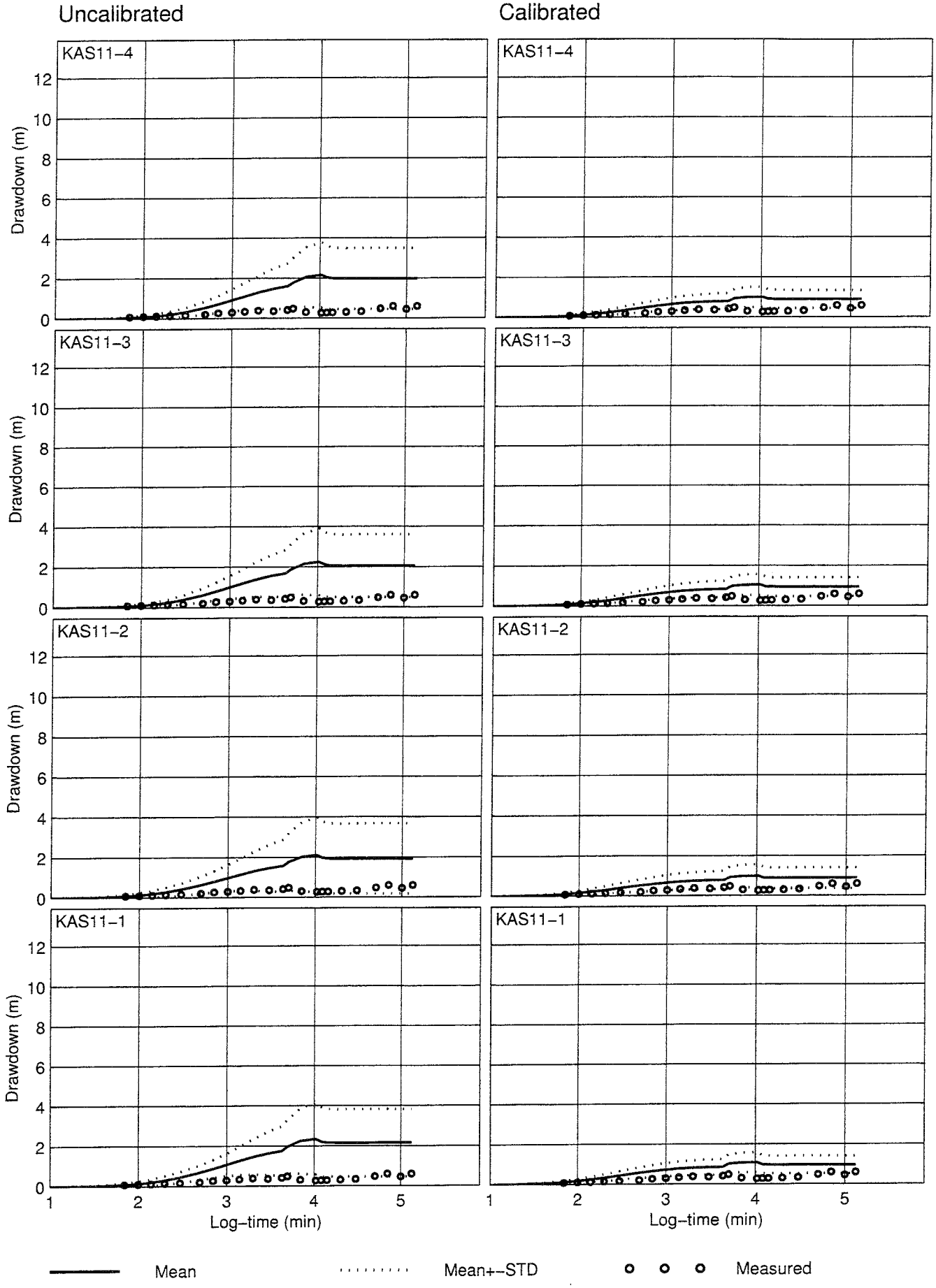

Noflow boundary condition on top, one kriging neighbourhood

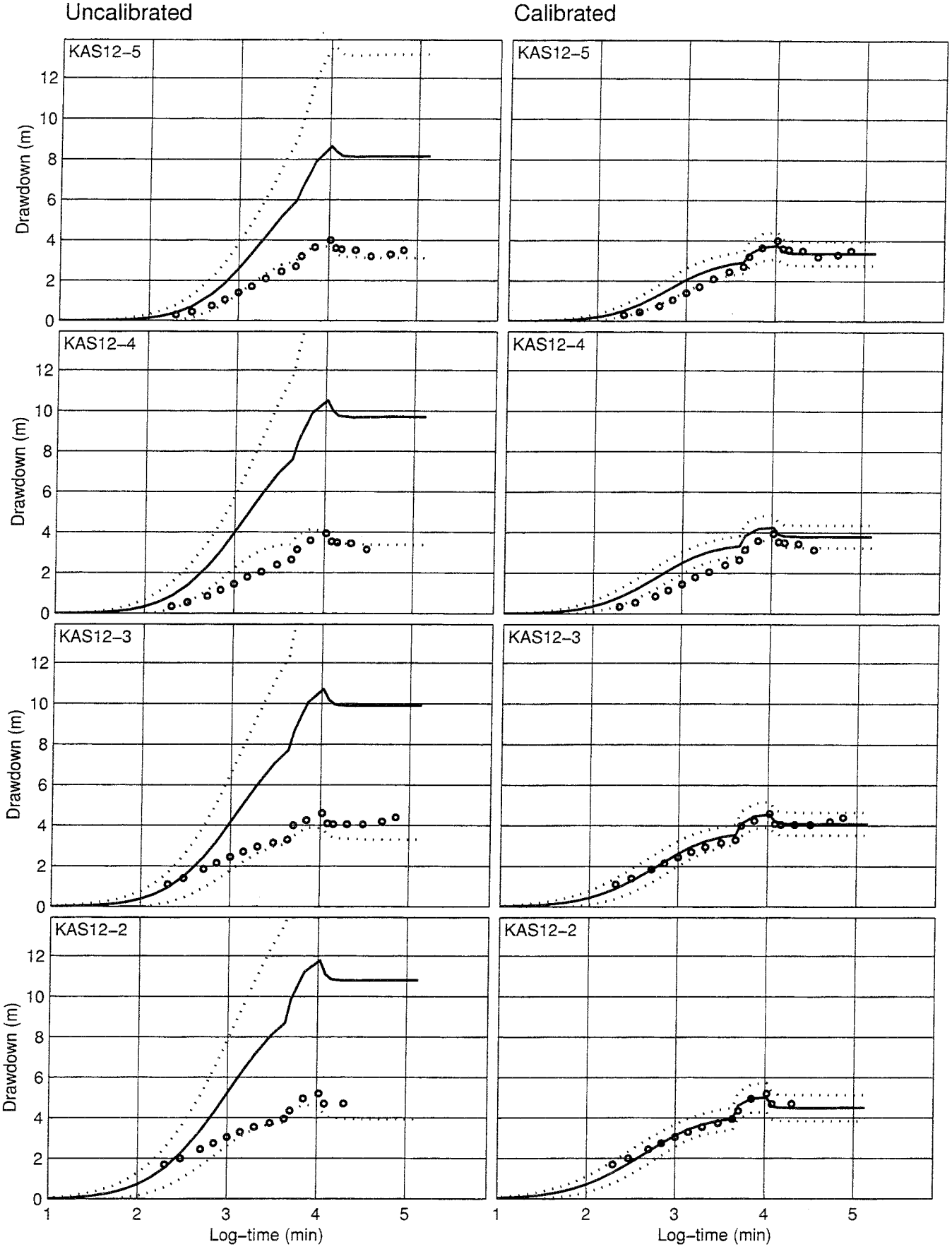

Noflow boundary condition on top, one kriging neighbourhood

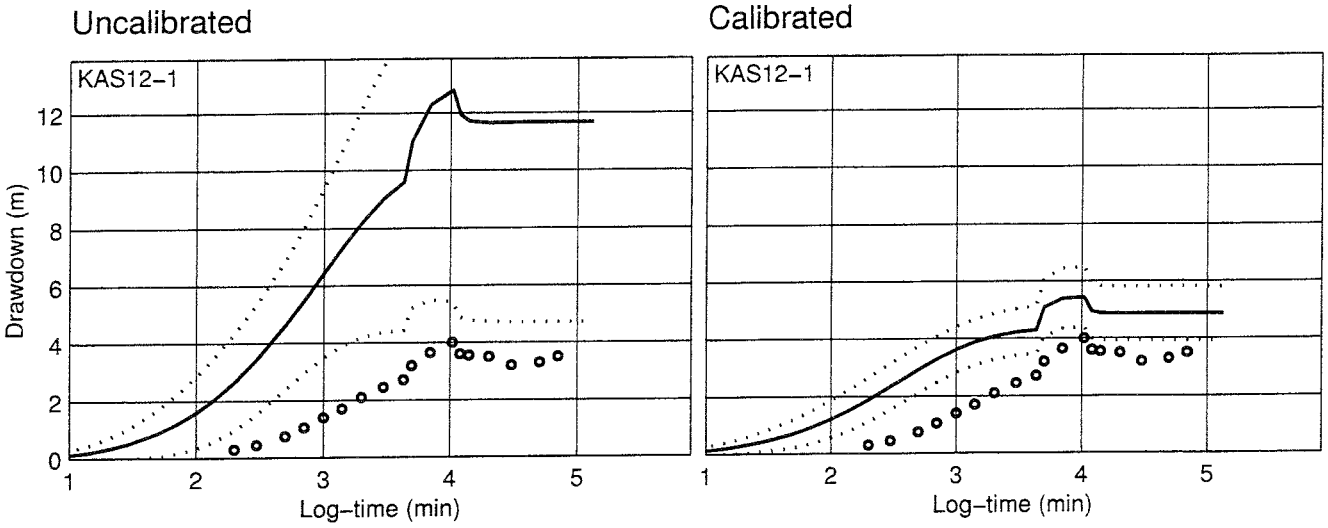

Mean Mean+-STD Measured

Noflow boundary condition on top, one kriging neighbourhood

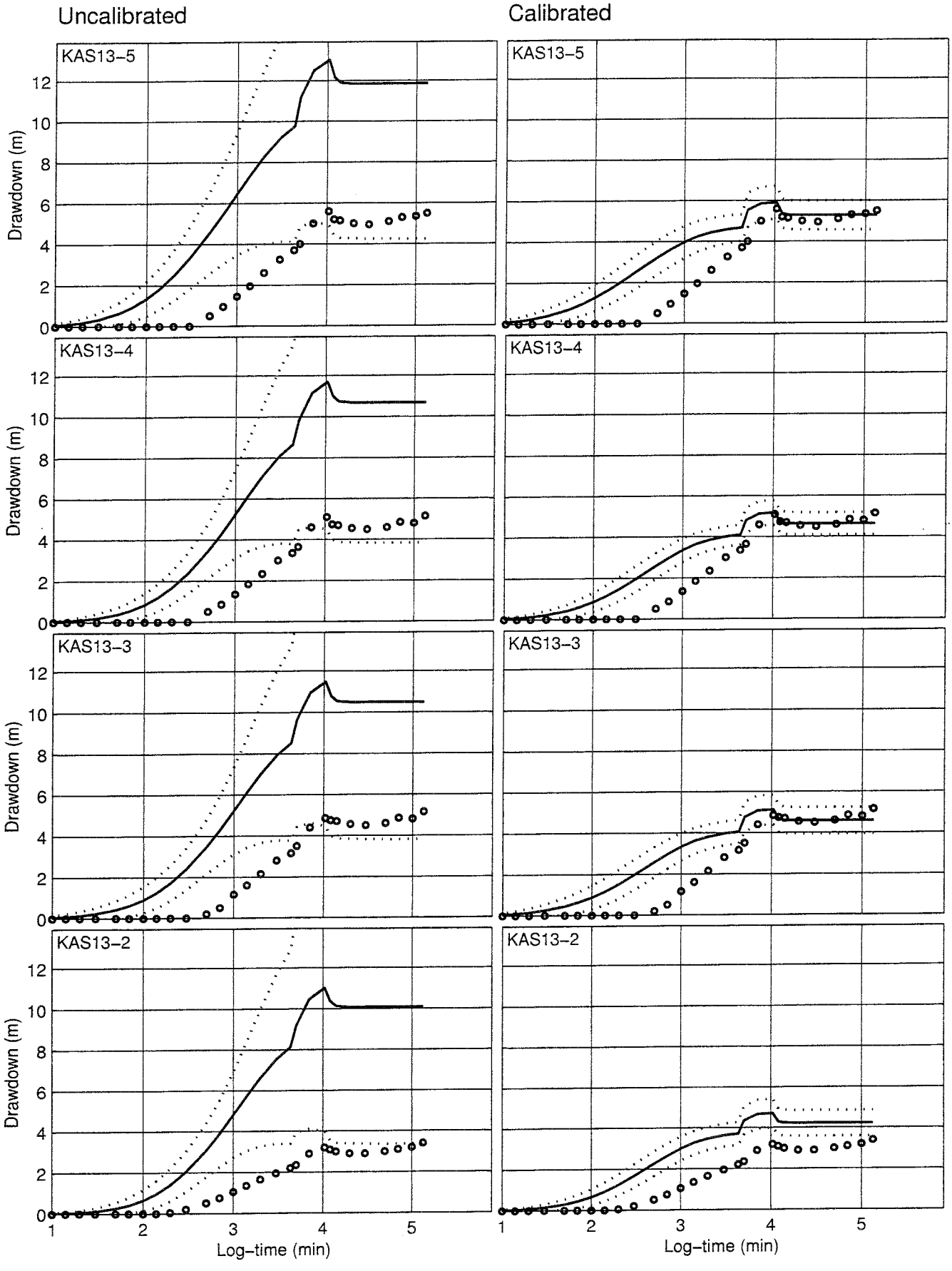

Noflow boundary condition on top, one kriging neighbourhood

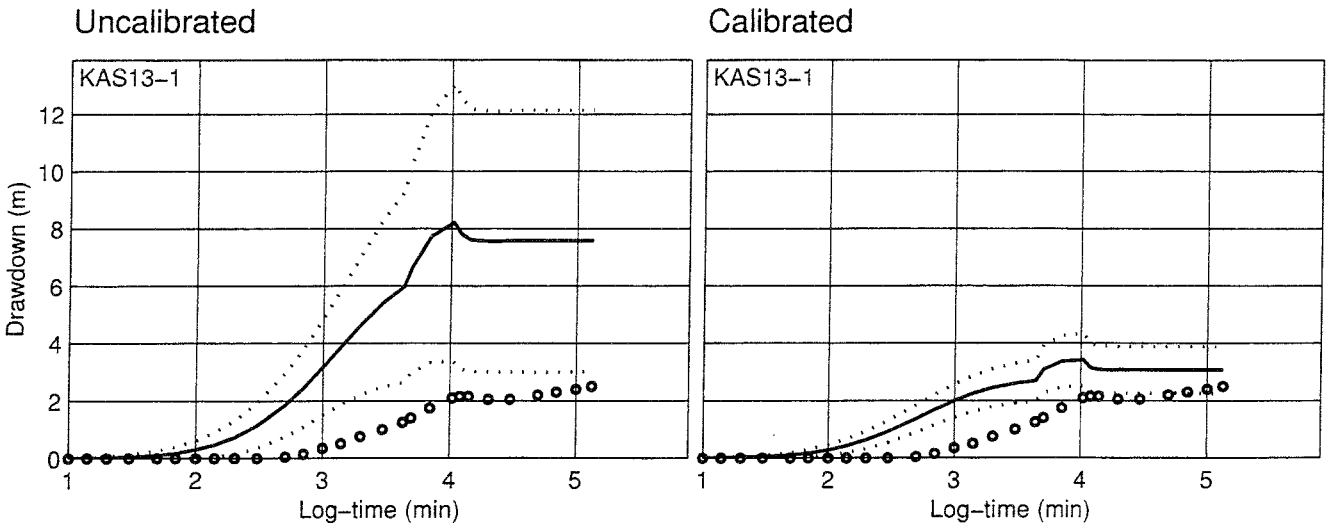

Mean Mean+-STD Measured

Noflow boundary condition on top, one kriging neighbourhood

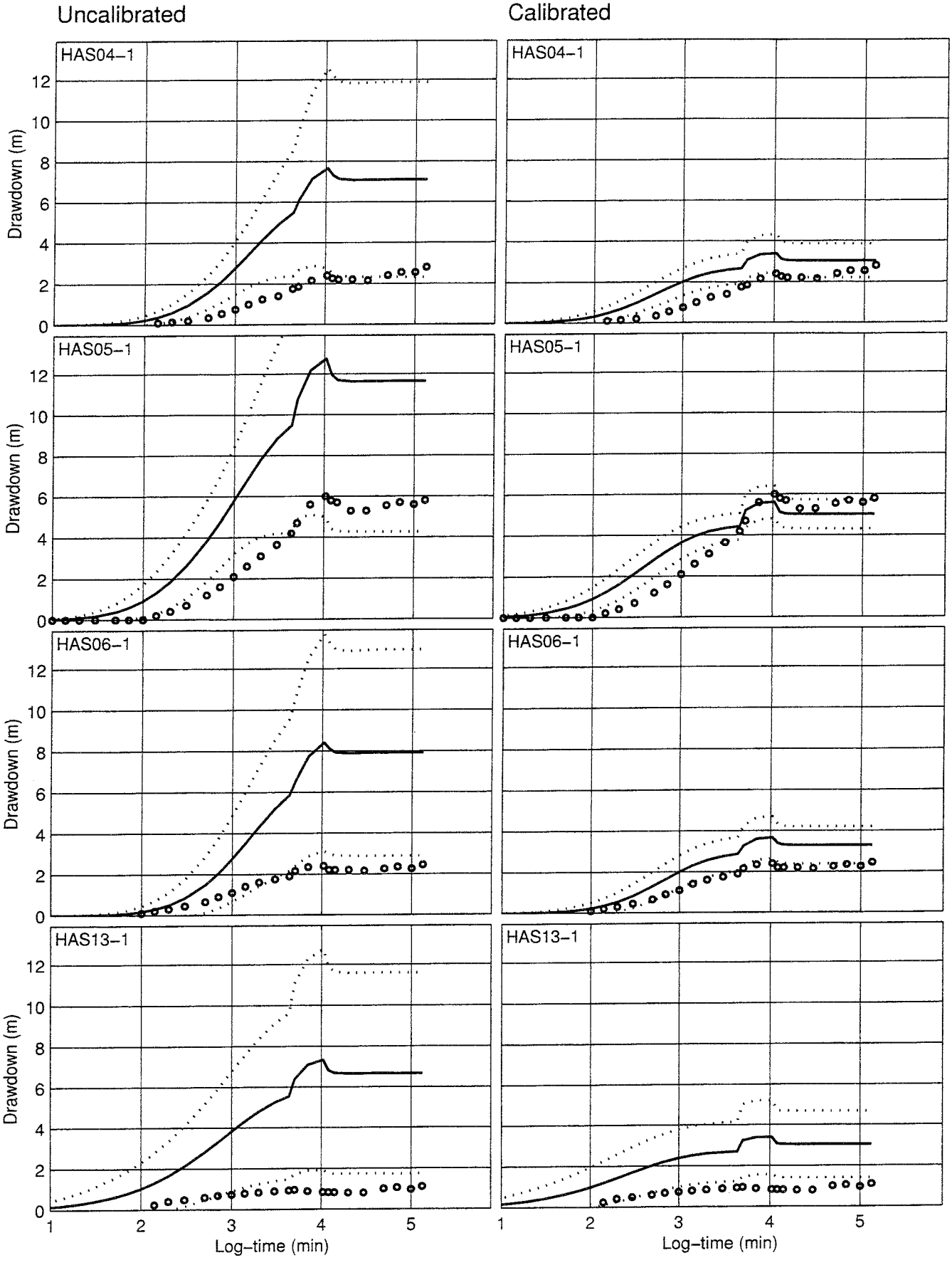

Noflow boundary condition on top, one kriging neighbourhood

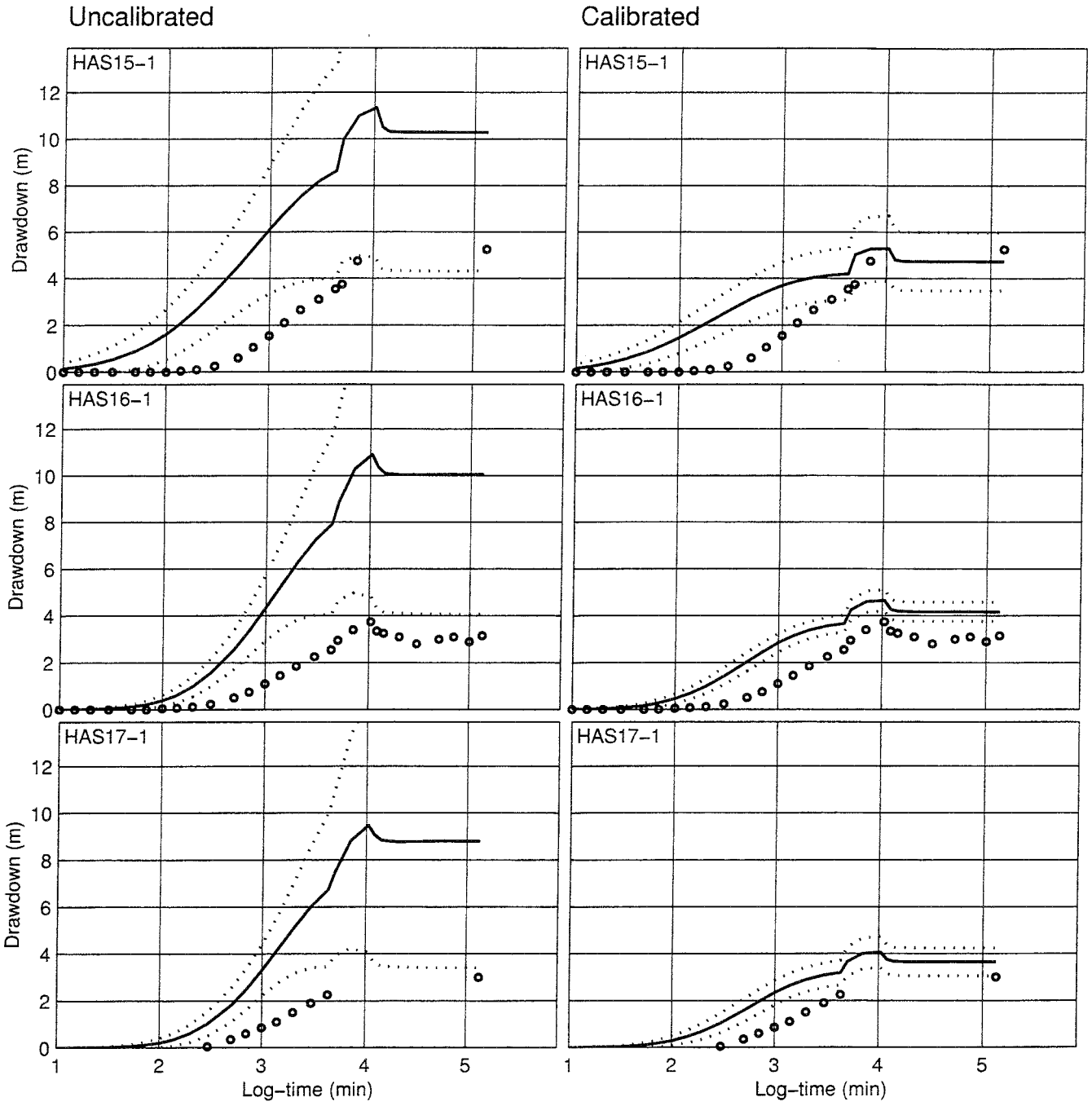

Noflow boundary condition on top, one kriging neighbourhood

APPENDIX D. DEFINITION OF PERFORMANCE MEASURES

As given in Gustafson and Ström, 1995, the performance measures used in this report are defined as follows:

MEAN ERROR

Non-weighted drawdown:

$$dh = \frac{\sum_{i=1}^{n} \left(h_i^m - h_i^c\right)}{n}$$

$$dh(abs) = \frac{\sum_{i=1}^{n} \left|h_i^m - h_i^c\right|}{n}$$

Two-dimensional weighted drawdown:

$$dh(\ln r) = \frac{\sum_{i=1}^{n} \left(h_i^m \cdot \ln\frac{r}{r_o} - h_i^c \cdot \ln\frac{r}{r_o}\right)}{n}$$

Three-dimensional weighted drawdown:

$$dh(r) = \frac{\sum_{i=1}^{n} \left(h_i^m \cdot \frac{r}{r_o} - h_i^c \cdot \frac{r}{r_o}\right)}{n}$$

ACCURACY

Non-weighted drawdown:

$$Dh = \sqrt{\frac{\sum_{i=1}^{n} \left(h_i^m - h_i^c - dh\right)^2}{n-1}}$$

Two- and three-dimensional weighted drawdown:

$$Dh(r) = \sqrt{\frac{\sum_{i=1}^{n} \left(h_i^m \cdot \frac{r}{r_o} - h_i^c \cdot \frac{r}{r_o} - dh(r)\right)^2}{n-1}}$$

$$Dh(\ln r) = \sqrt{\frac{\sum_{i=1}^{n} \left(h_i^m \cdot \ln \frac{r}{r_o} - h_i^c \cdot \ln \frac{r}{r_o} - dh(\ln r) \right)^2}{n-1}}$$

n: number of points with measured data, used to compare with calculated points

h: piezometric level (freshwater head)

index m: measured value

index c: calculated value

r: spherical distance between point of application in pumping well and observation section, in metres

r_o: reference radius, r_o = 1 m in the calculation shown.

APPENDIX E. HYDRASTAR INPUT FILE

This appendix presents an example of the HYDRASTAR main input file, refc11.hyd. The parameters of this particular input file correspond to the results of the calibrated simulations of Appendix C (i.e., Noflow (Neumann) upper boundary condition, calibrated, single kriging neighbourhood).

```
#-------------------------------------------------------
#
#  Name: faa.hyd
#  Desc: Fall aa  HYDRASTAR local Aespoe model
#  Date: 950406
#  User: Hans Widen, Kemakta
#
#  Version: HS 1.4
#
#-------------------------------------------------------
#
SYSTEM SAVE_SCRATCH_FILES
SYSTEM IGNORE_ERRORS
#SYSTEM SKIP_USER_INTERFACE
#
#
#BEGIN_BLOCK INPUT_DATA
# SEED 870505153
# NUM_MONTE   2
# PACKER_SCALE 24.0
# P_REG_TOL   0.95
# N_REG_TOL   0.8
# WRITE_COND   NOPRES
# BEGIN_FILE
#../inferens/kas02.txt
#../inferens/kas03.txt
#../inferens/kas04.txt
#../inferens/kas05.txt
#../inferens/kas06.txt
#../inferens/kas07.txt
#../inferens/kas08.txt
# END_FILE
#END_BLOCK
#
BEGIN_BLOCK COVARIANCE
# DETERMINISTIC   YES
#Spherival model
 VARIANCE      2.3
# VARIANCE      0.1
 RANGE        80.
BEGIN_DEF   ANISOTROPY
    KXX       1.0
    KXY       0.0
    KXZ       0.0
    KYY       1.0
    KYZ       0.0
    KZZ       1.0
 END_DEF
 RELATIVE_TOL   1.0E-8
 NUM_ICOSAHEDRON 4
 NUM_LINES     6
 ORIGIN        0.0 0.0 0.0
 MUL_FACTOR    0.2
 TRUNCATION    999.
END_BLOCK
#
BEGIN_BLOCK GEOM
#
# 24 meter block scale
```

```
 # NAMMU BC
 # Default transformation to the other coordinate systems
 #
 # AXISLENGTH     1008. 1200. 1008.
   AXISLENGTH     900. 1200. 900.
 # NUMBER_OF_NODES  43 51 43
   NUMBER_OF_NODES  31 41 31
   BOUNDARY       NAMMU
   NOFLOW_SIDES
    ZTOP
   END_SIDES
 # BOUNDARY       SIMPLE
 # GRADIENT 0.003 0.0 0.0
 # LEVEL    0.0
 #
 #
  BEGIN_def USER
    XY_ROTATE 0.
    ZY_ROTATE 0.
 #  TRANSLATE 624. 1300. 992.
    TRANSLATE 630. 1290. 1100.
    system RIGHT
  END_DEF
 #
   BEGIN_def WORLD
     XY_ROTATE  0.0
     ZY_ROTATE  0.0
 #   TRANSLATE 1624 6800 -1008
     TRANSLATE 1630 6790 -900
   system right
  END_DEF
 END_BLOCK
 #
 # SKB 91 values
 #
 BEGIN_BLOCK KRGE_NBH
  BEGIN_DEF SECONDARY
 #    NORMAL      -0.2 -0.2 .51
     NORMAL      0.0  0.0 1.0
     WIDTH       1000.0
     OVERLAP     85.0
     MEASUREMENTS 8
  END_DEF
 END_BLOCK
 #
 #
 #
 BEGIN_BLOCK KRIGE
  NUM_ITERATIONS  80
  RESIDUAL_TOL    1.0E-08
  METHOD          NR
  RESTART
 # PATH          /slow/usr7/kemanb/hwtmp/
   PATH  .
 END_BLOCK
 #
 #
 #
 BEGIN_BLOCK HYDROLOGY_EQ
```

```
 NUM_ITERATIONS  1500
 RESIDUAL_TOL   1.0E-09
 PRECOND       DIAGONAL
END_BLOCK
#
BEGIN_BLOCK TRANSPORT
 TRANSPORT_MODEL STREAM
 PLOT_TIMES     1
 TRACERS
700  1400  1550  1
800  1400  1550  1
900  1400  1550  1
1000  1400  1550  1
1100  1400  1550  1
1200  1400  1550  1
1300  1400  1550  1
1400  1400  1550  1
700  1500  1550  1
800  1500  1550  1
900  1500  1550  1
1000  1500  1550  1
1100  1500  1550  1
1200  1500  1550  1
1300  1500  1550  1
1400  1500  1550  1
700  1600  1550  1
800  1600  1550  1
900  1600  1550  1
1000  1600  1550  1
1100  1600  1550  1
1200  1600  1550  1
1300  1600  1550  1
1400  1600  1550  1
700  1700  1550  1
800  1700  1550  1
900  1700  1550  1
1000  1700  1550  1
1100  1700  1550  1
1200  1700  1550  1
1300  1700  1550  1
1400  1700  1550  1
700  1800  1550  1
800  1800  1550  1
900  1800  1550  1
1000  1800  1550  1
1100  1800  1550  1
1200  1800  1550  1
1300  1800  1550  1
1400  1800  1550  1
700  1900  1550  1
800  1900  1550  1
900  1900  1550  1
1000  1900  1550  1
1100  1900  1550  1
1200  1900  1550  1
1300  1900  1550  1
1400  1900  1550  1
700  2000  1550  1
800  2000  1550  1
```

```
 900 2000 1550 1
 1000 2000 1550 1
 1100 2000 1550 1
 1200 2000 1550 1
 1300 2000 1550 1
 1400 2000 1550 1
 700 2100 1550 1
 800 2100 1550 1
 900 2100 1550 1
 1000 2100 1550 1
 1100 2100 1550 1
 1200 2100 1550 1
 1300 2100 1550 1
 1400 2100 1550 1
 700 2200 1550 1
 800 2200 1550 1
 900 2200 1550 1
 1000 2200 1550 1
 1100 2200 1550 1
 1200 2200 1550 1
 1300 2200 1550 1
 1400 2200 1550 1
 700 2300 1550 1
 800 2300 1550 1
 900 2300 1550 1
 1000 2300 1550 1
 1100 2300 1550 1
 1200 2300 1550 1
 1300 2300 1550 1
 1400 2300 1550 1
 700 2400 1550 1
 800 2400 1550 1
 900 2400 1550 1
 1000 2400 1550 1
 1100 2400 1550 1
 1200 2400 1550 1
 1300 2400 1550 1
 1400 2400 1550 1
END_LIST
 BACK_INTERPOL  NOBACKINT
 INTERVALS     FIXED
 DELIMITERS
          1.0
          10.0
          100.0
          1000.0
 END_LIST
 LOGON
 TOLERANCE     0.2
 PRESENTATION   1.0
 CELL_SHIFTS    1024
 PLOTTING_MOMENTS 1.0E4
 STREAM_TUBES   88
 DIVISION      SPATIAL
 VIEW          ALL
END_BLOCK
#
BEGIN_BLOCK RESULT_ESTIMATION
  PERIOD         1
```

```
  SAVE_TRANSPORT  TRANSPORT
 END_BLOCK
 #
 BEGIN_BLOCK PRESENTATION
 #  POST_PROCESSOR   HYDRAPOST
  VIEW          ZDIR
  PRESENT       ALL
  NUM_REALIZATIONS 1
  INTERACTIVE     NO
  MODEL_NAME      faac
#
  BEGIN_DEF PSLICE
    NORMAL       0. 0. 1.
    DISTANCE     340.0
    WIDTH        30.
    C_THRESHOLD  0.
    V_THRESHOLD  0.
  END_DEF
  BEGIN_DEF PSLICE
    NORMAL       0. 0. 1.
    DISTANCE     440.0
    WIDTH        30.
    C_THRESHOLD  0.
    V_THRESHOLD  0.
  END_DEF
  BEGIN_DEF PSLICE
    NORMAL       0. 0. 1.
    DISTANCE     490.0
    WIDTH        30.
    C_THRESHOLD  0.
    V_THRESHOLD  0.
  END_DEF
  BEGIN_DEF PSLICE
    NORMAL       0. 0. 1.
    DISTANCE     640.0
    WIDTH        30.
    C_THRESHOLD  0.
    V_THRESHOLD  0.
  END_DEF
  BEGIN_DEF PSLICE
    NORMAL       0. 0. 1.
    DISTANCE     790.0
    WIDTH        30.
    C_THRESHOLD  0.
    V_THRESHOLD  0.
  END_DEF
END_BLOCK
#
BEGIN_BLOCK TRENDS
 REF_DEPTH  40.0
 ALFA       -8.0
 BETA       0.000
 STORATIVITY 1.0E-7
BEGIN_DEF PLANE
NAME   P1
EQUATION   -0.4889655   0.87168437   -0.032849   -5636.1812
TYPE   UPPER
END_DEF
BEGIN_DEF PLANE
```

```
NAME    P2
EQUATION  -0.4792322   0.85472816   -0.1994401   -5472.543
TYPE    UPPER
END_DEF
BEGIN_DEF PLANE
NAME    P3
EQUATION  -0.3032357   0.81050146   0.50113422   -5511.585
TYPE    UPPER
END_DEF
BEGIN_DEF PLANE
NAME    P4
EQUATION  -0.3032357   0.81050146   0.50113422   -5496.585
TYPE    UPPER
END_DEF
BEGIN_DEF PLANE
NAME    P5
EQUATION  -0.3032357   0.81050146   0.50113422   -5526.585
TYPE    UPPER
END_DEF
BEGIN_DEF PLANE
NAME    P6
EQUATION  -0.1993962   0.96115947   -0.1908235   -6409.2007
TYPE    UPPER
END_DEF
BEGIN_DEF PLANE
NAME    P7
EQUATION  -0.1993962   0.96115947   -0.1908235   -6394.2007
TYPE    UPPER
END_DEF
BEGIN_DEF PLANE
NAME    P8
EQUATION  -0.1993962   0.96115947   -0.1908235   -6424.2007
TYPE    UPPER
END_DEF
BEGIN_DEF PLANE
NAME    P9
EQUATION  -0.1993962   0.96115947   -0.1908235   -6409.2007
TYPE    UPPER
END_DEF
BEGIN_DEF PLANE
NAME    P10
EQUATION  -0.1993962   0.96115947   -0.1908235   -6394.2007
TYPE    UPPER
END_DEF
BEGIN_DEF PLANE
NAME    P11
EQUATION  -0.1993962   0.96115947   -0.1908235   -6424.2007
TYPE    UPPER
END_DEF
BEGIN_DEF PLANE
NAME    P12
EQUATION  -0.0142345   0.60171956   0.79858059   -4104.5356
TYPE    UPPER
END_DEF
BEGIN_DEF PLANE
NAME    P13
EQUATION  -0.0142345   0.60171956   0.79858059   -4089.5356
TYPE    UPPER
END_DEF
```

```
BEGIN_DEF PLANE
NAME  P14
EQUATION  -0.0142345  0.60171956  0.79858059  -4119.5356
TYPE  UPPER
END_DEF
BEGIN_DEF PLANE
NAME  P15
EQUATION  -0.2547729  0.94171762  -0.2196787  -5528.4541
TYPE  UPPER
END_DEF
BEGIN_DEF PLANE
NAME  P16
EQUATION  -0.2547729  0.94171762  -0.2196787  -5513.4541
TYPE  UPPER
END_DEF
BEGIN_DEF PLANE
NAME  P17
EQUATION  -0.2547729  0.94171762  -0.2196787  -5543.4541
TYPE  UPPER
END_DEF
BEGIN_DEF PLANE
NAME  P18
EQUATION  0  1  0  -7063.5
TYPE  UPPER
END_DEF
BEGIN_DEF PLANE
NAME  P19
EQUATION  0.45744616  0.88240653  -0.1100078  -7527.4409
TYPE  UPPER
END_DEF
BEGIN_DEF PLANE
NAME  P20
EQUATION  0.90743715  0.42018786  0  -5068.3945
TYPE  UPPER
END_DEF
BEGIN_DEF PLANE
NAME  P21
EQUATION  0  1  0  -6896.7202
TYPE  UPPER
END_DEF
BEGIN_DEF PLANE
NAME  P22
EQUATION  0  1  0  -7384.5
TYPE  UPPER
END_DEF
BEGIN_DEF PLANE
NAME  P23
EQUATION  -0.6026021  0.74425858  0.2880103  -3733.3003
TYPE  UPPER
END_DEF
BEGIN_DEF PLANE
NAME  P24
EQUATION  -0.6026021  0.74425858  0.2880103  -3708.3003
TYPE  UPPER
END_DEF
BEGIN_DEF PLANE
NAME  P25
EQUATION  -0.6026021  0.74425858  0.2880103  -3758.3003
TYPE  UPPER
```

```
END_DEF
BEGIN_DEF PLANE
NAME    P26
EQUATION  -0.6026021   0.74425858   0.2880103   -3733.3003
TYPE    UPPER
END_DEF
BEGIN_DEF PLANE
NAME    P27
EQUATION  -0.6026021   0.74425858   0.2880103   -3708.3003
TYPE    UPPER
END_DEF
BEGIN_DEF PLANE
NAME    P28
EQUATION  -0.6026021   0.74425858   0.2880103   -3758.3003
TYPE    UPPER
END_DEF
BEGIN_DEF PLANE
NAME    P29
EQUATION  -0.4454407   0.86145574   0.24387823   -4988.1753
TYPE    UPPER
END_DEF
BEGIN_DEF PLANE
NAME    P30
EQUATION  -0.4454407   0.86145574   0.24387823   -4963.1753
TYPE    UPPER
END_DEF
BEGIN_DEF PLANE
NAME    P31
EQUATION  -0.4454407   0.86145574   0.24387823   -5013.1753
TYPE    UPPER
END_DEF
BEGIN_DEF PLANE
NAME    P32
EQUATION  -0.4454407   0.86145574   0.24387823   -4988.1753
TYPE    UPPER
END_DEF
BEGIN_DEF PLANE
NAME    P33
EQUATION  -0.4454407   0.86145574   0.24387823   -4963.1753
TYPE    UPPER
END_DEF
BEGIN_DEF PLANE
NAME    P34
EQUATION  -0.4454407   0.86145574   0.24387823   -5013.1753
TYPE    UPPER
END_DEF
BEGIN_DEF PLANE
NAME    P35
EQUATION  -0.7882543   0.57274765   -0.2249786   -2588.8579
TYPE    UPPER
END_DEF
BEGIN_DEF PLANE
NAME    P36
EQUATION  -0.7882543   0.57274765   -0.2249786   -2603.8579
TYPE    UPPER
END_DEF
BEGIN_DEF PLANE
NAME    P37
EQUATION  -0.7882543   0.57274765   -0.2249786   -2573.8579
```

```
TYPE   UPPER
END_DEF
BEGIN_DEF PLANE
NAME   P38
EQUATION  -0.4814563   0.83386427   0.26994488   -4463.0518
TYPE   UPPER
END_DEF
BEGIN_DEF PLANE
NAME   P39
EQUATION  -0.4814563   0.83386427   0.26994488   -4448.0518
TYPE   UPPER
END_DEF
BEGIN_DEF PLANE
NAME   P40
EQUATION  -0.4814563   0.83386427   0.26994488   -4478.0518
TYPE   UPPER
END_DEF
BEGIN_DEF PLANE
NAME   P41
EQUATION  -0.4266499   0.86480469   -0.2647314   -4715.3848
TYPE   UPPER
END_DEF
BEGIN_DEF PLANE
NAME   P42
EQUATION  -0.4266499   0.86480469   -0.2647314   -4700.3848
TYPE   UPPER
END_DEF
BEGIN_DEF PLANE
NAME   P43
EQUATION  -0.4266499   0.86480469   -0.2647314   -4730.3848
TYPE   UPPER
END_DEF
BEGIN_DEF PLANE
NAME   P44
EQUATION  0.90743703   0.4201881   0   -5018.3833
TYPE   UPPER
END_DEF
BEGIN_DEF PLANE
NAME   P45
EQUATION  0.90743703   0.4201881   0   -5003.3833
TYPE   UPPER
END_DEF
BEGIN_DEF PLANE
NAME   P46
EQUATION  0.90743703   0.4201881   0   -5033.3833
TYPE   UPPER
END_DEF
BEGIN_DEF PLANE
NAME   P47
EQUATION  0.91595715   0.40127611   0   -4958.3926
TYPE   UPPER
END_DEF
BEGIN_DEF PLANE
NAME   P48
EQUATION  0.91595715   0.40127611   0   -4943.3926
TYPE   UPPER
END_DEF
BEGIN_DEF PLANE
NAME   P49
```

```
EQUATION 0.91595715 0.40127611 0 -4973.3926
TYPE UPPER
END_DEF
BEGIN_DEF PLANE
NAME P50
EQUATION 0.99950331 -0.0315147 0 -1921.1322
TYPE UPPER
END_DEF
BEGIN_DEF PLANE
NAME P51
EQUATION 0.99950331 -0.0315147 0 -1906.1322
TYPE UPPER
END_DEF
BEGIN_DEF PLANE
NAME P52
EQUATION 0.99950331 -0.0315147 0 -1936.1322
TYPE UPPER
END_DEF
BEGIN_DEF PLANE
NAME P53
EQUATION 0.98824656 0.12555167 0.08720932 -3176.6104
TYPE UPPER
END_DEF
BEGIN_DEF PLANE
NAME P54
EQUATION 0.98824656 0.12555167 0.08720932 -3161.6104
TYPE UPPER
END_DEF
BEGIN_DEF PLANE
NAME P55
EQUATION 0.98824656 0.12555167 0.08720932 -3191.6104
TYPE UPPER
END_DEF
BEGIN_DEF PLANE
NAME P56
EQUATION 0.99822807 0.05950383 0 -2399.2993
TYPE UPPER
END_DEF
BEGIN_DEF PLANE
NAME P57
EQUATION 0.99822807 0.05950383 0 -2384.2993
TYPE UPPER
END_DEF
BEGIN_DEF PLANE
NAME P58
EQUATION 0.99822807 0.05950383 0 -2414.2993
TYPE UPPER
END_DEF
BEGIN_DEF PLANE
NAME P59
EQUATION 0.99009866 0.14037316 0 -3266.7075
TYPE UPPER
END_DEF
BEGIN_DEF PLANE
NAME P60
EQUATION 0.99009866 0.14037316 0 -3251.7075
TYPE UPPER
END_DEF
BEGIN_DEF PLANE
```

```
NAME    P61
EQUATION  0.99009866   0.14037316   0    -3281.7075
TYPE    UPPER
END_DEF
BEGIN_DEF PLANE
NAME    P62
EQUATION  0.90399688   0.41862771   0.08683567   -4915.147
TYPE    UPPER
END_DEF
BEGIN_DEF PLANE
NAME    P63
EQUATION  0.90399688   0.41862771   0.08683567   -4900.147
TYPE    UPPER
END_DEF
BEGIN_DEF PLANE
NAME    P64
EQUATION  0.90399688   0.41862771   0.08683567   -4930.147
TYPE    UPPER
END_DEF
BEGIN_DEF PLANE
NAME    P65
EQUATION  0.36773312   0.33874565   0.8660391   -3132.4543
TYPE    UPPER
END_DEF
BEGIN_DEF PLANE
NAME    P66
EQUATION  0.36773312   0.33874565   0.8660391   -3117.4543
TYPE    UPPER
END_DEF
BEGIN_DEF PLANE
NAME    P67
EQUATION  0.36773312   0.33874565   0.8660391   -3147.4543
TYPE    UPPER
END_DEF
BEGIN_DEF PLANE
NAME    P68
EQUATION  0.04555526   0.99896181   0    -8112.6436
TYPE    UPPER
END_DEF
BEGIN_DEF PLANE
NAME    P69
EQUATION  0.04555526   0.99896181   0    -8012.6436
TYPE    UPPER
END_DEF
BEGIN_DEF PLANE
NAME    P70
EQUATION  0.04555526   0.99896181   0    -8212.6436
TYPE    UPPER
END_DEF
BEGIN_DEF PLANE
NAME    P71
EQUATION  -0.0064101   0.99997944   0    -8062.6548
TYPE    UPPER
END_DEF
BEGIN_DEF PLANE
NAME    P72
EQUATION  -0.0064101   0.99997944   0    -7962.6548
TYPE    UPPER
END_DEF
```

```
BEGIN_DEF PLANE
NAME    P73
EQUATION  -0.0064101   0.99997944   0   -8162.6548
TYPE   UPPER
END_DEF
BEGIN_DEF PLANE
NAME    P74
EQUATION  0.05815384   0.99830765   0   -8222.1777
TYPE   UPPER
END_DEF
BEGIN_DEF PLANE
NAME    P75
EQUATION  0.05815384   0.99830765   0   -8122.1777
TYPE   UPPER
END_DEF
BEGIN_DEF PLANE
NAME    P76
EQUATION  0.05815384   0.99830765   0   -8322.1777
TYPE   UPPER
END_DEF
BEGIN_DEF PLANE
NAME    P77
EQUATION  -0.5489014   0.83588713   0   -5818.5664
TYPE   UPPER
END_DEF
BEGIN_DEF PLANE
NAME    P78
EQUATION  -0.5489014   0.83588713   0   -5718.5664
TYPE   UPPER
END_DEF
BEGIN_DEF PLANE
NAME    P79
EQUATION  -0.5489014   0.83588713   0   -5918.5664
TYPE   UPPER
END_DEF
BEGIN_DEF PLANE
NAME    P80
EQUATION  -0.2334014   0.86342204   -0.4472428   -4675.2183
TYPE   UPPER
END_DEF
BEGIN_DEF PLANE
NAME    P81
EQUATION  -0.4194661   0.79003066   -0.4471016   -3832.0398
TYPE   UPPER
END_DEF
BEGIN_DEF PLANE
NAME    P82
EQUATION  -0.4194661   0.79003066   -0.4471016   -3732.0398
TYPE   UPPER
END_DEF
BEGIN_DEF PLANE
NAME    P83
EQUATION  -0.4194661   0.79003066   -0.4471016   -3932.0398
TYPE   UPPER
END_DEF
BEGIN_DEF PLANE
NAME    P84
EQUATION  -0.6670307   0.74503022   0   -4257.6597
TYPE   UPPER
```

```
END_DEF
BEGIN_DEF PLANE
NAME   P85
EQUATION  -0.6670307   0.74503022   0   -4157.6597
TYPE   UPPER
END_DEF
BEGIN_DEF PLANE
NAME   P86
EQUATION  -0.6670307   0.74503022   0   -4357.6597
TYPE   UPPER
END_DEF
BEGIN_DEF PLANE
NAME   P87
EQUATION  0.19783649   0.98023504   0   -7540.7715
TYPE   UPPER
END_DEF
BEGIN_DEF PLANE
NAME   P88
EQUATION  0.19783649   0.98023504   0   -7440.7715
TYPE   UPPER
END_DEF
BEGIN_DEF PLANE
NAME   P89
EQUATION  0.19783649   0.98023504   0   -7640.7715
TYPE   UPPER
END_DEF
BEGIN_DEF PLANE
NAME   P90
EQUATION  -0.9900235   0.14090222   0   -23.415733
TYPE   UPPER
END_DEF
BEGIN_DEF PLANE
NAME   P91
EQUATION  -0.9900235   0.14090222   0   1.58426666
TYPE   UPPER
END_DEF
BEGIN_DEF PLANE
NAME   P92
EQUATION  -0.9900235   0.14090222   0   -48.415733
TYPE   UPPER
END_DEF

BEGIN_DEF ZONE
NAME      Z01
ALFA   -6.7781513
BETA   0.0
STORATIVITY  1.0E-7
PLANE   P36
P_TYPE   UPPER
PLANE   P37
P_TYPE   LOWER
PLANE   P29
P_TYPE   LOWER
PLANE   P2
P_TYPE   UPPER
TEST_POINT   2106.81348   7248.91602   -434.5435
#DETERMINISTIC YES
END_DEF
BEGIN_DEF ZONE
```

```
NAME      Z02
ALFA   -6.0457575
BETA   0.0
STORATIVITY  1.0E-7
PLANE   P64
P_TYPE   UPPER
PLANE   P63
P_TYPE   LOWER
PLANE   P6
P_TYPE   LOWER
PLANE   P29
P_TYPE   LOWER
PLANE   P2
P_TYPE   UPPER
TEST_POINT   2121.43201   7246.64111   -417.63605
#DETERMINISTIC YES
END_DEF
BEGIN_DEF ZONE
NAME      Z03
ALFA   -6.1760913
BETA   0.0
STORATIVITY  1.0E-7
PLANE   P46
P_TYPE   UPPER
PLANE   P45
P_TYPE   LOWER
PLANE   P2
P_TYPE   UPPER
PLANE   P6
P_TYPE   LOWER
TEST_POINT   2215.32904   7158.9646   -975
#DETERMINISTIC YES
END_DEF
BEGIN_DEF ZONE
NAME      Z04
ALFA   -7.7781513
BETA   0.0
STORATIVITY  1.0E-7
PLANE   P8
P_TYPE   UPPER
PLANE   P7
P_TYPE   LOWER
PLANE   P29
P_TYPE   LOWER
PLANE   P90
P_TYPE   UPPER
TEST_POINT   1463.09003   6863.67725   -544.2039
#DETERMINISTIC YES
END_DEF
BEGIN_DEF ZONE
NAME      Z05
ALFA   -6.1760913
BETA   0.0
STORATIVITY  1.0E-7
PLANE   P11
P_TYPE   UPPER
PLANE   P10
P_TYPE   LOWER
PLANE   P23
```

```
P_TYPE   LOWER
PLANE   P29
P_TYPE   LOWER
PLANE   P90
P_TYPE   UPPER
TEST_POINT   1961.79977   7057.0248   -91.445001
#DETERMINISTIC YES
END_DEF
BEGIN_DEF ZONE
NAME      Z06
ALFA   -5.3309932
BETA   0.0
STORATIVITY  1.0E-7
PLANE   P55
P_TYPE   UPPER
PLANE   P54
P_TYPE   LOWER
PLANE   P29
P_TYPE   LOWER
PLANE   P2
P_TYPE   UPPER
TEST_POINT   2317.77905   7355.58724   -429.23267
#DETERMINISTIC YES
END_DEF
BEGIN_DEF ZONE
NAME      Z07
ALFA   -5.6320232
BETA   0.0
STORATIVITY  1.0E-7
PLANE   P49
P_TYPE   UPPER
PLANE   P48
P_TYPE   LOWER
PLANE   P2
P_TYPE   UPPER
PLANE   P29
P_TYPE   LOWER
TEST_POINT   2215.625   7299.1512   -423.95744
#DETERMINISTIC YES
END_DEF
BEGIN_DEF ZONE
NAME      Z08
ALFA   -5.7781513
BETA   0.0
STORATIVITY  1.0E-7
PLANE   P61
P_TYPE   UPPER
PLANE   P60
P_TYPE   LOWER
PLANE   P29
P_TYPE   UPPER
PLANE   P15
P_TYPE   LOWER
TEST_POINT   2339.83411   6767.96716   -975
#DETERMINISTIC YES
END_DEF
BEGIN_DEF ZONE
NAME      Z09
ALFA   -6.69897
```

```
BETA  0.0
STORATIVITY  1.0E-7
PLANE  P17
P_TYPE  UPPER
PLANE  P16
P_TYPE  LOWER
PLANE  P41
P_TYPE  UPPER
TEST_POINT  2842.33865  6412.13257  -975
#DETERMINISTIC YES
END_DEF
BEGIN_DEF ZONE
NAME  Z10
ALFA  -6.1760913
BETA  0.0
STORATIVITY  1.0E-7
PLANE  P14
P_TYPE  UPPER
PLANE  P13
P_TYPE  LOWER
PLANE  P90
P_TYPE  UPPER
PLANE  P2
P_TYPE  UPPER
PLANE  P20
P_TYPE  UPPER
PLANE  P29
P_TYPE  LOWER
TEST_POINT  1667.57528  7003.69756  -107.67738
#DETERMINISTIC YES
END_DEF
BEGIN_DEF ZONE
NAME  Z11
ALFA  -6.1760913
BETA  0.0
STORATIVITY  1.0E-7
PLANE  P52
P_TYPE  UPPER
PLANE  P51
P_TYPE  LOWER
PLANE  P18
P_TYPE  UPPER
PLANE  P21
P_TYPE  LOWER
TEST_POINT  2142.172  6980.10791  -975
#DETERMINISTIC YES
END_DEF
BEGIN_DEF ZONE
NAME  Z12
ALFA  -5.7781513
BETA  0.0
STORATIVITY  1.0E-7
PLANE  P58
P_TYPE  UPPER
PLANE  P57
P_TYPE  LOWER
PLANE  P22
P_TYPE  UPPER
PLANE  P41
```

```
P_TYPE   LOWER
TEST_POINT   1999.90527   6771.62659   -975
#DETERMINISTIC YES
END_DEF
BEGIN_DEF ZONE
NAME      Z13
ALFA   -4.9456423
BETA   0.0
STORATIVITY  1.0E-7
PLANE   P43
P_TYPE   UPPER
PLANE   P42
P_TYPE   LOWER
PLANE   P38
P_TYPE   UPPER
PLANE   P84
P_TYPE   UPPER
PLANE   P87
P_TYPE   UPPER
TEST_POINT   1461.19153   5922.58964   -819.39115
#DETERMINISTIC YES
END_DEF
BEGIN_DEF ZONE
NAME      Z14
ALFA   -4.8436528
BETA   0.0
STORATIVITY  1.0E-7
PLANE   P40
P_TYPE   UPPER
PLANE   P39
P_TYPE   LOWER
PLANE   P80
P_TYPE   LOWER
PLANE   P84
P_TYPE   UPPER
PLANE   P90
P_TYPE   UPPER
PLANE   P2
P_TYPE   UPPER
PLANE   P87
P_TYPE   UPPER
TEST_POINT   1106.6337   6311.8488   -990.4901
#DETERMINISTIC YES
END_DEF
BEGIN_DEF ZONE
NAME      Z15
ALFA   -7.60206
BETA   0.0
STORATIVITY  1.0E-7
PLANE   P89
P_TYPE   UPPER
PLANE   P88
P_TYPE   LOWER
PLANE   P29
P_TYPE   UPPER
TEST_POINT   4916.16177   6700.61243   -975
#DETERMINISTIC YES
END_DEF
BEGIN_DEF ZONE
```

```
NAME      Z16
ALFA   -5.39794
BETA   0.0
STORATIVITY  1.0E-7
PLANE   P31
P_TYPE   UPPER
PLANE   P30
P_TYPE   LOWER
PLANE   P84
P_TYPE   UPPER
PLANE   P90
P_TYPE   UPPER
PLANE   P2
P_TYPE   UPPER
PLANE   P19
P_TYPE   UPPER
TEST_POINT   1377.1912   6738.54932   -833.73433
#DETERMINISTIC YES
END_DEF
BEGIN_DEF ZONE
NAME      Z17
ALFA   -5.0457575
BETA   0.0
STORATIVITY  1.0E-7
PLANE   P34
P_TYPE   UPPER
PLANE   P33
P_TYPE   LOWER
PLANE   P84
P_TYPE   UPPER
PLANE   P19
P_TYPE   UPPER
TEST_POINT   1445.31678   6573.13281   -125
#DETERMINISTIC YES
END_DEF
BEGIN_DEF ZONE
NAME      Z18
ALFA   -5.39794
BETA   0.0
STORATIVITY  1.0E-7
PLANE   P25
P_TYPE   UPPER
PLANE   P24
P_TYPE   LOWER
PLANE   P19
P_TYPE   LOWER
PLANE   P2
P_TYPE   UPPER
PLANE   P74
P_TYPE   UPPER
TEST_POINT   2880.8645   7628.87927   -724.08417
#DETERMINISTIC YES
END_DEF
BEGIN_DEF ZONE
NAME      Z19
ALFA   -5.0457575
BETA   0.0
STORATIVITY  1.0E-7
PLANE   P28
```

```
P_TYPE   UPPER
PLANE   P27
P_TYPE   LOWER
PLANE   P19
P_TYPE   LOWER
PLANE   P74
P_TYPE   UPPER
TEST_POINT   3126.19092   7595.68091   -125
#DETERMINISTIC YES
END_DEF
BEGIN_DEF ZONE
NAME      Z20
ALFA   -6.6320232
BETA   0.0
STORATIVITY  1.0E-7
PLANE   P67
P_TYPE   UPPER
PLANE   P66
P_TYPE   LOWER
PLANE   P90
P_TYPE   UPPER
PLANE   P1
P_TYPE   LOWER
PLANE   P71
P_TYPE   UPPER
TEST_POINT   1693.14459   7860.99841   -176.72415
#DETERMINISTIC YES
END_DEF
BEGIN_DEF ZONE
NAME      Z21
ALFA   -6.1760913
BETA   0.0
STORATIVITY  1.0E-7
PLANE   P5
P_TYPE   UPPER
PLANE   P4
P_TYPE   LOWER
PLANE   P71
P_TYPE   UPPER
PLANE   P90
P_TYPE   UPPER
TEST_POINT   1878.38708   7765.35856   -424.34851
#DETERMINISTIC YES
END_DEF
BEGIN_DEF ZONE
NAME      Z22
ALFA   -7.60206
BETA   0.0
STORATIVITY  1.0E-7
PLANE   P70
P_TYPE   UPPER
PLANE   P69
P_TYPE   LOWER
PLANE   P71
P_TYPE   LOWER
TEST_POINT   -415   8140   -975
#DETERMINISTIC YES
END_DEF
BEGIN_DEF ZONE
```

```
NAME      Z23
ALFA   -7.60206
BETA   0.0
STORATIVITY  1.0E-7
PLANE   P73
P_TYPE   UPPER
PLANE   P72
P_TYPE   LOWER
PLANE   P68
P_TYPE   LOWER
PLANE   P74
P_TYPE   UPPER
TEST_POINT   1900   8075   -975
#DETERMINISTIC YES
END_DEF
BEGIN_DEF ZONE
NAME      Z24
ALFA   -7.60206
BETA   0.0
STORATIVITY  1.0E-7
PLANE   P76
P_TYPE   UPPER
PLANE   P75
P_TYPE   LOWER
PLANE   P71
P_TYPE   UPPER
TEST_POINT   3195   8050   -975
#DETERMINISTIC YES
END_DEF
BEGIN_DEF ZONE
NAME      Z25
ALFA   -7.60206
BETA   0.0
STORATIVITY  1.0E-7
PLANE   P79
P_TYPE   UPPER
PLANE   P78
P_TYPE   LOWER
PLANE   P90
P_TYPE   LOWER
TEST_POINT   -2072.5   5600   -975
#DETERMINISTIC YES
END_DEF
BEGIN_DEF ZONE
NAME      Z26
ALFA   -7
BETA   0.0
STORATIVITY  1.0E-7
PLANE   P92
P_TYPE   UPPER
PLANE   P91
P_TYPE   LOWER
PLANE   P84
P_TYPE   LOWER
TEST_POINT   1000   7192.5   -975
#DETERMINISTIC YES
END_DEF
# Z27 must not be included
# is outside local model boundaries
```

```
#BEGIN_DEF ZONE
#NAME      Z27
#ALFA   -7.60206
#BETA    0.0
#STORATIVITY  1.0E-7
#PLANE   P86
#P_TYPE   UPPER
#PLANE   P85
#P_TYPE   LOWER
#TEST_POINT   212.5   5905   -975
#DETERMINISTIC YES
#END_DEF
BEGIN_DEF ZONE
NAME      Z28
ALFA   -6.60206
BETA    0.0
STORATIVITY  1.0E-7
PLANE   P83
P_TYPE   UPPER
PLANE   P82
P_TYPE   LOWER
TEST_POINT   4620.35687   6751.88831   -975
#DETERMINISTIC YES
END_DEF
END_BLOCK

BEGIN_BLOCK TRANSIENT
 T_END   7.9557E6
# T_END   120.
 DT_START 60.0
# DT_START 1.0
# T_TOL   0.05
 T_TOL   0.05
# T_TOL   0.1
# CG_TOL   0.00001
 CG_TOL   0.1
 METHOD_KMAX 2
# METHOD_THETA 0.15
 METHOD_THETA 0.0
# H0     STATIONARY
 H0     CONSTANT
 VALUE   0.0
 TRACE   ON
# TRACE   OFF
 BEGIN DEF SOURCE
  TYPE LINE
#   START_AT  555  273 1008
#   START_AT  555  273  984
#   END_AT   621  595  503
#   START_AT  549  283  870
#   END_AT   615  605  395
   START_AT  551  300  870
   END_AT   611  598  395
   PUMPING_INTERVAL
    2.592E5  2.01E-3
    6.2634E5 2.52E-3
    2.0E7   2.25E-3
   END_LIST
#   HOLE_CONDUCTIVITY 1.0E-3
```

```
   HOLE_CONDUCTIVITY 1.0E-2
  END_DEF
END_BLOCK

BEGIN_BLOCK T_PRESENTATION
  PRES_TIMES
    0
    60
    84
    120
    180
    300
    420
    600
    840
    1200
    1800
    3000
    4200
    6000
    8400
    12000
    18000
    30000
    42000
    60000
    84000
    120000
    180000
    259200
    300000
    420000
    626340
    720000
    840000
    1200000
    1800000
    3000000
    4200000
    6000000
    7955700
  END_LIST
  PRES_POINTS
#   19  11  31
# kas06
    19  11  30
    19  12  29
#   20  12  28
    20  15  23
    20  16  22
    21  17  21
#   21  20  16
    21  20  15
    21  21  14
# kas02-4
#   17  18  21
# kas05-3
#   16  15  20
# kas07-4
```

```
#   18  13  25
# kas08-3
#   21  19  25
# kas08-1
#   24  14  17
# kas12-2
#   20  23  22
#
#   17  17  25
#   17  19   4
#   14  26  26
#   15  24  22
#   16  16  26
#   16  15  20
#   16  14  14
#   16  15  16
#   20  20  27
#   24  14  16
#    7  34  28
#    6  36  13
 END_LIST
END_BLOCK

BEGIN_BLOCK CALIBRATION
 CAL_TYPE          TRANSIENT
 CAL_TOL           0.001
# MAX_CAL_ITERATIONS 32
 MAX_CAL_ITERATIONS 8
# LINESEARCH_TOL    0.0005
 LINESEARCH_TOL    0.0005
 MAX_LS_ITERATIONS  3
# LS_STEP           0.1
# LS_STEP           0.5
# LS_STEP           1.5
 LS_STEP           1.5
# MAX_LS_STEP       0.5
# MAX_LS_STEP       1.0
# MAX_LS_STEP       3.0
 MAX_LS_STEP       3.0
 LS_GRADIENT       ON
 STAT_WEIGHT       1.0
# ADJOINT_WEIGHT    5000.0
 ADJOINT_WEIGHT    3.0E8
END_BLOCK
```

List of SKB reports

Annual Reports

1977-78
TR 121
KBS Technical Reports 1 – 120
Summaries
Stockholm, May 1979

1979
TR 79-28
The KBS Annual Report 1979
KBS Technical Reports 79-01 – 79-27
Summaries
Stockholm, March 1980

1980
TR 80-26
The KBS Annual Report 1980
KBS Technical Reports 80-01 – 80-25
Summaries
Stockholm, March 1981

1981
TR 81-17
The KBS Annual Report 1981
KBS Technical Reports 81-01 – 81-16
Summaries
Stockholm, April 1982

1982
TR 82-28
The KBS Annual Report 1982
KBS Technical Reports 82-01 – 82-27
Summaries
Stockholm, July 1983

1983
TR 83-77
The KBS Annual Report 1983
KBS Technical Reports 83-01 – 83-76
Summaries
Stockholm, June 1984

1984
TR 85-01
Annual Research and Development Report 1984
Including Summaries of Technical Reports Issued during 1984. (Technical Reports 84-01 – 84-19)
Stockholm, June 1985

1985
TR 85-20
Annual Research and Development Report 1985
Including Summaries of Technical Reports Issued during 1985. (Technical Reports 85-01 – 85-19)
Stockholm, May 1986

1986
TR 86-31
SKB Annual Report 1986
Including Summaries of Technical Reports Issued during 1986
Stockholm, May 1987

1987
TR 87-33
SKB Annual Report 1987
Including Summaries of Technical Reports Issued during 1987
Stockholm, May 1988

1988
TR 88-32
SKB Annual Report 1988
Including Summaries of Technical Reports Issued during 1988
Stockholm, May 1989

1989
TR 89-40
SKB Annual Report 1989
Including Summaries of Technical Reports Issued during 1989
Stockholm, May 1990

1990
TR 90-46
SKB Annual Report 1990
Including Summaries of Technical Reports Issued during 1990
Stockholm, May 1991

1991
TR 91-64
SKB Annual Report 1991
Including Summaries of Technical Reports Issued during 1991
Stockholm, April 1992

1992
TR 92-46
SKB Annual Report 1992
Including Summaries of Technical Reports Issued during 1992
Stockholm, May 1993

1993
TR 93-34
SKB Annual Report 1993
Including Summaries of Technical Reports Issued during 1993
Stockholm, May 1994

1994

TR 94-33

SKB Annual Report 1994

Including Summaries of Technical Reports Issued during 1994.
Stockholm, May 1995

1995

TR 95-37

SKB Annual Report 1995

Including Summaries of Technical Reports Issued during 1995.
Stockholm, May 1996

List of SKB Technical Reports 1996

TR 96-01

Bacteria, colloids and organic carbon in groundwater at the Bangombé site in the Oklo area

Karsten Pedersen (editor)
Department of General and Marine Microbiology, The Lundberg Institute, Göteborg University, Göteborg, Sweden
February 1996

TR 96-02

Microbial analysis of the buffer/container experiment at AECL´s Underground Research Laboratory

S Stroes-Gascoyne[1], K Pedersen[2], S Daumas[3], C J Hamon[1], S A Haveman[1], T L Delaney[1], S Ekendahl[2], N Jahromi[2], J Arlinger[2], L Hallbeck[2], K Dekeyser[3]

[1] AECL, Whiteshell Laboratories, Pinawa, Manitoba, Canada
[2] University of Göteborg, Department of General and Marine Microbiology, Göteborg, Sweden
[3] Guigues Recherche Appliquée en Microbiologie (GRAM), Aix-en-Provence, France
1996

TR 96-03

Reduction of Tc (VII) and Np (V) in solution by ferrous iron. A laboratory study of homogeneous and heterogeneous redox processes

Daqing Cui, Trygve E Eriksen
Department of Chemistry, Nuclear Chemistry, Royal Institute of Technology, Stockholm, Sweden
March 1996

TR 96-04

Revisiting Poços de Caldas. Application of the co-precipitation approach to establish realistic solubility limits for performance assessment

Jordi Bruno, Lara Duro, Salvador Jordana, Esther Cera
QuantiSci, Barcelona, Spain
February 1996

TR 96-05

SR 95

Template for safety reports with descriptive example
SKB
December 1995

TR 96-06

Äspö Hard Rock Laboratory Annual Report 1995

SKB
April 1996

TR 96-07

Criticality in a high level waste repository. A review of some important factors and an assessment of the lessons that can be learned from the Oklo reactors

Virginia M Oversby
VMO Konsult
June 1996

TR 96-08

A reappraisal of some Cigar Lake issues of importance to performance assessment

John Smellie[1], Fred Karlsson[2]

[1] Conterra AB
[2] SKB
July 1996

TR 96-09

The long-term stability of cement. Leaching tests

Ingemar Engkvist, Yngve Albinsson, Wanda Johansson Engkvist
Chalmers University of Technology, Göteborg, Sweden
June 1996

TR 96-10

Lake-tilting investigations in southern Sweden

Tore Påsse
Sveriges geologiska undersökning, Göteborg, Sweden
April 1996

TR 96-11
Thermoelastic stress due to an instantaneous finite line heat source in an infinite medium
Johan Claesson, Göran Hellström
Depts. of Building Physics and Mathematical Physics, Lund University, Lund, Sweden
September 1995

TR 96-12
Temperature field due to time-dependent heat sources in a large rectangular grid
– Derivation of analytical solution
Johan Claesson, Thomas Probert
Depts. of Building Physics and Mathematical Physics, Lund University, Lund, Sweden
January 1996

TR 96-13
Thermoelastic stress due to a rectangular heat source in a semi-infinite medium
– Derivation of an analytical solution
Johan Claesson, Thomas Probert
Depts. of Building Physics and Mathematical Physics, Lund University, Lund, Sweden
May 1996

TR 96-14
Oklo: Des reacteurs nucleaires fossiles (Oklo: The fossil nuclear reactors). Physics study (R Naudet, CEA)
– Translation of chapters 6, 13, and conclusions
V O Oversby
VMO Konsult
September 1996

TR 96-15
PLAN 96
Costs for management of the radioactive waste from nuclear power production
Swedish Nuclear Fuel and Waste Management Co
June 1996

TR 96-16
Diffusion of I^-, Cs^+ and Sr^{2+} in compacted bentonite
– Anion exclusion and surface diffusion
Trygve E Eriksen, Mats Jansson
Royal Institute of Technology, Department of Chemistry, Nuclear Chemistry, Stockholm
November 1996

TR 96-17
Hydrophilic actinide complexation studied by solvent extraction radiotracer technique
Jan Rydberg
Department of Nuclear Chemistry, Chalmers University of Technology, Gothenburg, Sweden and Radiochemistry Consultant Group AB, V. Frölunda, Sweden
October 1996

TR 96-18
Information, conservation and retrieval
Torsten Eng[1], Erik Norberg[2], Jarl Torbacke[3], Mikael Jensen[4]
[1] Swedish Nuclear Fuel and Waste Management Co (SKB)
[2] National Swedish Archives
[3] Department of History, Stockholm University
[4] Swedish Radiation Protection Institute (SSI)
December 1996

TR 96-19
Application of space geodetic techniques for the determination of intraplate deformations and movements in relation with the postglacial rebound of Fennoscandia
Hans-Georg Scherneck, Jan M Johansson, Gunnar Elgered
Chalmers University of Technology, Onsala Space Observatory, Onsala, Sweden
April 1996

TR 96-20
On the characterization of retention mechanisms in rock fractures
Jan-Olof Selroos, Vladimir Cvetkovic
Div. of Water Resources Engineering, Dep. of Civil and Environmental Engineering, Royal Institute of Technology, Stockholm, Sweden
December 1996

TR 96-21
Boring of full scale deposition holes using a novel dry blind boring method
Jorma Autio, Timo Kirkkomäki
Saanio & Riekkola Oy, Helsinki, Finland
October 1996

TR 96-22
Feasibility study for siting of a deep repository within the Malå municipality
Swedish Nuclear Fuel and Waste Management Co., Stockholm
March 1996